

Crosstalk between the lung microenvironment and CNS autoimmunity

Dissertation

for the award of the degree

“Doctor rerum naturalium”

of the Georg-August-Universität Göttingen

within the doctoral program “Molecular Biology of Cells”
of the Georg-August University School of Science (GAUSS)

submitted by

Roger Cugota Canals

born in Barcelona (Spain)

Göttingen, 2022

Thesis advisory committee

Prof. Dr. Alexander Flügel

Institute for Neuroimmunology and Multiple Sclerosis Research
University Medical Center Göttingen

Prof. Dr. Jürgen Wienands

Department of cellular and molecular immunology
University Medical Center Göttingen

Prof. Dr. Holger Reichardt

Department of cellular and molecular immunology
University Medical Center Göttingen

Members of the Examination Board

Referee: Prof. Dr. Alexander Flügel

Institute for Neuroimmunology and Multiple Sclerosis Research
University Medical Center Göttingen

2nd Referee: Prof. Dr. Jürgen Wienands

Institute for cellular and molecular immunology
University Medical Center Göttingen

Further Members of the Examination Board

Prof. Dr. Holger Reichardt

Institute for cellular and molecular immunology
University Medical Center Göttingen

Prof. Dr. Christine Stadelmann-Nessler

Institute of Neuropathology
University Medical Center Göttingen

Prof. Dr. Hannelore Ehrenreich

Clinical Neuroscience
Max Planck Institute of Experimental Medicine

Prof. Dr. Martin S. Weber

Institute of Neuropathology
University Medical Center Göttingen

Date of oral examination: 13.05.2022

(This page was intentionally left blank.)

To my mother and my father,
who supported me, even when it was not easy to understand.

To my brother Manel, who is always there.

Table of contents

Table of contents.....	IV
List of figures.....	VIII
List of abbreviations	XI
Summary.....	XIII
1. Introduction	1
1.1 Multiple Sclerosis.....	1
1.1.1 Aetiology of MS and Risk factors	1
Genetic risk factors	2
Environmental factors.....	2
1.1.2 MS risk factors directly associated with the lung.	2
1.2 Experimental autoimmune encephalomyelitis, EAE.....	3
1.2.1 Active EAE.....	4
1.2.2 Transfer EAE.....	5
1.3 The role of the lung in CNS autoimmunity	6
1.3.1 The lung microbiome as moderator of CNS autoimmunity.....	9
1.3.2 Oxygen levels as regulator factor of the immune response.....	10
2. Aims and objectives.....	15
2.1 Impact of <i>in vitro</i> hypoxia on T _{MBP} cell properties.	15
2.2 Impact of whole-body hypoxia on EAE	15
3. Material and Methods	17
3.1 Materials	17
3.1.1 Media and buffers.....	17
3.1.2 Reagents, chemicals and sera.....	18
3.1.3 Antigens and adjuvants	19
3.1.4 Antibodies.....	19
3.1.5 Q-PCR primers.....	19
3.1.6 Kits.....	20

3.1.7 Equipment and consumables	20
3.1.8 Instruments and machines	21
3.1.9 Software	21
3.2 Methods	22
3.2.1 Animals	22
3.2.2 Generation and culture of primary T cell lines	22
3.2.3 T cell culture under hypoxic conditions	23
3.2.4 Experimental autoimmune encephalomyelitis (EAE).....	23
Transfer EAE	23
Lung active EAE.....	23
EAE Clinical scoring	24
3.2.5 Exposition to whole body hypoxia	24
3.2.6 Organ retrieval and processing.....	25
Euthanasia and perfusion	25
Blood	25
Lungs	25
Spinal cord.....	26
Spleen	26
Lymph nodes	26
3.2.7 Fluorescence activated cell sorting (FACS).....	26
Staining	26
Staining of surface markers.....	27
Intracellular staining for cytokine production	27
Intranuclear staining for transcription factors	27
FACS cell counting.....	27
FACS cell sorting	28
3.2.8 RNA isolation and cDNA conversion	28
3.2.9 Quantitative real time PCR.....	28

3.2.10 Enzyme-linked immunosorbent assay (ELISA).....	28
3.2.11 Next generation sequencing.....	29
3.2.12 Treatment, analysis and statistical analysis of the data.....	29
4. Results.....	31
4.1 Environmental oxygen conditions affect T _{MBP} cell proliferation.....	31
4.2 Environmental oxygen conditions do not affect T _{MBP} cell viability but affect T _{MBP} cell proliferation	32
4.3 Environmental oxygen conditions affect the expression of activation markers on the surface of T _{MBP} cells.....	34
4.4 Environmental oxygen conditions affect cytokine production in T _{MBP} cells.....	36
4.5 Environmental oxygen conditions do not affect FOXP3 expression in T _{MBP} cells.....	38
4.6 Hypoxia induces changes in the global expression profile of T _{MBP} cells.....	40
4.7 An oxygen-deprived environment promotes transcriptional activity in T _{MBP} cells.....	42
4.8 Dynamic changes in the expression profile of T _{MBP} cells upon hypoxic conditions.....	44
4.9 Gene Set Enrichment Analysis as a tool to explore specific, hypoxia-dependent programmes	47
4.10 An oxygen-deprived environment during T _{MBP} activation triggers the upregulation of specific transcripts related to the glycolytic pathway.....	51
4.11 Environmental oxygen conditions during <i>in vitro</i> T cell activation affect the encephalitogenic potential of T _{MBP} cells.....	55
4.12 An oxygen-deprived environment during <i>in vitro</i> activation impairs T _{MBP} cell ability to invade the CNS.....	58
4.13 CNS inflammation correlates with the invasion pattern of T _{MBP} cells.....	61
4.14 The reactivation of hypoxic T _{MBP} cells in the target tissue is not impaired.....	62
4.15 Endogenous T cell recruitment to the CNS is reduced in animals that receive hypoxic T _{MBP} cells	67
4.16 Hypoxyprobe-1 allows the detection of the oxygenation status of T _{MBP} cells <i>in vitro</i>	70
4.17 T cells in different organs displayed a different oxygenation status.....	71
4.18 <i>In vivo</i> hypoxia impairs T _{MBP} cell proliferation in EAE induced via the lung.....	73
4.19 <i>In vivo</i> hypoxia impairs cytokine expression in T _{MBP} cells in EAE induced via the lung.....	77

4.20 <i>In vivo</i> hypoxia does not induce a main shift toward a regulatory phenotype in T _{MBP} cells in lung-EAE.....	79
4.21 <i>In vivo</i> hypoxia affects the encephalitogenic potential of T _{MBP} cells	80
5. Discussion.....	83
6. List of references	89
Acknowledgements.....	100

List of figures

Figure 1. Infographic depicting the protocol of transfer EAE.....	5
Figure 2 . In the transfer EAE set up, T _{MBP} cells home into the lung before invading the CNS.	6
Figure 3. A cell population in the lung is able to take up antigens from the airways.	7
Figure 4. T _{MBP} cells reactivated in vitro with APCs isolated from the lung are able to trigger a CNS autoimmune disease upon intravenous transfer.	8
Figure 5. The lung-microbiome regulates CNS autoimmunity by conditioning microglial reactivity.	10
Figure 6. Oxygen tensions in a selection of human tissues in comparison to standard cell culture conditions.	11
Figure 7. Experimental design for the in vitro set up.	31
Figure 8. An oxygen-deprived environment reduces the number of T _{MBP} cells retrieved after antigen stimulation.	32
Figure 9. T _{MBP} cells stimulated under hypoxic conditions are viable.	33
Figure 10. An oxygen-deprived environment affects T _{MBP} cell proliferation.	34
Figure 11. An oxygen-deprived environment affects the expression of surface activation markers in T _{MBP} cells.	35
Figure 12. An oxygen-deprived environment affects the percentage of T _{MBP} cells producing IFN γ	36
Figure 13. An oxygen-deprived environment affects pro-inflammatory cytokine production by T _{MBP} cells.....	37
Figure 14. No main shift toward a regulatory phenotype is observed in T _{MBP} cells stimulated under hypoxic conditions.....	38
Figure 15. Experimental design and workflow for the transcriptomic study.....	40
Figure 16. Time after antigen encounter and oxygen conditions determine transcriptional changes in T _{MBP} cells.	41
Figure 17. (next page). Hypoxia induces early and sustained changes in the expression profile of T _{MBP} cells.....	42
Figure 18. In hypoxic conditions, nearly 40% of the genes are uniquely upregulated at 48h.	44
Figure 19. Hypoxia induces upregulation of several genes regulated by HIF-1 alpha.	45
Figure 20. In hypoxic conditions, nearly 74% of the genes are uniquely downregulated at 48h....	46
Figure 21. Hypoxia induces early and sustained changes in the transcriptional program of T _{MBP} cells.	50
Figure 22. Hypoxia triggers the overexpression of a specific subset of hypoxia-related genes.....	52

Figure 23. Hypoxia promotes the upregulation of glycolysis rate-limiting enzymes. Scheme of the metabolic pathway	53
Figure 24. Experimental design of transfer EAE experiments.....	55
Figure 25. T _{MBP} cell blasts stimulated in vitro under hypoxic conditions trigger milder clinical signs in the transfer EAE.	56
Figure 26. Low numbers of hypoxic T _{MBP} cell blasts trigger a delayed and weaker clinical signs in the transfer EAE.	57
Figure 27. Hypoxic T _{MBP} cell blasts display a reduced capacity to infiltrate the CNS.....	59
Figure 28 . Different expression pattern of pro-inflammatory cytokines and Foxp3 in hypoxic and normoxic T _{MBP} cells in the CNS.	61
Figure 29. The expression of surface of activation markers in hypoxic T _{MBP} cells is not impaired in the CNS.	62
Figure 30. The expression of pro-inflammatory cytokines by hypoxic T _{MBP} cells in the CNS is not impaired.	64
Figure 31. The number of hypoxic T _{MBP} cells producing pro-inflammatory cytokines is reduced in the CNS.	65
Figure 32. Hypoxic blasts do not acquire a regulatory phenotype in the spinal cord.	66
Figure 33. Reduced infiltration of endogenous T cells in the target tissue upon transfer of hypoxic T _{MBP} cells.	67
Figure 34. Endogenous T cells recruited in the CNS upon transfer of hypoxic T _{MBP} cells are not functionally impaired.....	68
Figure 35. Activated endogenous T cells in the CNS are reduced upon transfer of hypoxic T _{MBP} cells.	69
Figure 36. T _{MBP} cells in vitro display a more intense HP1-staining in hypoxic than in normoxic conditions.....	70
Figure 37. T cells in different organs displayed different levels of oxygenation through the course of EAE.	71
Figure 38. Effect of hypoxic environment on T _{MBP} cell reactivation into the lung.	73
Figure 39. Hypoxia affects T _{MBP} cell proliferation in vivo upon lung immunisation.	74
Figure 40. T _{MBP} cell proliferation in the lung is affected by a hypoxic environment..	75
Figure 41. Proliferative status of T _{MBP} cells in the mediastinal lymph nodes is affected by a hypoxic environment.....	76
Figure 42. Hypoxia does not affect cytokine production by T _{MBP} at 48h after reactivation in the lung.	77

Figure 43. Hypoxia affects cytokine production by T_{MBP} at 24h after reactivation in the lung..... 78
Figure 44. Hypoxia promotes a mild increase in the expression of FOXP3 in T_{MBP} cells in the lungs.
..... 79
Figure 45. Hypoxia induce clinical differences in EAE induced via the lung..... 81

List of abbreviations

ACK	Ammonium-chloride-potassium
aEAE	Active experimental autoimmune encephalomyelitis
APC	Antigen presentig cell
APC (fluo)	Allophycocianin
BBB	Blood-brain barrier
BSA	Bovine serum albumin
BV421	Brilliant violet 421
cDNA	complementary DANN
CFA	Complete Freund's adjuvant
CIS	Clinical isolated syndrome
CMV	Cytomegalovirus
CNS	Central nervous system
CO ₂	Carbon dioxide
Cy7	Cyanine 7
DEG	Differentially expressed gene
DMEM	Dulbecco's modified Eagle medium
DMSO	Dimethylsulfoxid
DPBS	Dulbecco's phosphate-buffered saline
EAE	Experimental autoimmune encephalomyelitis
EBV	Epstein-Barr virus
EDTA	Ethylenediaminetetraacetic acid
EH	Eagle's-HEPES medium
ELISA	Enzym-linked immunosorbent analysis
FACS	Ffluorescence-activated Cell Sorting
FAM	Fluorescein
FC	Fold change
FCS	Fetal calf serum
FM	Freezing medium
G-418	Neomycin g418
GFP	Green ffluorescent protein
GO	Gene ontology
GSEA	Gene-set enrichment analysis
GWAS	Genome-wide assiciation study
HLA	Human leukocyte antigen
HP1	Hypoxyprobe 1
HRE	Hypoxia response element
HRP	Horseradish peroxydase
i. tr.	intratracheal (administration)
i. v.	intravenous (administration)
IFA	Incomplete Freund's adjuvent
IFN	Interferon
IL17a	Interleukin 17a
IL-2	Interleukin 2
IL-2R α	α subunit of receptor for Interleukin-2
IONO	ionomycin calcium salt
IU	International units
LPS	Lipopolysaccharide

LSM1077	Lymphocyte separation media 1077
MBP	Myelin basic protein
MHC	Major histocompatibility complex
mM	millimolar
mmHg	Millimetre of mercury
MOG	Myelin oligodendrocyte protein
MS	Multiple sclerosis
NGS	Next-generation sequencing
O ₂	Oxygen
OD	Optical density
OVA	Chicken ovoalbumin
p. i.	(days) post immunisation
p. t.	(days) post transfer
PBS	Phosphate-buffered Saline
PC	Principal component
PCA	Principial component analysis
PE	Phycoerythrin
PerCP	Peridinin Chlorophyll
PFA	Paraformaldehyde
PHD	Prolyl-hydroxylase domain
PLP	proteolipid protein
PMA	Phorbol 12-myriyate 13-acetate
PPMS	Primary progressive multiple sclerosis
qPCR	real time quantitative polimerase chain reaction
RCF	Relative centrifugal force
RNA	Ribonucleic acid
RRMS	relapsing-remitting multiple sclerosis
SEM	Standard error of the mean
SPF	Specific pathogen free
SPSM	Secondary progressive multiple sclerosis
SSD	Standard spin down
TAMRA	5-Carboxytetramethylrhodamine
TCGF	T cell growing factor
TCM	T cell medium
TCR	T cell receptor
tEAE	Transfer experimental autoimmune encephalomyelitis
T _{EM}	T-effector memory cell
TM	Thawing medium
T _{MBP}	T _{effector-memory} cells directed agains myelin basic protein
Treg	T regulatory cell
VHL	Von Hippel Lindau

Summary

The contribution of the lung in shaping CNS autoimmunity is gaining relevance in the last years. Central nervous system (CNS) reactive T cells can acquire in the lung the potential to invade the CNS in experimental autoimmune encephalomyelitis, an animal model for Multiple sclerosis. Furthermore, the lung microbiota by modulating the microglial phenotype can act on the effector phase of the CNS autoreactive process and regulate the disease severity. Finally, the lung can also represent a trigger site for CNS autoimmunity. Indeed, very low doses of CNS antigen delivered intra-trachea are sufficient to trigger myelin-reactive T cells to induce EAE. As a repercussion of its main task of gas-exchange, the lung represents the most extensive surface in contact with the outside environment and is the organ with the highest level of oxygenation in the body. In this work, in order to identify pulmonary factors that can potentially contribute to the efficiency of the lung in triggering autoimmunity, we investigated if oxygen availability determines the function of CNS-reactive T cells in the context of CNS autoimmunity.

In vitro, we could observe that an oxygen-deprived atmosphere impaired proliferation and effector functions of myelin-reactive T cells stimulated with the cognate antigen. These functional changes were associated with a global reprogramming of the transcriptional profile. The hypoxic stimulus, rather than impairing, triggered an upregulation of numerous transcripts mainly involved in glucose metabolism and cell signalling events. These transcriptional changes were clinically relevant. Indeed myelin-reactive T cells stimulated in a hypoxic environment and retransferred *in vivo* proliferated less than the normoxic counterpart did and induced a milder disease.

We then assessed if these *in vitro* findings could be translated *in vivo*. We could prove that T cells are able to sense different oxygen tensions as they circulate throughout the organism. Furthermore, we observed that myelin-reactive T cells residing in the lung were less activated and proliferated less when stimulated in the lung with the cognate antigen in animals kept under hypoxic conditions. These data confirmed that also *in vivo* the initial steps of T cell activation are depending on the environmental oxygen. Finally, when EAE was induced via intra-lung immunization in animals exposed to whole body hypoxia during the initial steps of T cell activation, the disease was milder and the animals displayed an atypical phenotype.

Taken together, our results indicated that the T cells are able to adapt their function to a broad range of environmental oxygen conditions by rapidly switching their metabolism and transcriptional profile. In the lung, the unique oxygen conditions favour T cells activation and proliferation and therefore contribute to the capacity of the lung to trigger CNS autoimmunity.

1. Introduction

1.1 Multiple Sclerosis

Multiple sclerosis (MS) is an inflammatory autoimmune condition affecting the central nervous system (CNS), characterized by demyelinating lesions in both grey and white matter leading to axonal loss and neurodegeneration (Compston & Coles, 2008; Ransohoff et al., 2015). MS generally first appears in young adults aged between 20 and 30 years and is more prevalent in women than in men in a 3 to 1 ratio (Alonso & Hernán, 2008). About 2.3 million people are affected worldwide and in Western countries MS represents one of the main causes of juvenile and adult disability, being responsible for a significant portion of the expenditure of public health and care systems in these countries (Feigin et al., 2017). The pathogenesis of the disease is still under discussion, but a body of data suggests that CNS-autoreactive CD4⁺ cells play a major role (Bahbouhi et al., 2010; Hohlfeld et al., 2016; Sospedra & Martin, 2016).

Regarding its clinical manifestations, MS usually first appears in the form of a so-called Clinical Isolated Syndrome (CIS), an episode of focal neurological dysfunction lasting at least 24 hours that generally remits completely within the period of one week. The most common signs and symptoms of CIS are unilateral sight loss, numbness and tingling or balance problems (Ransohoff et al., 2015).

Usually CIS gives rise to the most common form of the disease, known as relapsing-remitting MS (RRMS), in which the disease presents in the form of clinical flares, isolated or separated in time, and thereafter the patient can recover completely or some sequelae may remain. Typically, RRMS evolves into a secondary progressive MS (SPMS) characterised by a slow but relentless progression of the disease course. In 10 to 20% of patients (Compston & Coles, 2008), the disease manifests itself as a primary progressive disease form (PPMS), characterised by the lack of relapsing-remitting episodes and an ongoing steady progression from the disease onset. According to recent epidemiological studies, the age of onset of PPMS is around 45 years, the age at which RRMS also generally progresses to SPMS (McKay et al., 2015).

1.1.1 Aetiology of MS and Risk factors

The cause of MS remains unknown. As for other autoimmune disorders such as type 1 diabetes mellitus, MS is recognised as a multifactorial disease with a complex aetiology caused by a combination of genetic and environmental factors.

Genetic risk factors

Evidence for a genetic component of MS was found in population-based studies that pointed to an increased disease risk among close relatives of MS patients. The risk decreases with familiar distance, the higher concordance rate (about 25 to 30%) being observed in monozygotic twins (Robertson et al., 1996; Ebers et al., 2000; Compston & Coles, 2008). Over the years, multiple genome-wide association studies (GWAS) have identified more than 200 loci that can independently contribute to the pathogenesis of the disease. Several of the identified genetic risk factors are associated with immune-related genes and are shared with other immune diseases (Beecham et al., 2013). The first loci to be identified were mapped on the Human Leukocyte Antigen (HLA) system encoding for molecules of the major histocompatibility complex (MHC). Specifically, the allele DR15 of the HLA region (HLA-DRB1*15:01) has been linked with MS in both Northern European and Northern American populations (Goodin, 2014). In a more recent revision, this allele has been linked to both an increased risk of MS development and to a more severe disease phenotype (Baranzini & Oksenberg, 2017).

Among the other identified risk genes, IL2RA, IL17Ra, TNFR1, TNFRSF1A, IRF8, CD25, CD6 and BAFF, as well as genes involved in the metabolism of vitamin D have gained special attention (Dobson & Giovannoni, 2019; Sospedra & Martin, 2016).

Environmental factors

A variety of environmental risk factors has been associated with the development of MS. The most commonly reported are childhood obesity, viral infections, cigarette smoking and dysregulation of the gut microbiome as well as low levels of vitamin D related with low sunlight exposure (Ascherio, 2013; Ascherio & Munger, 2007a, 2007b; Compston & Coles, 2008). Regarding the latter, the exposure to ultraviolet radiation and increased vitamin D levels, especially before young adulthood, seems to exert a protective effect against MS (Lucas et al., 2015; Munger et al., 2006) and could therefore contribute to explain the well-described latitudinal gradient of MS incidence, prevalence and related mortality (Simpson et al., 2011).

1.1.2 MS risk factors directly associated with the lung.

Many of the environmental factors reported to increase the risk of MS are lung-associated.

Lung infections by influenza-viruses or members of the Human Herpes-Virus family such as Epstein-Barr Virus (EBV) and Cytomegalovirus (CMV) have been linked to both an increased risk of MS development and a worsening of the pre-existing disease (Halenius & Hengel, 2014; Lang et al., 2002; Oikonen et al., 2011). EBV is a human herpes virus infecting preferentially epithelial cells in the

oropharynges and B cells. After infection, the virus persists in latent form in B lymphocytes throughout life (Hatton et al., 2014). Elevated titers of anti-EBV antibodies are found in serum of MS patients, and an increased number of CD8⁺ T cells directed against EBV are found in the circulation during relapses of MS (Angelini et al., 2013; Pender et al., 2014). Post-mortem studies have also revealed a high number of EBV infected B cells in the CNS lesions of MS patients (Serafini et al., 2017). Recently, a longitudinal study conducted on 10 million young adults showed that EBV infection precedes MS onset and greatly increases the risk of subsequent MS (Bjornevik et al., 2022). At a mechanistic level, molecular mimicry between EBV and CNS autoantigens has been proposed for the involvement of EBV in MS pathogenesis (Lanz et al., 2022; Pender et al., 2014; Tengvall et al., 2019)

Regarding the relationship between tobacco smoke and MS, cigarette smoking has been found by several studies to be strongly associated with both an increased risk of developing MS and a stronger and more rapid disease progression (Ascherio & Munger, 2007b; Goodin, 2014; Hedström et al., 2013; Hernán et al., 2001; Jafari & Hintzen, 2011). Furthermore, the risk of disability progression is significantly increased in patients that started smoking earlier in their lives; these patients also show an increased risk of earlier development to a chronic clinical course of the disease (Sundström & Nyström, 2008). Even passive exposure to tobacco smoke (second hand smoke) has been related to an early onset of MS in children (Hedström et al., 2011).

Taken all together, these observations suggest that the lung could play a major role in the pathogenesis of MS.

1.2 Experimental autoimmune encephalomyelitis, EAE

The knowledge we nowadays possess about the pathogenesis of MS, as well as several currently used therapies, are grounded on observations made in animal models of the disease. Each model mimics specific aspects of the disease. Unfortunately, no one model can recapitulate the entire complexity of MS. One of the most relevant animal models to the study of MS is the so-called experimental autoimmune encephalomyelitis, shortly EAE.

The germinal idea of EAE appeared by the beginning of the last century, within the context of investigating the adverse effects derived from Pasteur's vaccination against rabies in 1882 (Pasteur & Illo, 1996). The vaccine was prepared from spinal cord of rabbits previously inoculated with the virus, and it led in some cases to paresis, ataxia, and impaired breathing and swallowing. In an attempt to understand these unexpected adverse effects, in 1925 Koritschoner and Schewinburg (Koritschoner & Schweinburg, 1925) observed that the injection of brain tissue from healthy sheep into rabbits led to limb paralysis, thus excluding a viral aetiology of the adverse effects. Shortly after, Thomas Milton

Rivers could showed that several Rhesus monkeys inoculated with rabbit brain developed demyelinating lesions in the CNS, preferentially localized around blood vessels (Rivers et al., 1933; Rivers & Schwentker, 1935; Schwentker & Rivers, 1934). He also observed a correlation between myelin content and disease-inducing capacity of the brain extract, suggesting that myelin could be responsible for the disease induction. These findings, together with the development of an adjuvant, namely Freund's complete adjuvant (CFA) composed by killed *Mycobacterium Tuberculosis* and paraffin oil able to boost the disease (Freund et al., 1945), led to the development of the EAE model (in this form called active EAE, aEAE). Since these initial observations, the pathogenesis of EAE has been extensively investigated. In the sixties, it was demonstrated that T cells and not antibodies are the trigger of the disease (Paterson, 1960). Two decades later, Wekerle and Ben Nun observed that the transfer of *in vitro* activated myelin basic protein (MBP)-specific CD4⁺ T cells into healthy syngeneic recipient animals was sufficient to induce the disease, thus identifying those cells as the culprit of EAE (Ben-Nun et al., 1981).

Since its establishment, the EAE model has been used in a wide variety of mammals, from pigs and rabbits to non-human primates. The gradual refinement of the rodent model has made EAE the most widely used model today to study CNS autoimmune threats. Although with variations mainly depending on animal species/backgrounds and experimental protocols, the clinical picture of EAE is mostly characterised by weight loss and ascending paralysis starting with tail tone affection that develops from ataxia and gait disturbances to complete paralysis of the hind and forelimbs.

EAE can be induced by two different protocols: 1) active EAE (aEAE) is induced by immunisation with CNS-related antigens; and 2) transfer EAE (tEAE) is induced by transferring of *in vitro* activated CNS-reactive CD4⁺ T cells in syngeneic recipients.

1.2.1 Active EAE

For the induction of aEAE, animals are immunised subcutaneously with myelin antigens such as myelin basic protein (MBP), myelin oligodendrocyte protein (MOG) or proteolipid protein (PLP) (Hemmer et al., 2002), emulsified in CFA. The myelin antigen is then presented to endogenous naïve T-cells by "professional" antigen presenting cells (APCs) in the lymph nodes draining the immunisation site. After being activated, the autoreactive T cells undergo clonal expansion through several rounds of proliferation and after some days, they are released into the bloodstream from where they enter the CNS by crossing the blood-brain barrier (BBB). In the target tissue, the CNS-reactive T cells are once more activated by encountering the cognate antigen presented by local APCs. This *in situ* activation step triggers the expression of pro-inflammatory cytokines and chemokines that induce a massive

recruitment of other immune cells including lymphocytes and monocytes/macrophages, finally leading to inflammation, demyelination and tissue destruction (Mix et al., 2010).

1.2.2 Transfer EAE

A crucial step in transfer EAE is the establishment of CNS-reactive T cells *in vitro*. For this purpose, animals are immunised subcutaneously with an emulsion of a myelin antigen and an adjuvant, as in the aEAE set up. Shortly before the onset of the disease (8-10 days after immunisation), the draining lymph nodes are removed and the isolated T cells are amplified *in vitro* for one or several rounds by stimulating them with the cognate antigen in presence of APCs (Ben-Nun et al., 1981). Fully activated T cell (blasts) are then transferred to naïve recipient animals. As with the aEAE model, a few days after transfer, CNS-reactive T cells are released into the bloodstream from where they enter the CNS, overcoming the BBB. Once in the CNS, the autoreactive T cells, upon *in situ* reactivation, trigger the CNS inflammation associated with tissue damage and clinical signs.

The choice of EAE protocol depends on the experimental question. aEAE makes it possible to investigate the initial event determining the priming of naïve T cell in the lymph nodes; the transfer model offers the possibility of genetically manipulating the culprit T cells *in vitro* and then tracking and functionally characterizing them *in vivo* during the entire disease course (Flügel et al., 1999a).

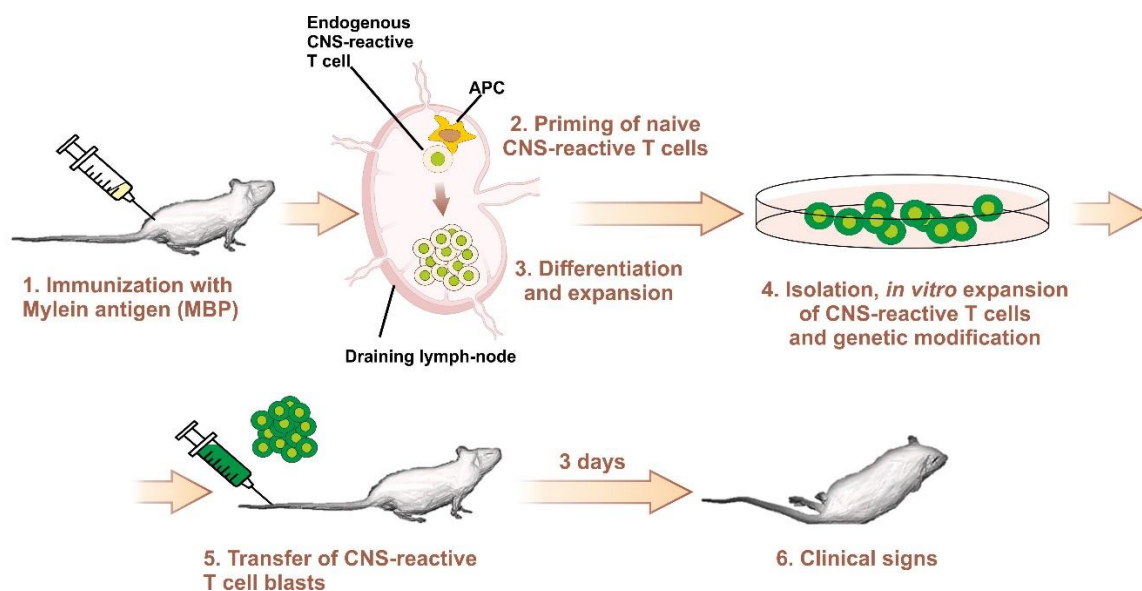


Figure 1. Infographic depicting the protocol of transfer EAE. The establishment of a transfer EAE protocol, making it possible to manipulate CNS-directed CD4⁺ T cells *in vitro* prior to their injection, for instance by expressing fluorescent proteins that allow the location of pathogenic cells to be tracked over the course of the disease. This has advanced research in the field of neuroimmunology. Scheme adapted from Merlini 2021.

1. 3 The role of the lung in CNS autoimmunity

The tEAE model has been employed to find out about the role of the lung in CNS autoimmunity. By tracking fluorescently labelled effector memory T cells directed against MBP (T_{MBP} cells) in tEAE in Lewis rats, it could be shown that T_{MBP} cells follow a precise migratory pattern. Immediately after intravenous transfer, T_{MBP} cells disappear from the blood circulation and home into the lung. Here, for the first 12h, T_{MBP} cells were found scattered in the lung tissue, whereas 24 to 48h after transfer they were mainly localized around the bronchial structures and in the bronchial associated lymphoid tissue. Two days after transfer, T_{MBP} cells were found in the lung-draining mediastinal lymph nodes and 24 hours later, they could be detected in blood, spleen and in peripheral organs. Starting on day 3 p.t., T_{MBP} cells entered the CNS, and this event coincided with the onset of the clinical symptoms (Flügel et al., 1999a; Odoardi et al., 2012). While residing in the lung, the gene expression profile of the transferred T_{MBP} cells underwent a drastic reprogramming: the expression of transcripts related to T cell activation and proliferation decreased, whereas the expression of genes related to T cell motility, migration and adhesion was upregulated (Figure 2). These global changes in the expression profile licensed T_{MBP} cells to enter the CNS. This work performed with tEAE not only indicated that the lung represents a hub for T_{MBP} cells on their way to the CNS, but also that the lung environment can shape the encephalitogenic potential of effector T cells.

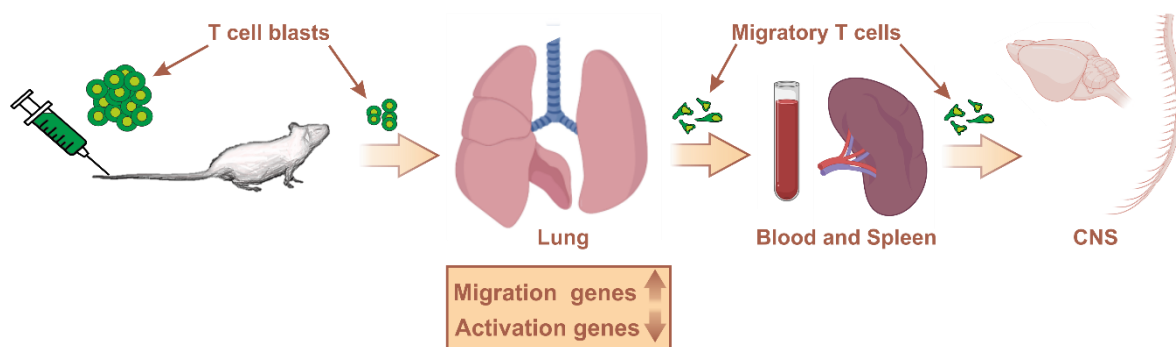


Figure 2 . In the transfer EAE set up, T_{MBP} cells home into the lung before invading the CNS. In a tEAE set up, upon intravenous transfer, encephalitogenic CD4+ T cells home into the lung of recipient animals where they undergo a refined change on their gene expression which confers them with the ability to invade the CNS (Odoardi et al., 2012). Infographic adapted from Ransohoff, 2012.

Further data also suggest that CNS autoimmunity can be initiated in the lung. Indeed long living memory T_{MBP} cells, instilled at neonatal age in recipient animals and persisting throughout adult life (Kawakami et al., 2005), could be activated in the lung by local delivery of the cognate antigen and were able to induce CNS disease (Odoardi et al., 2012).

In order to characterize the population of cells able to present the antigen in the lung, in a preliminary work I performed together with L. Hosang (*Figures 3 and 4*), we administered intra-tracheally (i.tr) a self-quenched conjugate of ovalbumin (OVA) that becomes fluorescent upon proteolytic degradation (DQ-OVA). We then quantified the fluorescently labelled APCs in the lung by flow cytometry. We observed that 24h after antigen delivery, 40% of MHC class II⁺ cells in the lung had been able to uptake the fluorescent antigen. About the 80% of these potential APCs had a myeloid lineage, evidenced by their expression of CD11b/c on their surface (*Figure 3*).

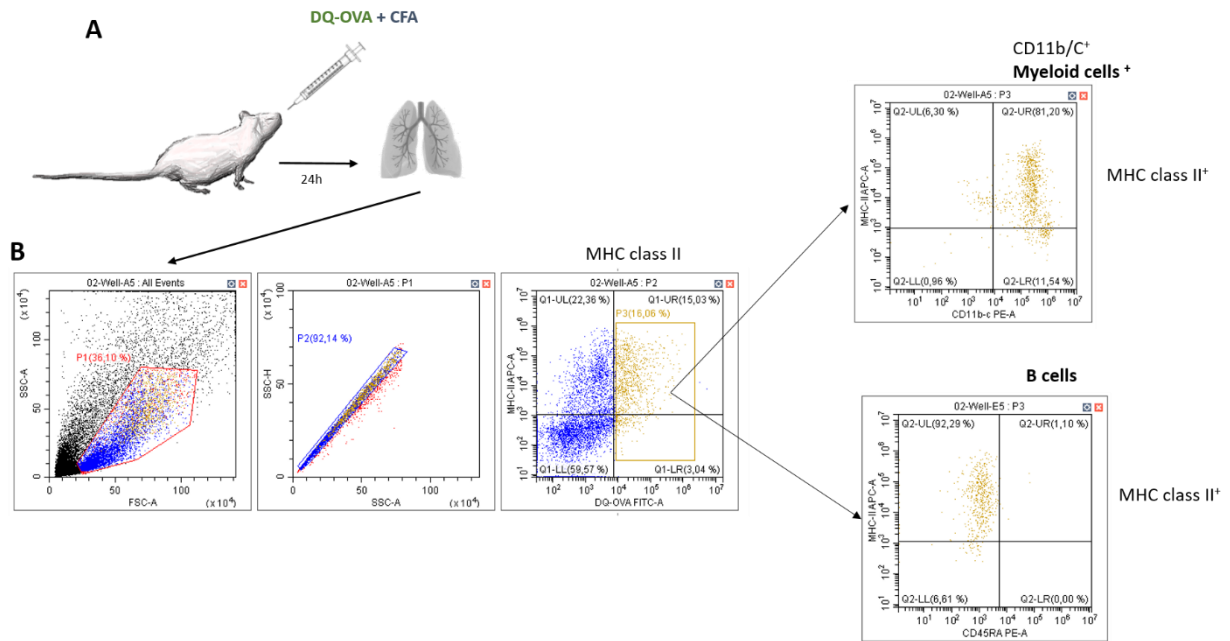


Figure 3. A cell population in the lung is able to take up antigens from the airways. Intratracheal immunisation of naïve Lewis rats with the fluorescent antigen DQ-OVA allowed our team to discover a subset of myeloid cells (CD11b/c⁺ MHCII⁺) residing in the lung able to uptake antigen from the airways and potentially present it to immune cells. **A.** Experimental set up. **B.** FACS plots showing the DQ-OVA derived fluorescence in the CD11b/c⁺ MHCII⁺ lung-residing population. Scheme provided by Dr. L. Hosang

To prove that these cells were indeed able to activate T cells, we isolated them from the lung and set them in culture together with resting T_{MBP} cells in the presence of cognate antigen; indeed, T_{MBP} cells could be activated *in vitro* by the lung-derived APCs and once transferred they were able to induce the disease (*Figure 4*).

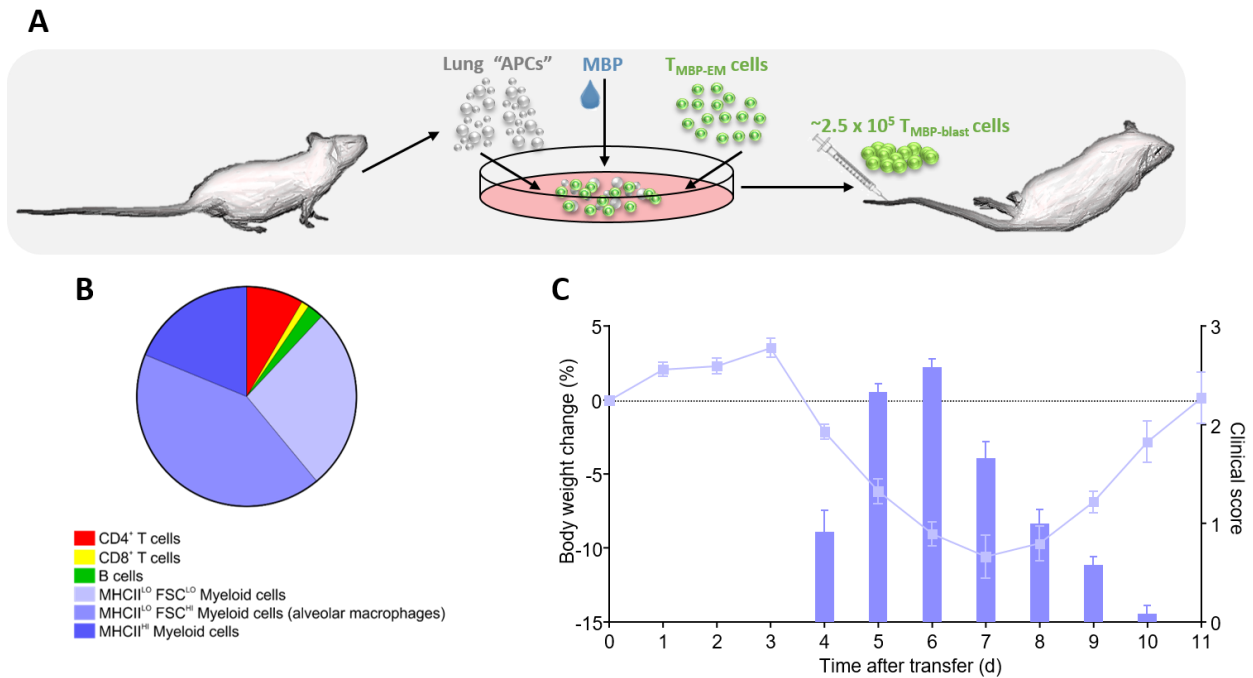


Figure 4. *T_{MBP} cells reactivated in vitro with APCs isolated from the lung are able to trigger a CNS autoimmune disease upon intravenous transfer.* Antigen presenting cells (APCs) isolated from the lung tissue were able, when set in culture, to fully reactivate myelin specific CD4⁺ T effector memory cells in presence of the cognate antigen. Upon intravenous transfer, these fully reactivated T cells triggered in the recipient animals an EAE. **A.** Schematic infographic of the experimental set-up. APCs, antigen presenting cells. MBP, myelin basic protein (here, cognate antigen) T_{MBP-EM}, Effector memory T cells directed against MBP. **B.** Immune cell composition of the lung tissue. Pie chart representing the different immune cell populations found in the lung in matters of their frequency. **C.** Clinical course of EAE induced by intravenous transfer of T_{MBP} cells reactivated *in vitro* with APCs isolated from the lung tissue. Dots connected by lines represent the changes of body weight in matters of percentage. Bars represent the clinical score of EAE. Means ±SEM (standard error of the mean) are represented. n=4. Edited image courtesy of Dr. L. Hosang.

Finally, in order to establish a system where the role of the lung in triggering CNS autoimmunity could be systematically investigated, we transferred naïve recipient animals with resting T_{MBP} cells, and immunised the animals in the lung with the cognate antigen. Upon immunisation, these animals developed a classical paralytic disease (Hosang et al., 2022), similar to the one observed in the transfer set up.

The most striking feature of this lung-induced EAE model was that very low doses of antigen, i.e. 100 to 1000 fold lower than the one used in the classical subcutaneously-induced active EAE, were sufficient to trigger the disease.

These observations indicate that the lung is not just capable but also extremely efficient in triggering CNS autoimmunity.

The main task of the lungs is to supply the organism with oxygen required for the most basic chemical reactions that define life. To do this, the lung tissue has a huge exchange surface of over 100 m² with the inhaled ambient air, which only lately has been acknowledged as a non-sterile environment, colonized by a rich microbiome. The observations made in MS animal models with the epidemiological observations identifying lung infections, inflammatory processes and cigarette smoking as risk factor for MS, together with the lungs' role of providing oxygen to the body and the presence of a lung microbiome, prompted us to investigate the role of the lung environment in the context of CNS autoimmunity. We decided to focus on two unique features of the lung tissue:

- The presence of a distinct lung microbiome.
- The environmental oxygen availability that is higher in the lung than in any other organ

1.3.1 The lung microbiome as moderator of CNS autoimmunity

Humans are colonised by microbial flora at all contact surfaces with the outside world. While the structure and function of the microbiome of the intestine or skin is well understood, it was long assumed that the lungs were sterile, i.e. had no bacterial colonisation at all.

In a recently published work, which I took part of, (Hosang et al., 2022) we were able to determine that the composition of the lung microbiome plays an important role in EAE. We showed that a low dose of locally applied antibiotic, able to alter the composition of the lung microbiome, was sufficient to strongly alter the susceptibility of the CNS to an autoimmune process in animal models for MS.

Searching to explain how changes in the composition of the lung microbiome affect autoimmune processes in the CNS, we excluded T cells, different populations of myeloid cells (resident and circulating) and endothelial cells from the CNS blood vessels as a target of the lung dysbiosis and found the effect to occur directly inside the CNS. Upon local application of antibiotic in the lungs, we described a change in the phenotype of microglial cells of the brain. In the CNS of antibiotic-treated animals, microglial cells showed a lower number of processes, with thicker and shortened ramifications in comparison with non-treated animals. These phenotypic changes of the microglia went along with profound functional changes: the microglia reacted significantly less upon inflammatory stimulations, which resulted in a reduced recruitment of immune cells into the inflamed brain tissue justifying a reduction of the disease strength in antibiotic treatment animals (*Figure 5*).

Furthermore, we identified a compound in the bacterial wall of Gram-negative bacteria, namely lipopolysaccharide – shortly LPS – as the one being responsible for the remote effect observed in microglial cells.

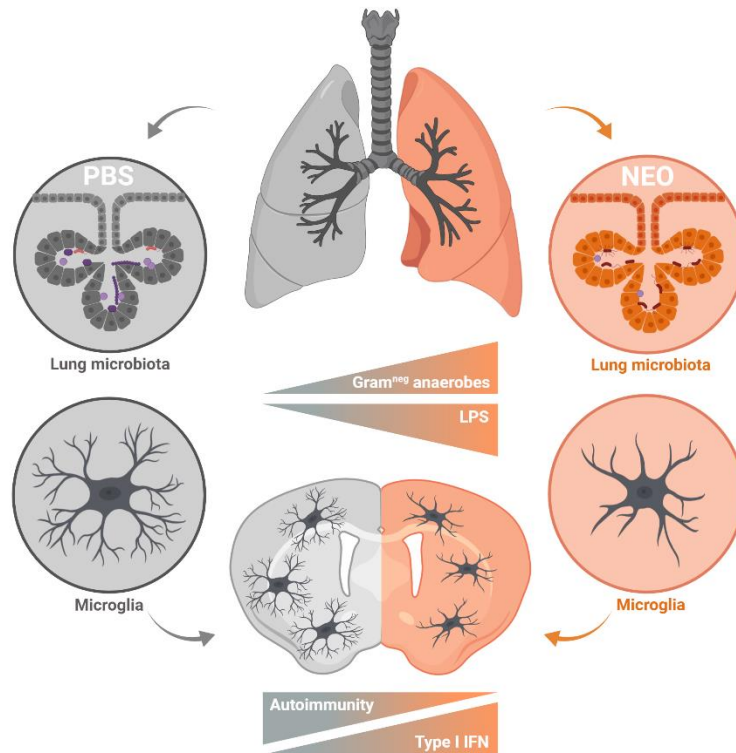


Figure 5. The lung-microbiome regulates CNS autoimmunity by conditioning microglial reactivity. The LPS-producing subset of lung microbiome was identified as modulator of CNS autoimmunity by a distal effect exerted on microglial reactivity. Local treatment in the lung with antibiotics modified the composition of the lung microbiome and showed a protective effect against CNS autoimmunity in a novel EAE model based on the reactivation of myelin directed T cells into the lung. Reproduced from Hosang et al, Nature 2022.

1.3.2 Oxygen levels as regulator factor of the immune response

In the adult human, the lung alveoli represent the largest surface in contact with external environment, covering about 70m² of surface (Holt et al., 2008; Wiebe & Laursen, 1995). Such a broad surface is needed to efficiently fulfil the task of gas exchange that the lung is solely in charge of. Facilitating and allowing the uptake of O₂ by haemoglobin in red blood cells and the release of CO₂ from blood in order to make possible the metabolism of all tissues and systems in the organism, was long thought to be the only function of the lung.

As direct repercussion of the anatomy of mammalian organisms, the oxygen availability within the organism differs significantly from organ to organ and tissue to tissue, the lung and the upper airways being constantly exposed to a higher oxygen tension, which decreases as the vascular system diverges and integrates into the different organs (Michiels, 2004; Semenza, 2003). Moreover, it has been demonstrated by the use of oxygen-sensing probes in laboratory animals, that in healthy conditions certain organs are characterized by a very low oxygen availability within their parenchyma. This is the case of the small intestine but also of several immune organs such as lymph nodes, thymus or spleen

(Braun et al., 2001; Caldwell et al., 2001; Keeley & Mann, 2019; Taylor & Colgan, 2017). This steady state oxygen level can change in altered physiological conditions. Inflammation, for example, is well known to promote a hypoxic environment (Karhausen et al., 2005).

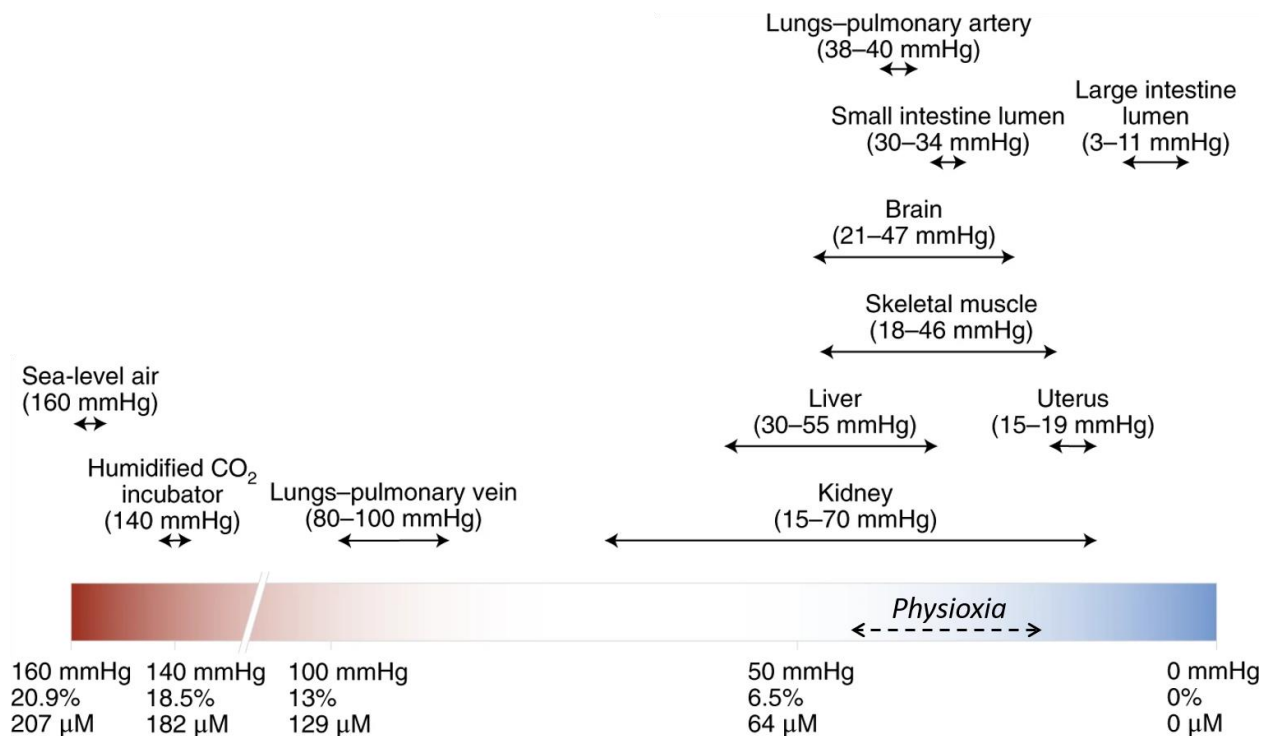


Figure 6. Oxygen tensions in a selection of human tissues in comparison to standard cell culture conditions. Cell culture conditions used in most of research works represent usually a hyper-oxygenated atmosphere to cultured cells reaching levels up to ten times in fold higher than the physiological oxygen tensions reported in living tissues. Adapted from Ast & Mootha, 2019

There are substantial differences between oxygen tension experienced by cells in tissues in a living organism and the cell culture conditions routinely used in the labs. The oxygen tension in room air at sea level or in a humidified incubator are 160 mmHg (20.9%) or 140mmHg (18.5%), respectively, and therefore even higher than the oxygen tension experienced by a cell within the pulmonary vein (100 mmHg, 13%) (Figure 6). These supraphysiological oxygen tensions can affect cell metabolic processes (Prabhakar & Semenza, 2015), generating changes in cell proliferation (Hubbi & Semenza, 2015) and differentiation (Hawkins et al., 2013), among others. Based on these observations, in the last years, several new concepts have emerged such as, physioxia or physiological hypoxia referring to cell culture performed at oxygen conditions, more similar to the ones experienced by a cell embedded in a tissue of the organism. These concepts broke the long established conceptual dichotomy between normoxia and hypoxia (Atkuri et al., 2005; McKeown, 2014; Ast & Mootha, 2019).

In the field of immunology, it has become increasingly clear that oxygen availability shapes the function of both the innate and adaptive immune response modulating immune cell differentiation, function and overall metabolism (reviewed in Krzywinska & Stockmann, 2018). The response to oxygen is orchestrated mainly by the transcriptional regulator hypoxia-inducible factor (HIF), which controls a wide range of oxygen responsive target genes (Krzywinska & Stockmann, 2018; Larbi et al., 2010; Tao et al., 2015; Tripmacher et al., 2008).

Under normoxic conditions, the cytoplasmic prolyl-hydroxylase domain (PHD) proteins catalyze the oxygen-dependent hydroxylation of HIF1 α proteins allowing it to be recognized by the von Hippel-Lindau (VHL) protein, which serves as E3 ubiquitin ligase triggering the degradation of HIF1 α by the proteasome. Under hypoxic conditions, the lack of oxygen available impairs the activity of PHD proteins and non-hydroxylated HIF1 α can bind with HIF1 β . The HIF1 $\alpha\beta$ -heterodimer translocates into the nucleus where it binds to hypoxia responsive elements (HRE) on the DNA and promotes the transcription of hypoxia-induced genes. (Cerychova & Pavlinkova, 2018; Fong & Takeda, 2008; Weidemann & Johnson, 2008).

Regarding T cell biology, it has been demonstrated that culturing T cells under more physiological oxygen concentrations induces numerous changes in T cell properties. Firstly, upon antigen mediated T cell stimulation in 1% to 5% of oxygen environment, T cell proliferation is reduced as compared to a “normoxic” environment (about 21% O₂) (Atkuri et al., 2005, 2007; Larbi et al., 2010; Loeffler et al., 1992; Naldini et al., 1997). This effect was maintained even when a strong mitogenic stimuli (such as CD28 or IL-2) were provided (Clambey et al., 2012) and was due – at least in part – to hypoxia-mediated alterations of the T cell receptor (TCR) signaling via impaired calcium entry (Makino et al., 2003). Secondly, in physiological oxygen conditions, T cell metabolism is shifted towards glycolysis and the redox status of T cells increases, resembling more closely the one observed *in vivo* (Atkuri et al., 2007; Larbi et al., 2010; Tripmacher et al., 2008). Thirdly, also T cell differentiation and effector function are influenced. Indeed, in 5% oxygen conditions, the differentiation of naïve T cells in Th17 cells was accelerated. Furthermore, in similar oxygen conditions, the lytic capacity of CD8⁺ T cells and their cytokine production were increased. Finally, the survival of T cells was also shown to crucially depend on the oxygen conditions (Caldwell et al., 2001). Overall, these *in vitro* data demonstrate the impact of oxygen availability on T cell function, but in addition they imply that T cells are extremely plastic at being able to perform their function within a large range of environmental oxygen conditions. Even in severe hypoxic condition, T cells are still functional.

This capacity of T cells to adapt their function to different oxygen conditions can be of relevance *in vivo*. Here, T cells encounter a wide range of oxygen tensions while migrating through the different

tissues to affect their function. During development, thymocytes are localized in the relatively low oxygen environment (<5 mmHg) of the thymus. Later, mature T cells travel in any organ of the body experiencing oxygen tension ranging from 3 mmHg to 100 mmHg (approx. 0.99% to 13%) (*Figure 8*). In pathological conditions such as inflammation and tumor, T cells can be exposed for prolonged periods to a hypoxic environment. How these different oxygen tensions affect T cell function is poorly investigated even if some evidence comes from the tumor field. Indeed, by using a model of lung metastasis, it has been shown that in the lung the relatively high tension of oxygen determines a local tolerogenic environment restraining inflammatory CD4⁺ and CD8⁺ T cell responses and permitting immunosuppressive T_{reg} cell differentiation. Such oxygen-dependent immunosuppressive pulmonary environment prevents inflammatory responses against innocuous foreign antigens but it fosters tumor colonization (Clever et al., 2016; Deng et al., 2013; McNamee et al., 2013; Westendorf et al., 2017). A further study showed that cytolytic activity and effector functions in CD8⁺ T cells were increased *in vivo* in the hypoxic tumor environment through the activation of the HIF signaling pathway (Doedens et al., 2013).

2. Aims and objectives

The aim of my project was to investigate the role of lung microenvironment in CNS autoimmunity.

Specifically, I tested the hypothesis that a unique characteristic of the lung, namely the presence of an oxygen tension higher in the lung than in any other tissue, could play a role in the capacity of the lung to trigger CNS autoimmunity.

2.1 Impact of *in vitro* hypoxia on T_{MBP} cell properties.

In order to examine the relevance of environmental oxygen tensions on T cell function in the context of CNS autoimmunity, we stimulated T_{MBP} cells *in vitro* under normoxic (20% oxygen) and hypoxic (1% oxygen) conditions and we then evaluated the consequences of these manipulations at several levels.

- At cellular level, by *in vitro* assessing proliferation, cell viability and effector functions.
- At transcriptomic level, by performing a systematic transcriptome study in order to tie down the changes in the gene expression triggered by the hypoxic stimulus in the context of T_{MBP} reactivation at different time points upon antigen encounter.
- At clinical level, by testing the encephalitogenic potential of T_{MBP} cells stimulated *in vitro* under hypoxic conditions in the context of transfer EAE.

2.2 Impact of whole-body hypoxia on EAE

To investigate whether the oxygen tension present in the lung can affect CNS autoimmunity, we induced active EAE via intra-tracheal immunization in animals previously transferred with T_{MBP} cells. We then exposed the animals to whole body hypoxia (10% oxygen) during the phase of T_{MBP} cell activation in the lung. Finally, we evaluated the consequences of these manipulations at several levels.

- At cellular level, by assessing *ex vivo* T_{MBP} cell proliferation and effector functions.
- At clinical level, by testing the encephalitogenic potential of T_{MBP} cells stimulated *in vivo* in hypoxic conditions in the context of active EAE induced via the lung.

3. Material and Methods

3.1 Materials

3.1.1 Media and buffers

Unless otherwise indicated, all buffers were prepared with water purified with a Mili-Q purification system (Merck, Germany).

Phosphate buffered saline (10x PBS)	8.1 mM	Na ₂ HPO ₄ (Roth, Germany)
	1.47 mM	Na ₂ H ₂ PO ₄ (Roth, Germany)
	137 mM	NaCl (Roth, Germany)
	2.68 mM	KCl (Roth, Germany)
		adjusted to pH 7.2 - 7.4 with HCl (Roth, Germany)
Ammonium-chloride-potassium	150 mM	NH ₄ Cl (Roth, Germany)
	1 mM	KHCO ₃ (Roth, Germany)
	0.1 mM	Na ₂ xEDTA (Roth, Germany)
		adjusted to pH 7.2 - 7.4 with HCl (Roth, Germany)
Dulbecco's Modified Eagle Medium	13.4 g /l	DMEM Powder (Thermo Fisher Scientific, USA)
	3.72 g /l	NaHCO ₃ (Roth, Germany)
Eagle's HEPES medium (EH)	75%	DMEM
	25%	HEPES 1M (Thermo Fischer Scientific, USA)
T cell medium (TCM)	950 ml	DMEM
	10 ml	Penicillin/Streptomycin (Thermo Fisher Scientific,
	10 ml	Sodium Pyruvate (Thermo Fisher Scientific, USA)
	10 ml	L-Asparagine monohydrat (Sigma-Aldrich, Germany)
	10 ml	L-Glutamine (PAN Biotech, Germany)
	10 ml	Non-Essential Aminoacids (Thermo
	4 µl	β-Mercaptoethanol (Roth, Germany)
Re-stimulation Media (RM)	99%	TCM
	1%	Rat serum (in house production)
T cell growth factor medium (TCGF)	88%	TCM
	10%	Horse serum (Merck, Germany)
	2%	IL-2 containing supernatant
FACS buffer	2 mM	Na ₂ xEDTA (Roth, Germany)
	0.5%	Albumin Fraction V (Roth, Germany) in 1x DPBS (-Ca ²⁺ -Mg ²⁺)

Freezing medium (FM)	80%	Horse serum (Merck, Germany)
	10%	TCM
	10%	Dimethylsulfoxid, DMSO (Roth, Germany)
Thawing medium (TM)	90%	EH
	10%	Fetal calf serum (Merck, Germany)
Isotonic percoll (Isopercoll)	90%	Percoll (Cytivia USA)
	10%	10x PBS
Underlying percoll	7 ml	Isotonic percoll (Isopercoll)
	3.9 ml	1x PBS
ELISA blocking buffer	5%	BSA in 1xPBS
ELISA washing buffer	0.05%	Tween20 (Roth, Germany) in 1xPBS

3.1.2 Reagents, chemicals and sera

<u>Reagent</u>	<u>Source</u>
Albumin Fraction V	Roth, Germany
APC beads (BD Calibrite)	BD Biosciences, USA
β -mercaptoethanol	Roth, Germany
Collagenase from C.Hystolyticum	Merck, Germany
Chloroform	Roth, Germany
Diethylether	Roth, Germany
Dimethyl Sulfoxide (DMSO)	Roth, Germany
DMEM powder	Thermo Fisher Scientific, USA
DNase	Roche, Switzerland
DPBS (10x) without CaCl ₂ and MgCl ₂	Thermo Fisher Scientific, USA
Fetal Calf serum	Merck, Germany
Glycogen	Roche, Switzerland
Glycoblue coprecipitant	Thermo Fisher Scientific, USA
G-418 sulfate solution	Capricorn Scientific, Germany
HEPES	Thermo Fisher Scientific, USA
Horse serum	Merck, Germany
Hydrochloric acid (HCl)	Roth, Germany
Incomplete Freund's Adjuvant (IFA)	BD Biosciences, USA
Recombinant Rat Interferon γ	Preprotech, Germany
Isopropanol (2-Propanol)	Roth, Germany
Lymphocyte separation medium 1077 (LSM1077)	PromoCell, Germany
Ketamine	Medistar, Germany
Paraformaldehyde	Roth, Germany
TRI-Reagent	Merck, Germany
Trypsin EDTA solution (10x)	Merck, Germany

qPCR Martermix	Eurogentec, Belgium
Xylazine	Echuphar, Belgium
Nuclease-free water	Thermo Fisher Scientific, USA
Percoll	Cytivia, Sweden
Rat serum	In house production
eBioscience FoxP3/transcription factor staining.	Thermo Fisher Scientific, USA
BD Perm/Wash 10x Buffer	BD Biosciences, USA
Pimonidazole HCl	Hypoxyprobe, USA

3.1.3 Antigens and adjuvants

<u>Product</u>	<u>Specifications</u>	<u>Source</u>
Myelin Basic Protein (MBP)	Isolated from guinea pig's brains	In-house production
Ovalbumin (OVA) from chicken egg white	None	Merck, Germany
DQ-OVA	None	Thermo Fisher Scientific, USA
Complete Freund's Adjuvant	40 mg M. tuberculosis H37Ra	BD Biosciences, USA
	10 ml Incomplete Freund's Adjuvant	BD Biosciences, USA

3.1.4 Antibodies

<u>Antigen</u>	<u>Antibody</u>	<u>Fluorochrome</u>	<u>Clone</u>	<u>Dilution</u>	<u>Producer</u>
$\alpha\beta$ TCR	Mouse IgG1 anti-rat	AF647	R73	1:200	BioLegend, USA
CD4	Mouse IgG1 anti-rat	PE/Cy7	W3/25	1:200	BioLegend, USA
CD8a	Mouse IgG1 anti-rat	PerCP	OX-8	1:200	BioLegend, USA
CD25	Mouse IgG1 anti-rat	PE	OX-39	1:200	BioLegend, USA
OX40	Mouse IgG2b, κ anti-rat	BV421	OX-40	1:200	BD Biosciences, USA
FOXP3	Mouse IgG1, κ anti-mouse/rat/human	PE	150D	1:200	BioLegend, USA
IFN γ	Mouse IgG1, κ anti-rat IFN γ	PE	DB-1	1:200	BioLegend, USA
IL17a	Rat IgG1, κ anti-mouse IL17A	BV421	TC11-18H10.1	1:200	BioLegend, USA
None	Mouse IgG1 κ Isotype ctrl	PE	MOPC-21	1:200	BioLegend, USA
None	Mouse IgG2b Isotype ctrl	BV421	MPC-11	1:200	BD Biosciences, USA
None	Rat IgG1, κ Isotype ctrl	BV421	R3-34	1:200	BD Biosciences, USA
HP1	Mouse IgG1 mAb conjugated	ATTO 594		1:200	Hypoxyprobe, USA

3.1.5 Q-PCR primers

<u>Gene (Abbreviation)</u>		<u>Sequence</u>
β actin	Forward (5'-3')	GTA CAA CCT CCT TGC AGC TCC T
	Reverse (3'-5')	TTG TCG ACG ACG AGC GC
	Probe: FAM- 5'-3'-TAMRA	CGC CAC CAG TTC GCC ATG GAT

rat IFN γ	Forward (5'-3') Reverse (3'-5') Probe: FAM- 5'-3'-TAMRA	AAC AGT AAA GCA AAA AAG GAT GCA TT TTC ATT GAC AGC TTT GTG CTG G CGC CAA GTT CGA GGT GAA CAA CCC
rat IL17A	Forward (5'-3') Reverse (3'-5') Probe: FAM- 5'-3'-TAMRA	GAG TCC CCG GAG AAT TCC AT GAG TAC CGC TGC CTT CAC TGT ATG TGC CTG ATG CTG TT
rat FoxP3	Forward (5'-3') Reverse (3'-5') Probe: FAM- 5'-3'-TAMRA	TGG CAA ACG GAG TCT GCA A TCT CAT CCA AGA GGT GAT CTG CTT AGC CGG GAG AGT TTC TCA AGC ACT GC

3.1.6 Kits

<u>Kit</u>	<u>Producer</u>
RevertAid First Strand DNA Synthesis kit	Thermo Fisher Scientific, USA
Rat IFN- γ Standard ABTS ELISA Development Kit	PreproTech, Germany
Rat IL17a ELISAMAX™ Deluxe Set	BioLegend™, USA

3.1.7 Equipment and consumables

3.1.7.1 Equipment

<u>Equipment</u>	<u>Source</u>
Cryobox	Nalgene, USA
Metal cell strainer (100 μ m)	UMG technical workshop,
Multichannel micropipette 30-300 μ l	Starlab, Germany
Pipettes (1; 2.5; 10; 20; 100; 200;	Eppendorf, Germany
Pipettus	Hirschmann, Germany
Rat intubation stack	UMG technical workshop,
Small animal laryngoscope	Penn Century, USA
Small animal laryngoscope LS-2	Penn Century, USA
Surgical instruments	Fine surgical tools (FST), Germany
Tuberculin glass syringes	Poulsen & Graf, Germany

3.1.7.2 Consumables

<u>Item</u>	<u>Source</u>
Cannulas (18G, 20G, 24G, 26G)	B. Braun, Germany
Cell culture plates (6-, 12-, 24-, 96-)	Thermo Fisher Scientific, USA

Cell strainers (40, 70, 100µm)	Greiner Bio-One, Austria/Germany
Conical centrifuge tubes (15, 50mL)	Greiner Bio-One, Austria/Germany
FACS tubes	BD Biosciences, USA
gentle MACS C Tubes	Miltenyi Biotec, Germany
Parafilm	Pichiney Plastic Packaging, USA
Petri dishes	Greiner Bio-One, Austria/Germany
Pipette filter tips (10, 20, 100, 200, 1000µL)	StarLab, Germany
Pipette tips (10, 20, 100, 200, 1000µL)	StarLab, Germany
qPCR plates	StarLab, Germany
Reaction tubes (0.2, 1.5, 2mL)	Sarstedt, Germany
Surgical suture	B. Braun, Germany
Syringes	B. Braun, Germany
Winged catheter (18G)	B. Braun, Germany

3.1.8 Instruments and machines

Item	Source
Cytoflex S	Beckman-coulter, USA
FACS-AriaII ASORP	BD Biosciences, USA
gentleMACS dissociator	Miltenyi Biotec, Germany
Heracell™ 240cell culture incubator	Thermo Scientific, USA
InvivoO2 I400 hypoxia workstation	Baker-Ruskin, USA
Laminar flow hood HERA safe KSP	Thermo Scientific, USA
Microcentrifuge 5418 R	Eppendorf Germany
Small animal laryngoscope	Penn Century, USA
Sorvall Heraeus multifuge 1 S-R	Thermo Scientific, USA
StepOne Plus RT-PCR system	Applied Biosystems, USA
Sunrise Plate reader system	Tecan, USA
T100™ Thermal Cycler	BioRad, United Kingdom
Tissue chopper	Mcllian, USA

3.1.9 Software

Microsoft Office (2010, 2016)	Microsoft, USA
StepOnePlus Software (Version 2.0)	Applied Biosciences, USA
R (version 3.6.0)	R Core Team
R Studio	Rstudio, USA
DAVID Bioinformatics Resources (2021 Update)	NIAID/NIH
GraphPad Prism (version 8)	GraphPad, USA
FlowJo (version 10)	BD Biosciences, USA
FACSDiva Software (version 8.0.1)	BD Biosciences, USA

3.2 Methods

3.2.1 Animals

Wild-type (wt) rats on a Lewis (LEW/Crl) background (*Rattus norvegicus*) were bred at the animal facility of the University Medical Centre Gottingen (UMG, Germany). The animals were kept in GR 9000 IVC (individually ventilated cages) under specific pathogen-free (SPF) conditions on a 12-hour light-dark cycle and ad libitum access to food and drink. No differences in experimental outcome were noted between sexes. All experiments were performed in accordance with the local regulations.

3.2.2 Generation and culture of primary T cell lines

Rat CD4⁺ T cells reactive against myelin basic protein (MBP) engineered with a retroviral system to express green fluorescent protein (GFP) were generated as previously described (Flügel et al., 1999b; Kawakami et al., 2005; Lodygin et al., 2013). Shortly, 6 to 8 weeks old female wild type Lewis rats were subcutaneously immunised with a 1:1 emulsion of complete Freund adjuvant (CFA) containing *Mycobacterium tuberculosis* extract (BD Biosciences, USA) at a concentration of 1mg/ml (final concentration) and MBP at a 0,5mg/ml concentration (final concentration) under short-lasting diethyl ether anaesthesia. The immunization emulsion was directly prepared inside the tuberculin glass syringes (Poulten & Graf, Germany) used for the injection. A total of 150µl was injected at the base of the tail (50µl each side) and into the popliteal cavities (25µl each side). Nine days after subcutaneous immunisation the animals were euthanized by CO₂ asphyxiation and the draining lymph nodes (popliteal, inguinal and paraaortic) were isolated, retrieved and mashed through a 100µm sterile metal cell strainer. The lymph node's cell suspension was co-cultured with GP+E86 packaging cell lines producing replication-deficient retroviruses carrying a Neomycin G-418 resistance cassette.

Prior to the co-culture establishment, the packaging cells were previously expanded in 75mm² cell culture flasks in T cell media (TCM) containing 10% FCS at 5% CO₂ and 37°C. Afterwards, the GP+E86 cells were suspended in restimulation media (RM) and plated in 96-well U-bottom plates at a concentration of 1.5 x10⁶ cells per plate. At least five hours later, the lymph node cell suspension was added to the GP+E86 cells in each well at a concentration of 20 x10⁶ cells per plate. Antigen was then added to a final concentration of 20µg /ml. Cells were cultured at 10% CO₂ and 37°C for 48 hours, prior to the addition of 50µl of T cell growth factor media (TCGF) per well. One to two days after TCGF addition, cells were transferred to 96-well flat-bottom plates and negative T cell selection was started by supplementing the culture media with G-418 to a final concentration of 0.4mg/ml.

Seven days (D7) after the initial *in vitro* stimulation, T cells were re-challenged with the cognate antigen (first restimulation). For this purpose, 100µl of supernatant was carefully removed in each

well and substituted with 100µl of fresh RM containing 1.4×10^6 irradiated (30Gy) rat thymocytes, serving as antigen presenting cells (APCs), 10µg/ml of MBP and 0.4mg/ml of G-418. Two days later, 50µl/well of TCGF supplemented containing G-418 were added to each well. The day after, T cells were selected according to the confluence reached in each well and their fluorescence brightness and pooled into 10cm cell culture dishes. Seven days after this first restimulation, T cells were again challenged with MBP at a 10µg/ml concentration (second restimulation) in presence of irradiated rat thymocytes at a 20 to 1 ratio (20 thymocytes per counted T cell). This seven-day restimulation cycle could be repeated up to the 6th restimulation. After the 2nd restimulation, T cells could be frozen and stored in liquid nitrogen. For that purpose, T cells in a resting state (day 5 or 6 after antigen encounter) were counted and centrifuged at 300 RCF and 4°C for 6 minutes, resuspended in freezing medium (FM) and aliquoted into freezing vials in volumes of 1.5ml per vial. The freezing vials were cooled down to -80°C into freezing boxes (Cryobox, Nalgene, USA) before being transferred for long term into liquid nitrogen storage system.

3.2.3 T cell culture under hypoxic conditions

Prior to each cell culture experiment, T_{MBP} cells were thawed in pre-warmed Thawing medium (TM) at 37°C, spun down for 6 minutes at 4°C and 300 RCF; then counted and resuspended at the required concentration. For the culture of T cells under hypoxic conditions, an InvivoO2 I400 workstation (Baker Ruskin, USA) system set at 1% O₂, 5% CO₂, 37°C of temperature and 65% of relative humidity was used. The control (normoxic) group for hypoxic restimulation experiments was kept in a normal cell culture incubator under 5% CO₂ conditions.

3.2.4 Experimental autoimmune encephalomyelitis (EAE)

Transfer EAE

Transfer EAE (tEAE) was induced in naïve recipient Lewis rats with aged between 8 to 10 weeks. Animals were shortly anaesthetised with diethyl-ether and intravenously transferred with either 2×10^6 or 0.25×10^6 T_{MBP} cell blasts (2nd day after *in vitro* antigen encounter). After transfer, clinical score and body weight changes were registered on a daily basis.

Lung active EAE

Lung EAE was induced as recently described (Hosang et al., 2022). Shortly, naïve animals aged 7 to 10 weeks were injected intravenously with 7.5×10^6 resting T_{MBP} cells (five or six days after antigen encounter) under short-lasting diethyl-ether anaesthesia. 4 hours after that, the animals were immunised into the lung with an emulsion consisting of equal parts of guinea pig MBP at a 20 µg /ml (cognate antigen) in CFA containing 200 µg /ml of *Mycobacterium tuberculosis* H37Ra extract in mineral oil. For the immunisation procedure, the rats were fixed on a stand in upright position and

slightly leaning backwards (at 70° in relationship with the operating table). 100 µl of emulsion per each 300 g of body weight were instilled in the trachea, previously located with the help of a veterinary laryngoscope for small animals (Penn Century, USA) through an 18G flexible winged catheter. The complete procedure lasted typically about one minute per animal. After immunisation, clinical score and body weight changes were registered on a daily basis.

EAE Clinical scoring

The severity assessment of EAE semiology was done using a 0 to 5 scoring scale, where 0 corresponds to no neurological affection and 5 relates to a moribund state. The detailed scale is described in the table that follows:

Score	EAE signs
0	No neurological affection
1	Tail paralysis
2	Ataxia
3	Hind limb paralysis
4	Tetraparesis
5	Moribund state

Disease states located in between two grades of the scale were given a score of +0.5 complementing the last fulfilled scale-step.

In some experimental set-up (specified in the text), animals developed an atypical clinical course. In such circumstances, one point was given for every completely fulfilled category in the previous table and 0.5 scoring points were given for partially affected criteria.

3.2.5 Exposition to whole body hypoxia

For the *in vivo* hypoxia experiments, the cage used for the regular housing of the animals was placed without lid into a in house-built hypoxia station made out of methacrylate planks, sealed together to prevent atmosphere exchange. The gradual establishment of the final atmosphere containing 10% O₂ was achieved within the first 30 minutes of exposure. Afterwards, the oxygen composition of the atmosphere inside the hypoxia station was kept constant for the period contemplated in the experimental design. After the selected time, animals were brought back to room air and housed as regular.

To achieve proper atmosphere control, the set up was equipped with a ProOx360 Unit atmosphere control unit (BioSpherix, USA). The ProOx360 unit is equipped with an oxygen sensor inserted into the wall of the hypoxia station. The ProOx360 incorporates an integrated gas injection system, used to

pump Nitrogen gas into the hypoxia station until the set atmosphere is achieved. A silent fan is integrated into the construction of the hypoxia station in order to guarantee the equal composition of the generated atmosphere.

3.2.6 Organ retrieval and processing

Euthanasia and perfusion

Animals were euthanized by subcutaneous injection of a lethal dose of ketamine/xylazine, i.e. 150 mg /Kg ketamine (Ecuphar, Germany) combined with 30 mg /Kg xylazine (Medistar, Germany) and transcardially perfused with ice cold 1x PBS containing heparin at a final concentration of 10000 IU /l. After perfusion, the organs of interest were isolated and processed for cytofluorimetric analysis as it follows:

Blood

Blood samples were drawn by heart puncture in syringes previously moistened with 80 mM EDTA solution after euthanasia and before the perfusion procedure began. The volume of retrieved blood (commonly between 3.5 and 5 ml in adult rats) was combined with the same volume of room temperature 1x PBS in a 15ml conic bottom tube. Half of volume of blood of Lymphocyte separation medium LSM1077 (Promocell, Germany) was carefully underlayered to the blood-PBS mix and a density gradient separation was run in a centrifuge for 30 minutes at room temperature and 800 RCF, with low acceleration and no brake. After the centrifugation, the cloudy interface containing lymphocytes was retrieved with a 1 ml pipette and washed with 1x PBS into a new tube. Finally, the sample was spun down for 6 minutes at 300 RCF and 4°C, the supernatant was sucked up and the cell pellet taken up in the required amount of Eagle's-HEPES (EH) medium and kept on ice.

Lungs

After perfusion, lungs were dissected at the bronchi level and chopped into 1mm cubes with a tissue chopper (McIllian, USA). Chopped up lungs were washed with cold EH medium in a gentleMACS C-tubes (Miltenyi Biotec, Germany). After a standard spin down (SSD) for 6 minutes at 4°C and 300 RCF, the washing medium was discarded and the samples were digested by adding 2 ml of 0.03% Collagenase IV from *Clostridium histolyticum* (Sigma-Aldrich, Germany) in 1x PBS. The samples were then processed with gentleMACS (Miltenyi biotech, Germany) tissue dissociator (program Multi_C_01 run for two times in each sample), incubated for 30 minutes at 37°C while shaking and finally submitted to the program Multi_C_02 of the gentleMACS system. After that, the digested lungs were washed with 1xPBS and sequentially filtered through 100µm and 70µm cell strainers (Grenier-bioOne, Germany). After SSD, the supernatant was discarded, the cell pellet resuspended in 5ml 40% Percoll

solution in a 15 ml conical bottom tube and 5ml of 70% Percoll solution were carefully underlayered with the help of a long hard cannula (70 mm 20 G) attached to a 5ml syringe. A density gradient was run at 4°C, 800 RCF for 30 minutes at the minimum acceleration and without breaks. The lymphocyte rich interphase was retrieved and washed in 1x PBS to be finally taken up in the required amount of EH medium supplemented with EDTA, typically 1 ml.

Spinal cord

Spinal cord from perfused animals was carefully dissected and the surrounding meninges were removed prior to mash the tissue through a 100µm metallic mesh. The mashed spinal cord tissue was adjusted to a final volume of 15ml of EH medium and 5ml of isopercoll solution were added to the tube. The samples were gently mixed by inversion and a density gradient was run at 4° and 1600 RFC for 30min, at the minimum acceleration and without breaks. The upper layer containing myelin was removed, the supernatant was discarded and the pellet containing single cells was resuspended and washed in 1x PBS to be finally taken up in the required amount of EH medium supplemented with EDTA, typically 500µL.

Spleen

After perfusion, the spleen was isolated, mashed through a 100µm metallic mesh and the resulting cell suspension was washed one time in 1xPBS and spun down. The supernatant was then removed and the pellet was resuspended in 3 ml of ammonium-chloride-potassium (ACK) buffer for removing the erythrocytes. After 3 minutes on ice, the reaction was stopped by adding 20 ml ice-cold 1xPBS and spun down. Supernatant was then discarded and the cell pellet resuspended in the required amount of EH-medium supplemented with EDTA, typically 5 ml.

Lymph nodes

After perfusion, lymph nodes were dissected, mashed through a 70µm cell strainer (Grenier-bioOne, Germany), washed in EH-medium and spun down. The cell pellet was then resuspended in the required amount of EH-medium supplemented with EDTA, typically 500 µl.

3.2.7 Fluorescence activated cell sorting (FACS)

Staining

FACS staining was performed, if else not indicated, in a V bottom 96-well plate. The list of antibodies used within the context of this work for FACS-staining can be find under the section 3.1.4.

Staining of surface markers

For the surface staining, the samples were washed one time with cold FACS buffer and then taken up in a cocktail of the required fluorescently labelled antibodies (1:200 dilution) in FACS buffer. Samples were stained for 30 minutes on ice and protected from light. After that, samples were washed once in FACS buffer and taken up in the wished volume of FACS buffer prior to the analysis.

In case that a two-step staining was needed, an additional step of washing with ice-cold FACS buffer was added in between of incubations with antibodies.

Intracellular staining for cytokine production

Prior to the staining, samples were stimulated or not with 1 µg /ml Phorbol 12-myriylate 13-acetate (PMA)(Sigma-Aldrich, Germany) and 5 µM ionomycin calcium salt (Sigma-Aldrich, Germany) in RM for 30 min in a cell incubator at 37°C. Brefeldin A (Sigma-Aldrich, Germany) at a concentration of 5 µg /ml was then add to block cytokine secretion for two hours. If required, the sample were stained for surface markers as above and then fixed in a solution of 2% Paraformaldehyde (PFA) on ice for 20 minutes, protected from light. After fixation, samples were washed three times with 200µL of 1x PBS each prior to permeabilisation with 200 µl of BD Fix/Perm (BD Biosciences, USA) working solution containing 10% of rat serum. Samples were incubated in permeabilisation buffer for 30 minutes, on ice and protected from light. After the permeabilisation step, samples were spun down and incubated with a mix of the required antibodies prepared in permeabilisation buffer for at least 30 minutes, on ice and protected from light. Finally, the samples were washed once in permeabilisation buffer and finally taken up in the volume of FACS buffer required for the analysis.

Intranuclear staining for transcription factors

If required, the sample were stained for surface markers as above, and then fixed in FoxP3 Fixation/Permeabilisation working solution (eBiosciences, USA) for 20 minutes, on ice and protected from light. After that, cells were washed once with 1x FOXP3 Permeabilisation buffer (eBiosciences, USA) containing 5% of rat serum, taken up in the permeabilisation buffer containing the required intranuclear antibody and incubated on ice and protected from light for at least 30 minutes. After the incubation time with the antibody, all samples were washed once with the permeabilisation buffer and finally taken up in the volume of FACS buffer required for the analysis.

FACS cell counting

Prior to FACS analysis, and in order to prevent clogging of the FACS instrument, all samples were filtered through a filtered-cap conical FACS tube (BD biosciences, USA). A known volume of beads suspension containing BD calibrate beads (BD biosciences, USA) in 1xPBS at a known concentration

was added to each sample immediately before acquisition in order to make possible cell quantification.

FACS cell sorting

Prior to FACS cell sorting and in order to prevent clogging of the FACS instrument, all samples were filtered through a filtered-cap conical FACS tube (BD biosciences, USA). Cells were sorted by using a FACS- AriaII SORP system (BD Biosciences, USA) which allowed keeping sorted samples at 4°C during the procedure. Sorted cells were retrieved in 5ml conical-bottom FACS tubes (BD biosciences, USA) coated with cell culture medium supplemented with serum containing 500 µL of EH-medium. Cell purity was assessed for each sample. Immediately after sorting, the samples were transferred to 1.5 ml centrifuge tubes (Eppendorf, Germany) spun down, resuspended in the required amount of TRI-Reagent (Sigma-Aldrich, Germany) and stored at -80°C until RNA extraction was performed.

3.2.8 RNA isolation and cDNA conversion

RNA from sorted cells or total tissue samples, preserved in TRI-Reagent (Sigma-Aldrich, Germany) at -80°C, was extracted by phase separation with chloroform followed by isopropanol precipitation according to manufacturer's instructions. The RNA pellet was then solubilized in 12µL of RNase-free water (Thermo Fisher Scientific, USA) and stored at -80°C until cDNA conversion.

Reverse transcription of the RNA samples into cDNA was performed with the RevertAid First Strand cDNA synthesis kit (Thermo Fisher Scientific) according to manufacturer's instructions

3.2.9 Quantitative real time PCR

To perform quantitative PCR (qPCR) cDNA from Total Tissue samples was diluted in Nuclease-free water (Thermo Fisher Scientific, USA) at a 1:30 ratio. qPCR was performed on a StepOnePlus Real-Time PCR system (Applied Biosystems, USA) with target-specific TaqMan probes labeled with FAM and quenched with TAMRA.

Rat-beta actin transcript (β -actin) was used as a house-keeping gene. All measurements were performed in duplicates and the difference in the CT values between the individual values did not exceed 0.5 amplification cycles. The sequences of primers and probes used are listed in section 3.1.5.

3.2.10 Enzyme-linked immunosorbent assay (ELISA)

Cell culture supernatant was frozen at -80°C at the time of harvest. Later on, the ELISA method was used to quantify the amount of cytokine present in the samples according to the manufacturer's

protocols. Briefly, Nunc™ MaxiSorp™ 96 well-ELISA plates (Thermo Fisher, USA) were coated overnight with capture antibody diluted in 1x PBS. The next day, the samples were thaw and diluted in ELISA blocking buffer (see table). Unbound capture antibody was removed from the plate. The plate was then washed three times with ELISA washing buffer, and triplicate samples were plated and incubated for 2 hours. Afterwards, the plate was washed three times with washing buffer prior to the addition to each well of detection antibody, diluted in blocking buffer, which was incubated for two more hours. Plates were then washed with washing buffer three times and Avidin-HRP conjugate was added to each well and incubated at room temperature for 30 minutes. After that, the plate was washed three times with washing buffer and ABTS liquid substrate was added to each well. Optical density (OD) of each well was measured at 405nm with wavelength correction set at 650nm by a Sunrise plate reader (Tecan, Switzerland)

3.2.11 Next generation sequencing

Transcriptome analysis using next generation sequencing (NGS) of T_{MBP} cells sorted at different times after antigen encounter under either normoxic or hypoxic cell culture conditions was performed at the Transcriptome and Genome Analysis Laboratory (TAL) of the University Medical Center Göttingen (UMG) under the supervision of Dr. Gabriela Salinas. Sequencing data analysis was performed by Dr. Orr Shomroni.

Additional statistical analysis and graphical depiction was performed by Michael Haberl and myself by using Microsoft Excel (2010, 2016; Microsoft, USA) and GraphPad Prism (V8; GraphPad, USA). Principle component analysis (PCA), gene set enrichment analysis (GSEA) and hierarchical clustering analysis were performed using R (V3.6.0; R Core Team). Biological processes Gene Ontology (GO) term enrichment analysis, as well as pathway enrichment analysis was performed using DAVID (V6.8; LHRI, USA).

3.2.12 Treatment, analysis and statistical analysis of the data

Flow cytometric data were analysed by using the softwares FlowJo™ v10 (BD Biosciences, USA) and CytExpert v 2.4 (Beckman-Coulter inc., USA).

Statistical analysis were performed by using the software GraphPad Prism (V8; GraphPad, USA). ANOVA test was used to compare parametric variables among three or more groups, Tukey's correction for multiple samples was apply when applicable. To compare means between unpaired groups with an assumption of unequal variance between sample sets, the independent t-test was used. P values less than 0.05 were considered to indicate statistical significance.

4. Results

4.1 Environmental oxygen conditions affect T_{MBP} cell proliferation

In order to assess the effect that a hypoxic environment may have on T cell function we started by assessing its effects on the antigen-driven proliferation of $T_{effector\ memory}$ (T_{EM}) cells. To this end, T_{EM} cells expressing green fluorescent protein, GFP, and directed against myelin basic protein, MBP (T_{MBP} cells), were plated together with irradiated thymocytes (serving as antigen presenting cells, APCs). T_{MBP} cells were stimulated with different doses of the cognate antigen, (MBP, 10 $\mu\text{g/ml}$, 1 $\mu\text{g/ml}$ or 0.1 $\mu\text{g/ml}$) or a non-cognate antigen, namely chicken ovalbumin (OVA, 10 $\mu\text{g/ml}$), serving as control. T_{MBP} cells were then cultured for 48 hours under the following environmental conditions: 1) normoxic (approx. 20% O_2) conditions (48N); 2) hypoxic (1% O_2) conditions (48H); 3) 24 hours in hypoxic conditions followed by 24 hours in normoxic conditions (24H+24N); and 4) 24 hours in normoxic conditions followed by 24 h in hypoxic conditions (24N+24H). An infographic illustrating the experimental design is depicted in *Figure 7*.

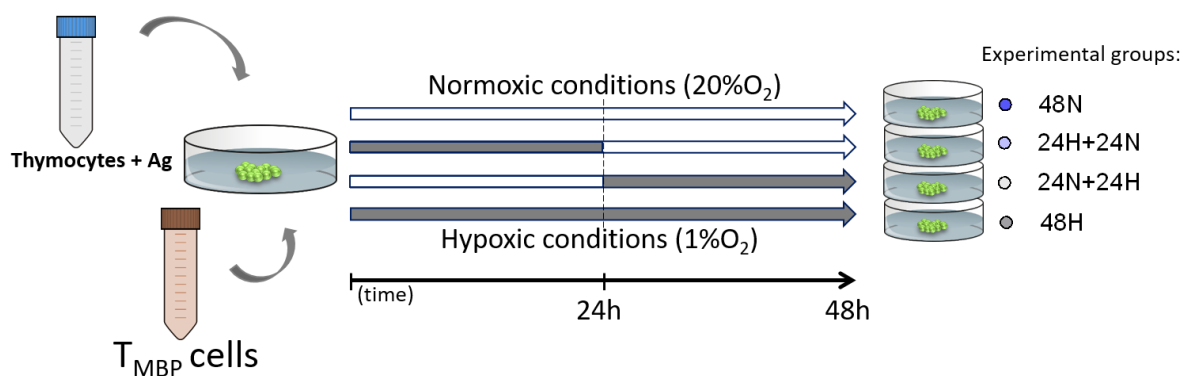


Figure 7. Experimental design for the *in vitro* set up. Resting T_{MBP} cells were cultured for 48 hours with thymocytes serving as APCs in presence of different doses of the cognate antigen (MBP) or non-cognate antigen (OVA) in different experimental conditions. 48N: normoxic environment for 48 hours; 48H: hypoxic conditions for 48 hours; 24N+24H: 24 hours in normoxic conditions followed by 24 hours in hypoxic conditions; 24H+24N: 24 hours in hypoxic conditions followed by 24 hours in normoxic conditions.

After 48 hours upon antigen encounter, the number of T_{MBP} cells was measured by FACS (*Figure 8*). Under optimal antigen concentration (10 μg MBP/ml), T_{MBP} cell proliferation was reduced by 60 to 70% in the group submitted to hypoxic conditions for 48 hours (48H) in comparison with the control group kept in normoxic conditions (48N). A similar trend (two-fold reduction) in relation to the controls was observed in T_{MBP} cells cultured for 24 hours in normoxic conditions followed by 24 hours

in hypoxia (24N+24H). In contrast, T_{MBP} cells cultured for 24 hours in hypoxia followed by 24 hours in normoxia (24N+24H) behaved similarly to the control group.

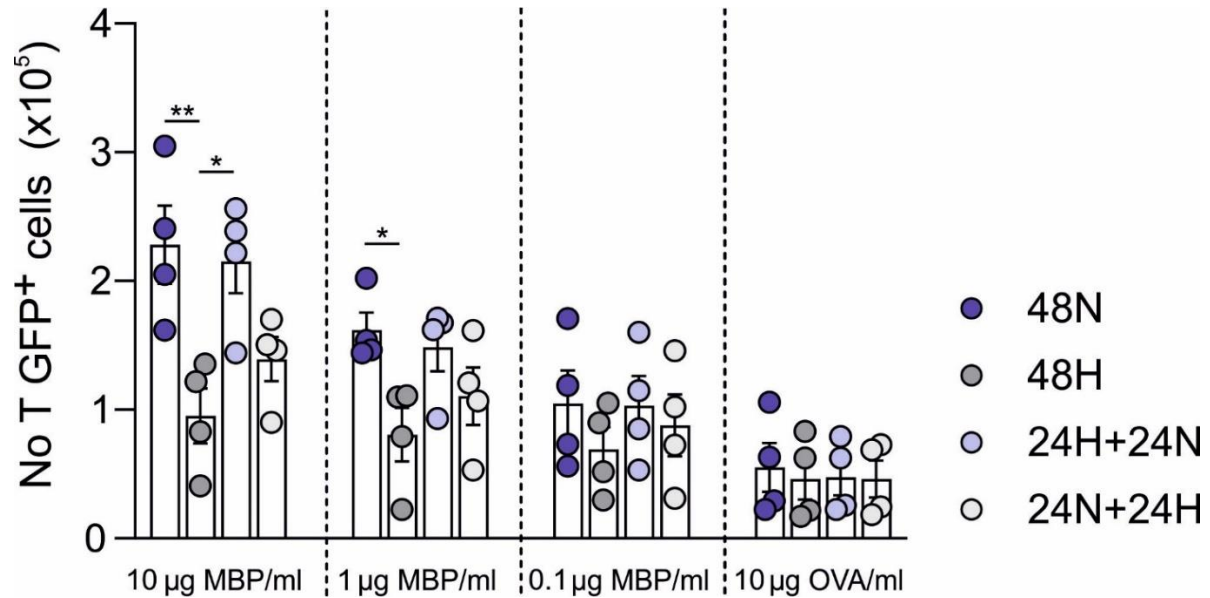


Figure 8. An oxygen-deprived environment reduces the number of T_{MBP} cells retrieved after antigen stimulation. Number of T_{MBP} cells quantified by flow cytometry 48 hours after exposure to the indicated doses of antigens in the indicated environmental conditions. 48N, 48 hours in normoxic environment; 48H, 48 hours in hypoxic environment; 24H+24N, 24 hours under hypoxic conditions followed by 24 hours under normoxic conditions; 24N+24H, 24 hours under normoxic conditions followed by 24 hours under hypoxic conditions. Mean \pm SEM. Cumulative data of four independent experiments. Ordinary one-way ANOVA with Tukey's correction for multiple comparisons. * $p \leq 0.05$; ** $p \leq 0.01$

When exposed to a lower dose of antigen (1 μ g MBP/ml), the numbers of T_{MBP} cells in the 48H group were on average 50% less than the normoxic control group. At the higher antigen dose, the 24N+24H group behaved as the 48H group while the 24H+24N group resembled the normoxic controls.

At the lowest investigated MBP dose (0.1 μ g/ml), no significant difference was observed between the different experimental conditions, though there was a tendentially lower (approx. 20% reduction) count of T_{MBP} cell in the 48H group when compared with the reference 48N group.

In the presence of the non-cognate antigen (OVA), no differences in T_{MBP} cell proliferation could be observed between the four different cell culture conditions.

4.2 Environmental oxygen conditions do not affect T_{MBP} cell viability but affect T_{MBP} cell proliferation

Next, we wanted to elucidate whether the reduced number of T_{MBP} cells observed in hypoxic conditions upon antigen stimulation was caused by cell death or to a direct impairment of T cell

proliferation. To this end, expression of phosphatidylserine on the cell surface was measured using flow cytometry by Annexin-V staining in T_{MBP} cells stimulated with different doses of MBP and cultured for 48 hours under normoxic or hypoxic conditions.

Phosphatidylserine is a lipid localized in the inner layer of the cell membrane in viable cells. In apoptotic cells, phosphatidylserine translocates to the outer surface of the cell. Annexin-V covalently binds phosphatidylserine residues. The presence of phosphatidylserine in the cell surface can be assessed by FACS using a fluorescently labelled Annexin-V.

As shown in *Figure 9*, the percentage of Annexin-V⁺ T_{MBP} cells in the control group was dose-dependent, being higher when T_{MBP} cells were stimulated with the lowest antigen doses. However, no significant differences in the percentage of Annexin-V⁺ cells were observed between T_{MBP} cells stimulated in the two environmental oxygen conditions at any of the tested antigen doses.

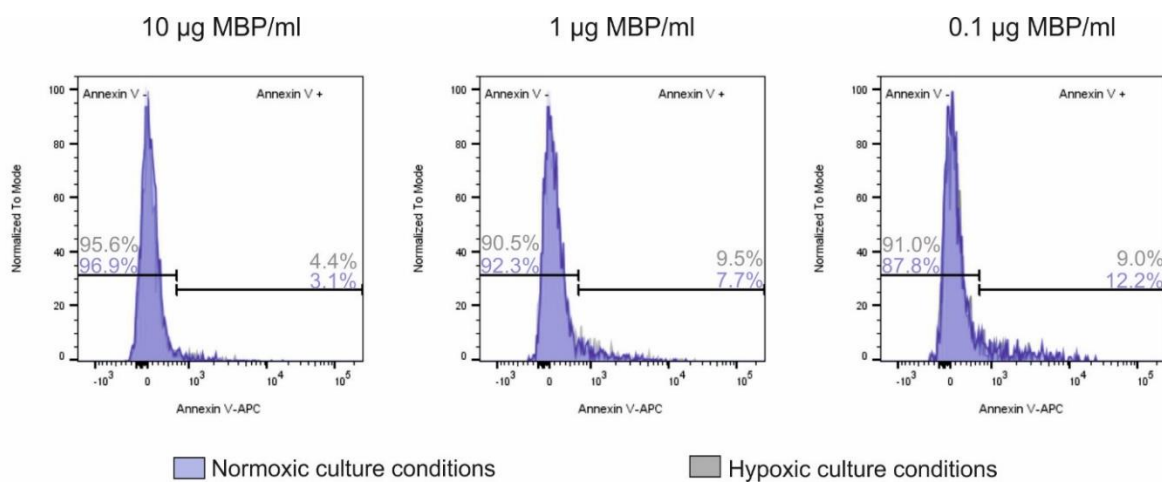


Figure 9. T_{MBP} cells stimulated under hypoxic conditions are viable. T_{MBP} cells were stimulated *in vitro* under normoxic or hypoxic conditions with the indicated doses of MBP for 48 hours. Representative overlay histograms (normalized to mode) depicting Annexin-V binding to T_{MBP} cell surface. Percentage of Annexin-V⁺ and Annexin-V⁻ T_{MBP} cells in the normoxic and hypoxic cohorts is indicated

Next, in order to investigate if the hypoxic environment had a direct effect on the T_{MBP} cell capacity to proliferate, T_{MBP} cells were stained with the cell proliferation tracking dye Tag-It Violet before reactivation under normoxic or hypoxic conditions as previously described. The proliferation dye diffuses into the cytoplasm where cellular enzymes modify it, allowing for its covalent attachment to cytosolic proteins. When Tag-It Violet⁺ cells proliferate, with every cell division the intensity of the staining in the daughter cells decreases 50% compared to the parent cell.

By using this technique, we observed that under hypoxic conditions T_{MBP} cells underwent fewer cycles of proliferation compared to the normoxic counterpart. This reduced proliferation could be observed at all antigen concentrations but was more pronounced at higher antigen doses (*Figure 10*). When

stimulated in the presence of 10 μg MBP/ml, around 30% of the hypoxic T_{MBP} cells underwent less than two cell division cycles whereas this percentage was 13% in the normoxic group. At 1 μg MBP/ml, the percentage of hypoxic T_{MBP} cells that underwent less than two cell division cycles was almost twice that of the normoxic T_{MBP} cells. At the lowest antigen dose (0.1 μg MBP/ml), the percentage of T_{MBP} cells that did not proliferate was 56% and 41% in the hypoxic and normoxic conditions, respectively.

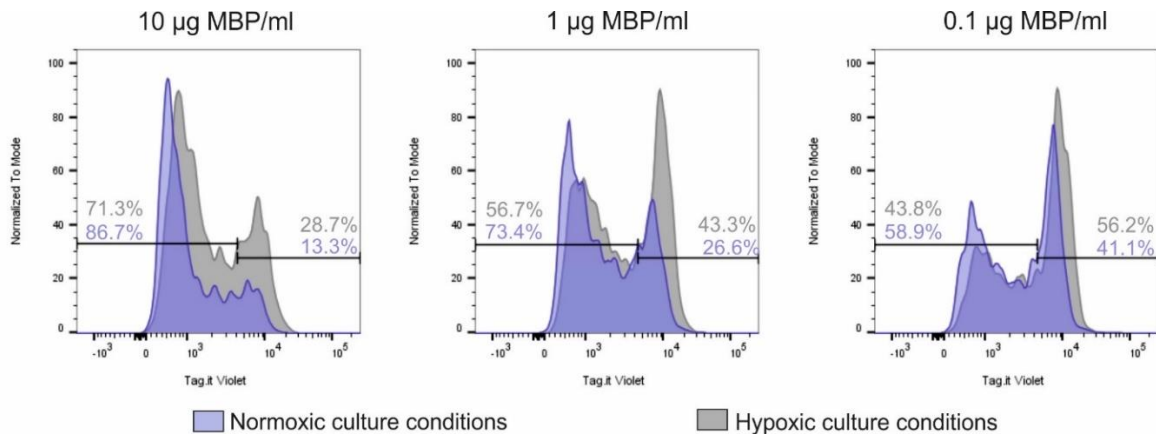


Figure 10. An oxygen-deprived environment affects T_{MBP} cell proliferation. Representative overlay histograms (normalized to mode) depicting T_{MBP} cell proliferation measured by dilution of the cell trace violet 48 hours after *in vitro* stimulation under normoxic or hypoxic conditions in presence of the indicated doses of MBP. Numbers indicate the percentage of divided and non-divided T_{MBP} cells per each condition

Taken together these results indicate that environmental oxygen availability does not influence T_{MBP} cell viability but rather affects the proliferation capacity of T_{MBP} cells in an antigen dose-dependent manner. At higher antigen concentrations, the suppressive effect of hypoxia on T cell proliferation is more pronounced.

4.3 Environmental oxygen conditions affect the expression of activation markers on the surface of T_{MBP} cells

In order to assess the effects of environmental oxygen tension on the activation of T_{MBP} cells *in vitro*, we performed a cell surface staining for CD134 and CD25 (IL2R α) on T_{MBP} cells stimulated in hypoxic or normoxic conditions in the presence of MBP (10 $\mu\text{g}/\text{ml}$, 1 $\mu\text{g}/\text{ml}$ and 0.1 $\mu\text{g}/\text{ml}$) or OVA (10 $\mu\text{g}/\text{ml}$). The expression of both of these molecules is increased upon T cell activation and can be detected by FACS (Figure 11).

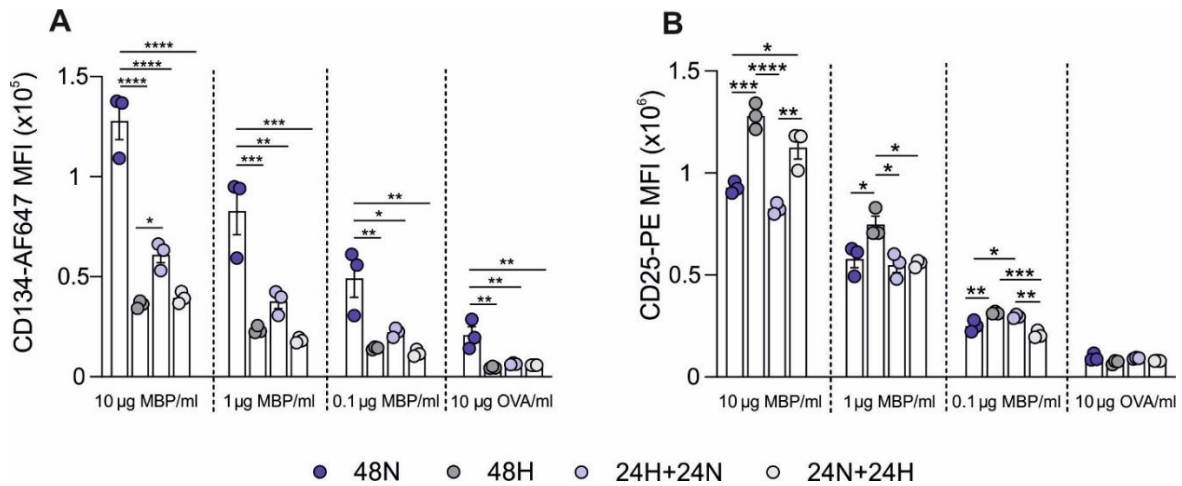


Figure 11. An oxygen-deprived environment affects the expression of surface activation markers in T_{MBP} cells. Expression levels of CD134 (A) and CD25 (B) on T_{MBP} cells after 48 hours of stimulation under the indicated environmental oxygen conditions and in presence of the indicated concentrations of MBP or OVA. Flow cytometry. 48N, 48 hours in normoxic environment; 48H, 48 hours in hypoxic environment; 24H+24N, 24 hours under hypoxic conditions followed by 24 hours under normoxic conditions; 24N+24H, 24 hours under normoxic conditions followed by 24 hours under hypoxic conditions. Cumulative data of 3 independent experiments. Mean ±SEM. Ordinary one-way ANOVA with Tukey's correction for multiple comparisons. * $p \leq 0.05$; ** $p \leq 0.01$; *** $p \leq 0.001$; **** $p \leq 0.0001$

We observed that the expression of CD134 (clone OX40) (Figure 11A) was higher in the normoxic group compared with any of the other experimental groups that were at some point exposed to an oxygen-deprived environment (48H, 24H+24N and 24N+24H). This holds true for all the investigated antigen conditions. When comparing the three hypoxic conditions, irrespectively of the MBP concentration, CD134 expression was higher in the group switched from hypoxia to normoxia (24H+24N) compared to the other two conditions. However, this difference reached statistical significance only in the 24H+24N group compared to the hypoxia group at the optimal MBP concentration (10 µg/ml). In such conditions, the expression of CD134 in the 24H+24N doubled the expression of the hypoxic group (48H).

In contrast to CD134, at optimal MBP dose condition (10µg/ml) the expression of CD25 (Figure 11B) was 37.8% higher on average in T_{MBP} cells stimulated under hypoxic conditions compared to the control group (48N). The 24N+24H group behaved similarly to the 48H group, displaying an increase of 21.1% on average in comparison with the control group, whereas the 24H+24N group was similar to the 48N group. At lower MBP doses (1 mg MBP/ml and 0.1 µg MBP/ml), there was still a significantly higher CD25 expression in the groups subjected to hypoxia for 48 hours (29.3% and 25.7% respectively) when compared with the normoxic group. No differences between the other two hypoxic conditions (24N+24H and 24H+24N) and the normoxic group could be observed.

4.4 Environmental oxygen conditions affect cytokine production in T_{MBP} cells

To further investigate the effects of environmental oxygen availability on T_{MBP} cell function, we assessed *in vitro* the capacity of T_{MBP} cells to produce pro-inflammatory cytokines upon antigen stimulation using two different techniques.

In brief, T_{MBP} cells were stimulated with MBP at different doses or with OVA under the four environmental oxygen conditions aforementioned. After 48 hours, intracellular staining for IFN γ was performed in T_{MBP} cells and acquired by FACS. Furthermore, the cell-culture supernatant was collected to detect IFN γ and IL17a by ELISA.

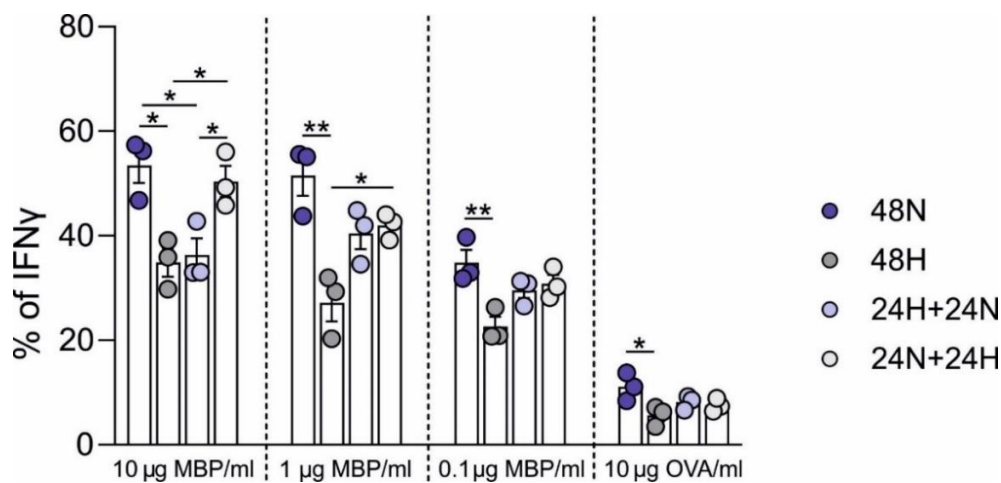


Figure 12. An oxygen-deprived environment affects the percentage of T_{MBP} cells producing IFN γ . Percentage of IFN γ ⁺ T_{MBP} cells 48 hours after *in vitro* antigen stimulation under the indicated environmental oxygen conditions. Flow cytometry. 48N, 48 hours in normoxic environment; 48H, 48 hours in hypoxic environment; 24H+24N, 24 hours under hypoxic conditions followed by 24 hours under normoxic conditions; 24N+24H, 24 hours under normoxic conditions followed by 24 hours under hypoxic conditions. Cumulative data of three independent experiments. Mean \pm SEM. Ordinary one-way ANOVA with Tukey's correction for multiple comparisons. * p \leq 0.05; ** p \leq 0.01

In the intracellular staining assay (Figure 12) we observed that, when provided with an optimal dose of the cognate antigen (10 μ g MBP/ml), the percentage of IFN γ ⁺ T_{MBP} cells was lowered in the hypoxic group by 20% in comparison with the normoxic group. As observed for the CD134 surface expression, the 24N+24H group behaved as the 48H group did (33% reduction compared to the normoxic group), whereas the 24H+24N group was similar to the 48N group.

At lower MBP conditions (1 μ g and 0.1 μ g MBP/ml) and when T_{MBP} cells were cultured in the presence of OVA, a 35% to 50% reduction in IFN γ ⁺ T_{MBP} cells was still observable in the 48H group in comparison with the reference group (48N). At these antigen doses, no differences were observed between the 24N+24H group or 24H+24N group and the normoxic group.

When cytokine production was assessed by ELISA (Figure 14), no significant differences in IFN γ amount could be observed between the experimental conditions (Figure 13A). However, in all the tested conditions, both the 48H and the 24H+24N group behaved similarly and both produced on average less IFN γ than the normoxic group. This decrease ranged from 9.5% in the 48H group and 9.7% in the 24H+24N group in the 10 μ g MBP/ml group to 28.2% and 33.6% respectively when T_{MBP} cells were stimulated with OVA. At all tested antigen doses, the 24N+24H group behaved as the 48N group did.

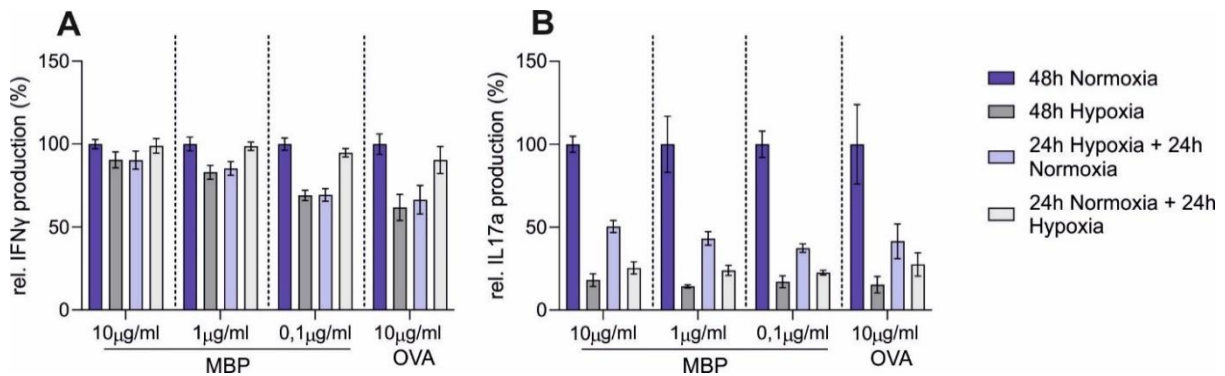


Figure 13. An oxygen-deprived environment affects pro-inflammatory cytokine production by T_{MBP} cells. Relative amount of IFN γ (A) and IL17a (B) normalized to the normoxic control produced by T_{MBP} cells under the indicated environmental oxygen conditions 48 hours after the encounter with MBP or OVA at the indicated concentrations. Mean \pm SD. Representative data of two independent experiments.

Regarding the production of IL17a (Figure 14B), in all the tested antigenic conditions T_{MBP} cells cultured for 48 hours in hypoxic conditions (48H) displayed on average a 84% reduced capacity to produce IL17a compared to the normoxic group. This decrease on IL17 production was lower in the 24N+24H, 75% on average and even lower (56% on average) in the 24H+24N group.

Taken together these results suggested that the production of pro-inflammatory cytokines depended on the environmental oxygen availability. Upon T_{MBP} cell stimulation the production of IL17a was very sensitive to any tested environmental oxygen condition whereas the effect of oxygen on the IFN γ production was more dependent on specific oxygen conditions. Furthermore, we could observe that the availability of oxygen in the first 24 hours but not in the following 24 hours upon antigen encounter critically influenced cytokine production.

4.5 Environmental oxygen conditions do not affect FOXP3 expression in T_{MBP} cells

It has been reported that a hypoxic environment could polarize naive T cell towards a regulatory phenotype (Westendorf et al., 2017). For this reason, we assessed the expression of the transcription factor FOXP3, a marker of regulatory phenotype in T cells, in T_{MBP} cells stimulated by MBP or OVA in the previously described environmental conditions. Intranuclear staining for FOXP3 was assessed by FACS 48 hours after antigen encounter (Figure 14).

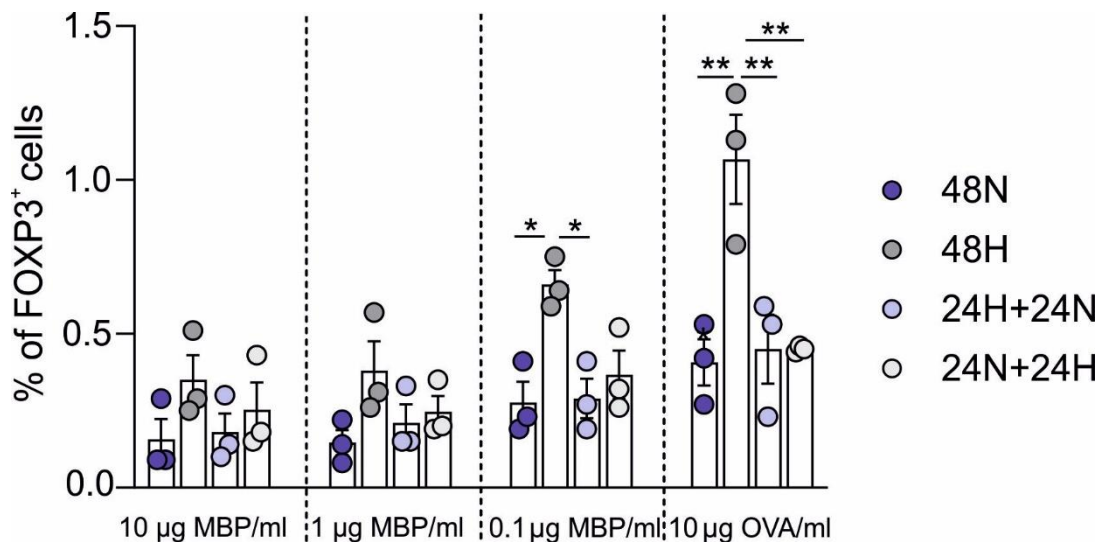


Figure 14. No main shift toward a regulatory phenotype is observed in T_{MBP} cells stimulated under hypoxic conditions. Percentage of FOXP3⁺ T_{MBP} cells 48 hours after stimulation with the indicated doses of antigens under different environmental oxygen conditions. Flow cytometry. 48N, 48 hours in normoxic environment; 48H, 48 hours in hypoxic environment; 24H+24N, 24 hours under hypoxic conditions followed by 24 hours under normoxic conditions; 24N+24H, 24 hours under normoxic conditions followed by 24 hours under hypoxic conditions. Cumulative data of three independent experiments. Mean ± SEM. Ordinary one-way ANOVA with Tukey's correction for multiple comparisons. **p* ≤ 0.05; ***p* ≤ 0.01.

Irrespectively of the type and dose of antigen and the environmental conditions, the percentage of FOXP3⁺T_{MBP} cells was always lower than 1.5%. In the hypoxic group (48H) the percentage FOXP3⁺T_{MBP} cells was always higher than in the normoxic group. This effect became significant when T_{MBP} were stimulated either with the lowest dose of MBP (0.1 µg/ml) or with OVA. No differences were observed between the two experimental groups that were switched from one oxygen condition to another after 24 hours of *in vitro* stimulation, or between these groups and the control 48N group.

These *in vitro* results suggest that a reduction in the environmental oxygen availability during T_{MBP} cell stimulation crucially affects both T cell proliferation and cytokine production, as well the expression of surface activation markers, without affecting T_{MBP} cell viability or inducing a switch in the T_{MBP} cells towards a regulatory phenotype. These effects were dose-dependent: They were more pronounced when T_{MBP} cells were stimulated in the presence of an optimal concentration of the cognate antigen. Cytokine production and CD134 expression were affected also in presence of a non-cognate antigen,

which points to an antigen-independent effect of the hypoxic environment on T_{MBP} cells. Furthermore, the timing of the exposure seemed crucial. The reduced oxygen availability in the first 24 hours after antigen exposure predominantly affected the expression of costimulatory molecules and cytokine production whereas in the following 24 hours mainly T_{MBP} cell proliferation was affected.

4.6 Hypoxia induces changes in the global expression profile of T_{MBP} cells

To evaluate the global effect of environmental oxygen availability on T_{MBP} cell function, we performed a transcriptome analyses of the T cells. To this purpose, resting T_{MBP} cells were stimulated *in vitro* under normoxic (approx. 20%O₂) or hypoxic (1% O₂) cell culture conditions. At 3 hours, 6 hours, 12 hours, 24 hours and 48 hours after antigen encounter, T_{MBP} cells were isolated by FACS-cell sorting (scheme in *Figure 15*).

A minimum of 2 x10⁴ T_{MBP} cells were sorted per experimental condition. After assessment of sorting purity, samples containing at least 98% of T_{MBP} cells were processed for RNA extraction. Isolated RNAs were then submitted to transcriptomic analysis.

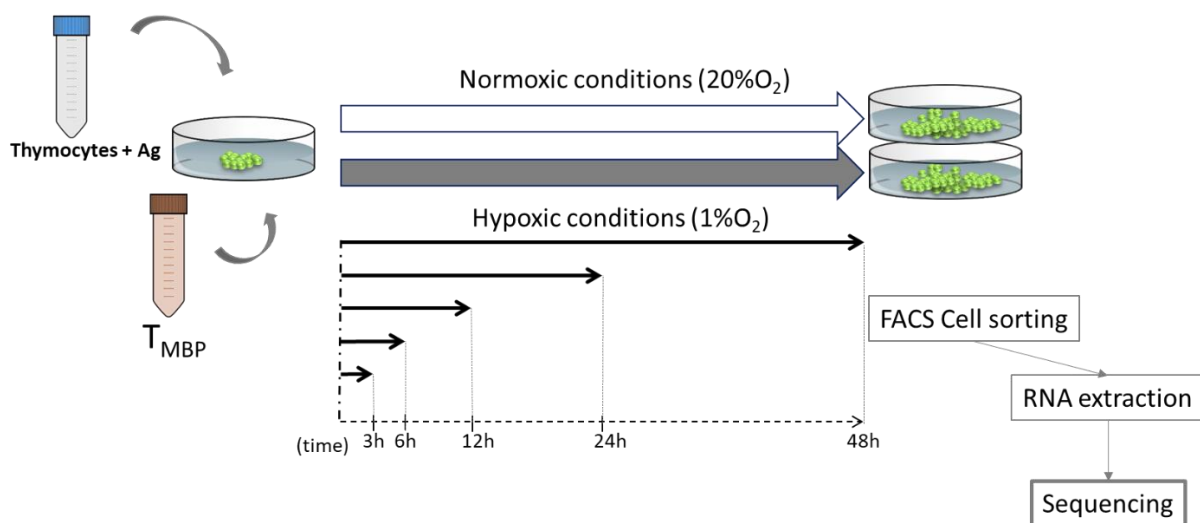


Figure 15. Experimental design and workflow for the transcriptomic study. T_{MBP} cells were cultured with irradiated thymocytes serving as APCs in presence of the cognate antigen (MBP). Plated cell mixes were cultured either in normoxic conditions (white-filled arrow, approx. 20% O₂) or in hypoxic conditions (grey-filled arrow; 1% O₂). At the indicate time points, T_{MBP} cells were FACS-sorted, RNA was extracted and, after quantification and purity assessment, the samples were submitted to transcriptome analysis.

In order to get an overview of the sequencing data, principal component analysis was used as an exploratory tool. Principle component 1 (PC1) and principle component 2 (PC2) captured 54% and 15% of the variation in the data set, respectively (*Figure 16*). The samples clustered according to the time point along PC1, indicating that this experimental condition is the main source of variation in the data. Additionally, samples clustered according to the hypoxic or normoxic states, suggesting that oxygen conditions also contributed to the variation in the data. Therefore, we proceeded in our analysis to investigate transcriptional changes induced by oxygen in T_{MBP} cells in more detail.

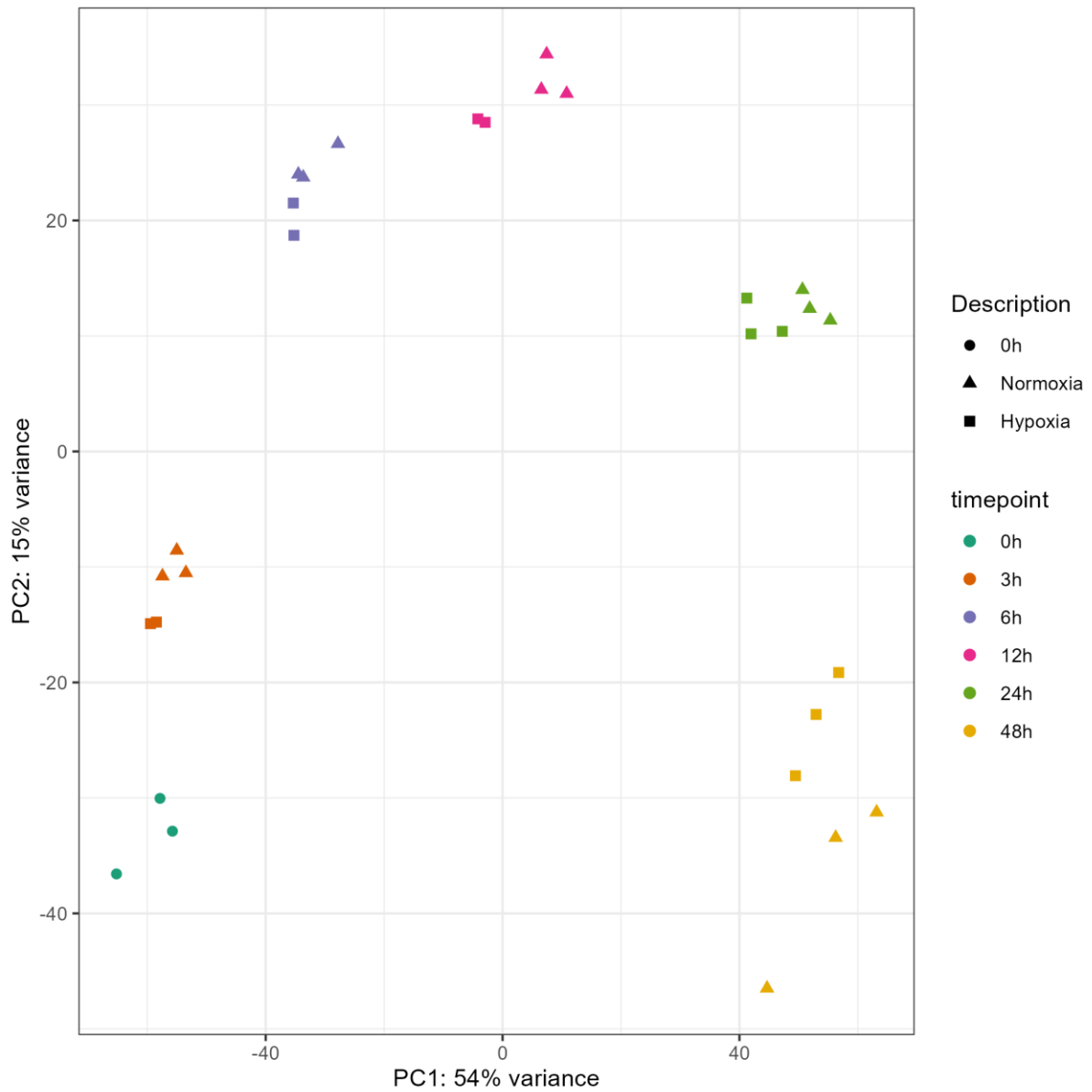


Figure 16. Time after antigen encounter and oxygen conditions determine transcriptional changes in T_{MBP} cells. Principal component analysis of T_{MBP} cells cultured under normoxic (triangles) or hypoxic (squares) conditions at the indicated time points (colours) after antigen encounter. Circles: resting T_{MBP} cells (time point 0).

4.7 An oxygen-deprived environment promotes transcriptional activity in T_{MBP} cells

The sequencing analysis detected 14850 transcripts present in all the samples. The differentially expressed genes (DEGs) detected at each time point are indicated and displayed as volcano plots (Figure 17). Volcano plots are a type of scatterplot that shows statistical significance (P value) versus magnitude of change (fold change). They enable a quick visual identification of the most regulated genes i.e. genes with large fold changes that are also statistically significant.

As early as 3 hours after antigen stimulation (Figure 18A), several genes ($n=147$) were differentially regulated between the two experimental conditions, the number of transcripts upregulated in hypoxic conditions ($n_{UP3h}=141$) being considerably higher than the one of downregulated transcripts ($n_{DOWN3h}=6$). This observation remained true for most the other time points (Figure 18A-D). The number of upregulated and downregulated transcripts promoted by hypoxia, was similar only at the last time point, namely 48 hours upon antigen encounter (Figure 18E).

At a first glance, it stands out that in all the investigated time points the most upregulated genes in the hypoxic group (e.g. *Egln3*, *Vegfa*, *Slc2a*, *Ak4* and *Ndr1*) were all directly regulated by the oxygen-sensitive transcription factor Hypoxia-inducible factor 1 α (*HIF1 α*). Of note, activation of the HIF1 α pathway is a very early and critical step in the transcriptional response to hypoxia and the same pathway can be also induced by TCR signalling (Cho et al., 2019; Palazon et al., 2014). Among the genes regulated in hypoxia, *EGLN3* displayed the most consistent and robust overexpression. *EGLN3* encodes for the prolyl hydroxylase 3, a cytoplasmic protein directly involved in the negative regulation of the HIF1 α response in eukaryotic cells.

Figure 17. (next page). Hypoxia induces early and sustained changes in the expression profile of T_{MBP} cells. A-D Volcano plots depicting the differences in expression profile of T_{MBP} cells cultured under normoxic or hypoxic condition at 3 hours (A), 6 hours (B), 12 hours (C), 24 hours (D) and 48 hours (E) after antigen encounter. Red: transcripts with $|\text{Log}_2\text{FC}| \geq 1$ and $-\text{Log}_{10}p > 6$; Green, transcripts with $|\text{Log}_2\text{FC}| \geq 1$ and $-\text{Log}_{10}p < 6$; Blue, transcripts with $|\text{Log}_2\text{FC}| < 1$ and $-\text{Log}_{10}p > 6$; Grey, transcripts with $|\text{Log}_2\text{FC}| < 1$ and $-\text{Log}_{10}p < 6$. Horizontal and vertical dotted lines show the cut-off used for identifying DEGs.

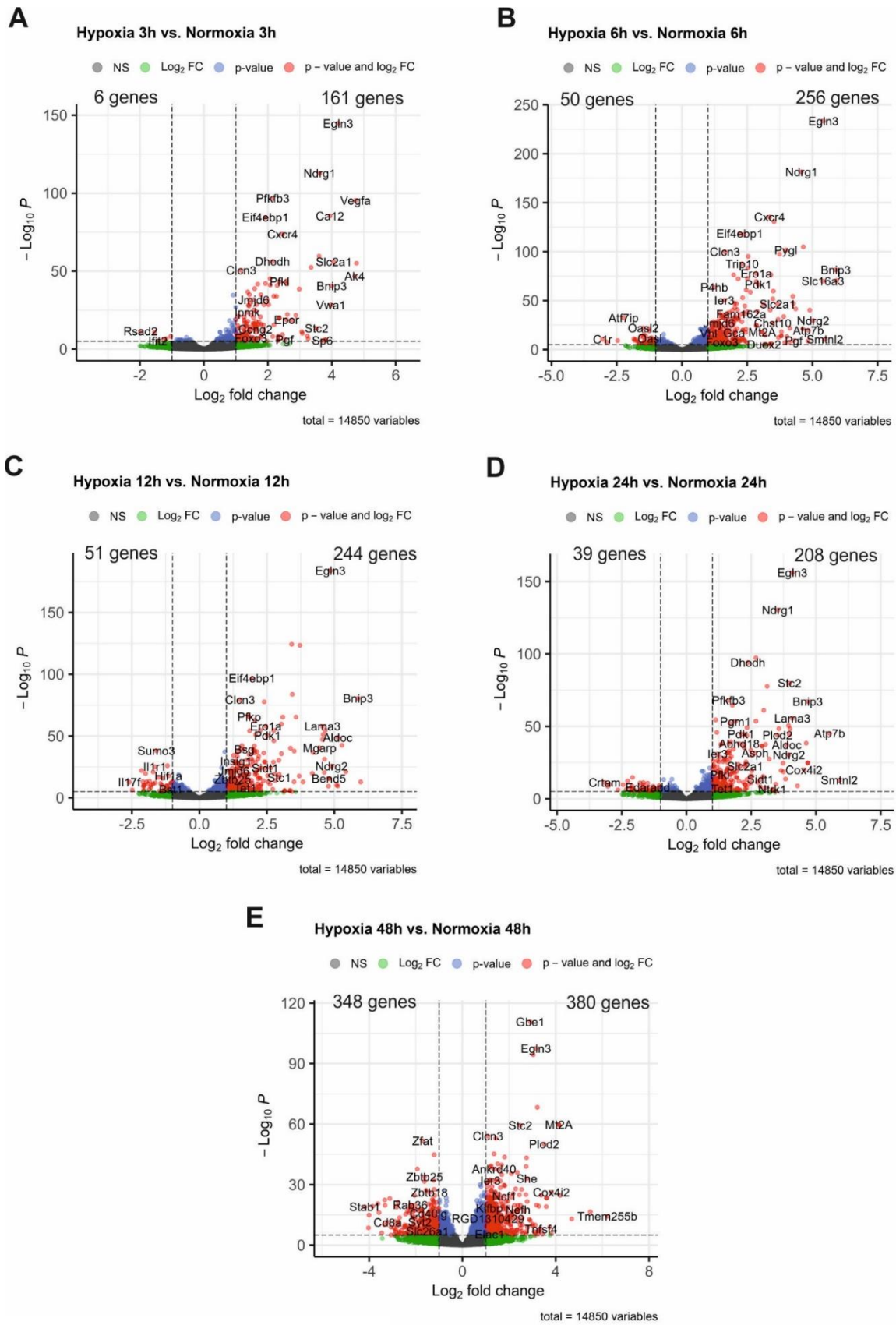


Figure 17. (Legend at the end of previous page)

4.8 Dynamic changes in the expression profile of T_{MBP} cells upon hypoxic conditions

Aiming to identify how the expression profile of T_{MBP} cells changes over time upon hypoxia, we quantified DEGs in the two experimental conditions at each time point. We visualized intersections between the DEGs of the analysed time points using UpSet plots to gain an overview of genes differentially expressed in one or several time points. UpSet plots are an alternative to Venn diagrams when the number of data sets compared at once is too large. In an UpSet plot, the total size of each set is represented on the left bar plot. Every possible intersection is represented by interconnected nodes on the bottom plot and their occurrence is shown on the top bar plot.

Two different UpSet plots were generated depicting genes upregulated or downregulated under hypoxic cell culture conditions (Figures 18 and 20).

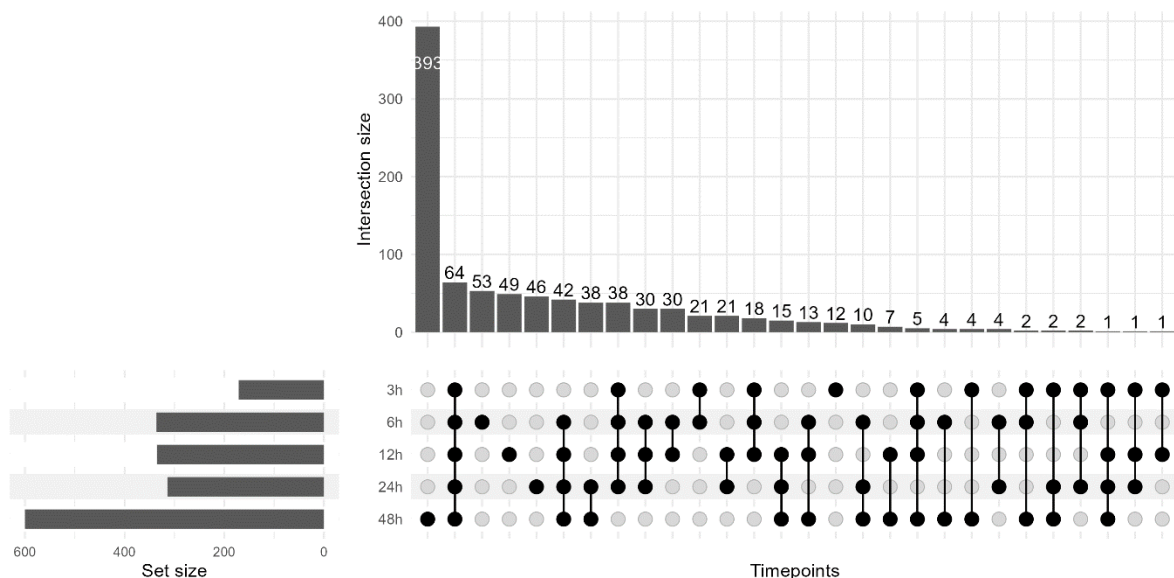


Figure 18. In hypoxic conditions, nearly 40% of the genes are uniquely upregulated at 48h. UpSet plot for the representation of the transcripts upregulated in T_{MBP} cells stimulated in hypoxic condition compared to normoxic. Sets of genes upregulated at a given time point or at a given intersection of time points are represented by interconnected nodes on the bottom plot and their occurrence is shown on the top bar plot. Only intersections considered statistically significant ($p_{adj} \leq 0.05$ and $\text{Log}_2\text{FC} > 1$) have been represented ($n=926$ transcripts).

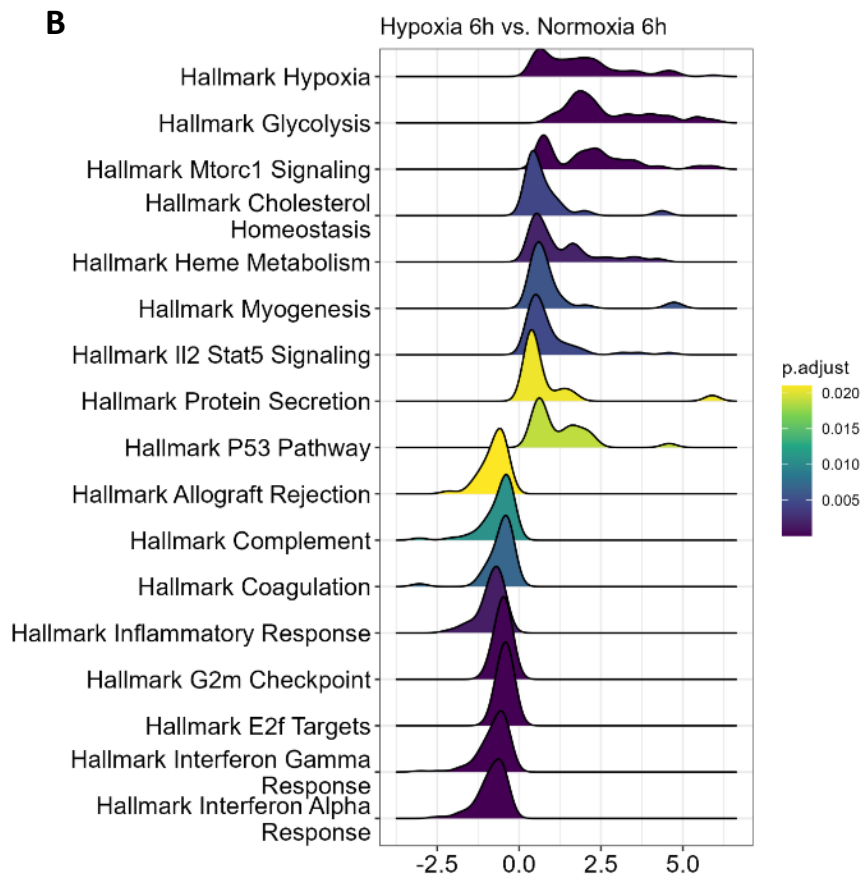
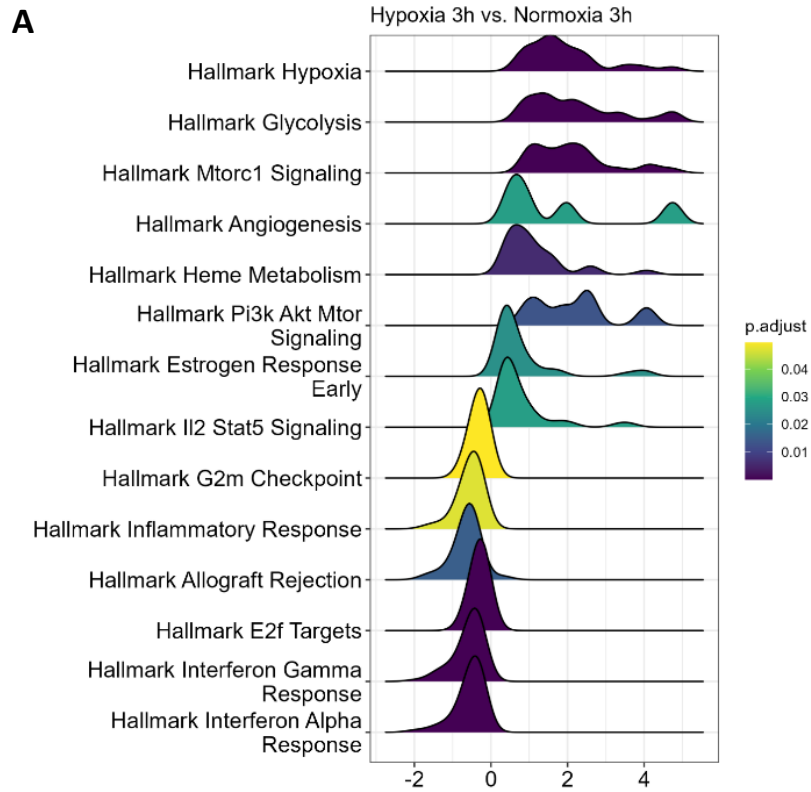
We detected 926 transcripts upregulated under oxygen-deprived cell culture conditions (Figure 19). A relevant part of them (393 transcripts) was exclusively upregulated at the latest time point, namely 48 hours after antigen encounter. Functional annotation clustering analysis of genes involved in biological processes applied to this gene set revealed an enrichment in transcripts related to kinase signalling activity and negative regulation of transcription.

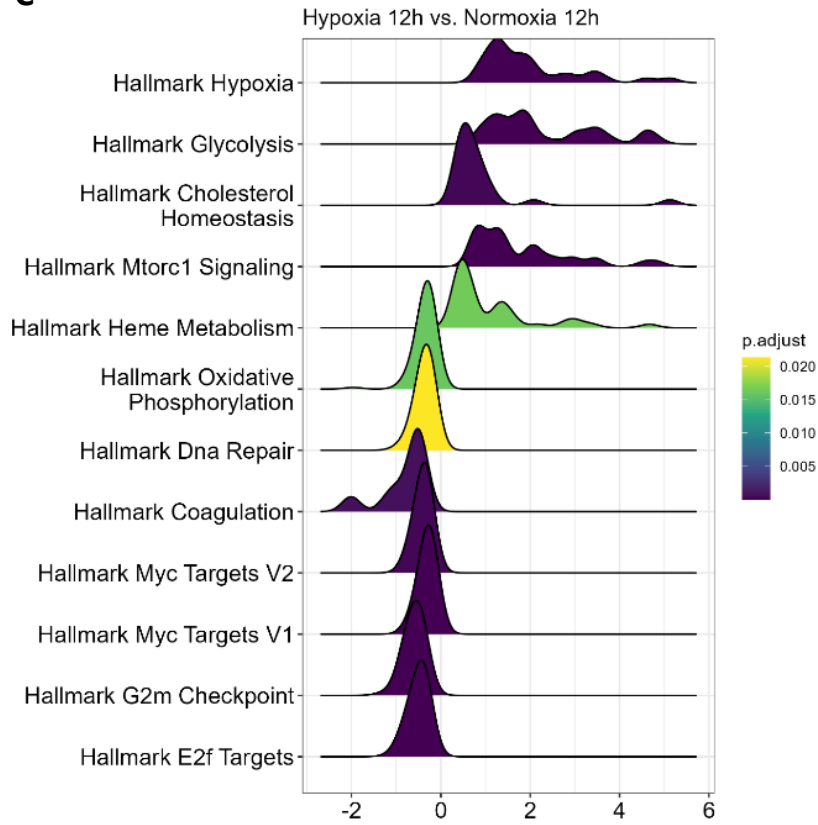
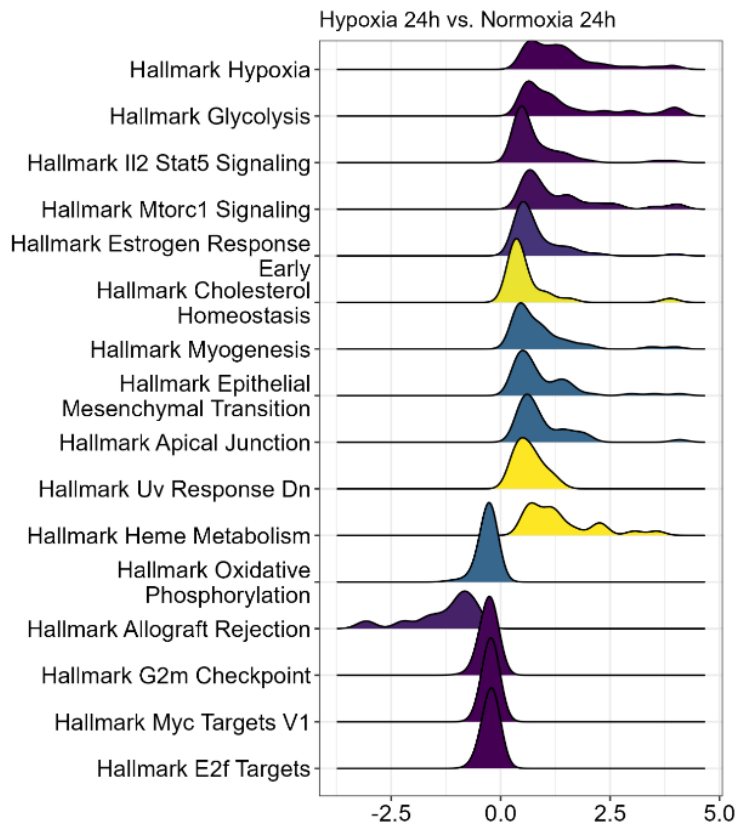
4.9 Gene Set Enrichment Analysis as a tool to explore specific, hypoxia-dependent programmes

In order to identify functional programme differentially regulated in T_{MBP} cells activated under either normoxic or hypoxic conditions, we evaluated the sequencing data by gene set enrichment analysis (GSEA). GSEA is a computational method that determines whether an a priori defined set of genes shows statistically significant differences between two biological states (Mootha et al., 2003; Subramanian et al., 2005).

We performed GSEA based on the hallmark gene sets from the Molecular Signatures Database (MiSigDB). MiSigDB is one of the largest repositories of gene sets. It annotates well-defined biological states or processes generated by a computational methodology based on identifying overlaps between gene sets in other molecular signatures database collections and retaining genes that express a coordinate expression.

The results of the GSEA are shown in *Figure 21 A-E* as sets of histograms per each time point. The X-axis represents the magnitude of the fold change (FC) for each gene set. If the peak of a histogram is localized above 0, the indicated gene set is enriched in hypoxic vs normoxic conditions whereas if the peak is localized below zero, the specific gene subset is underrepresented in the hypoxic vs the normoxic group. The colour of the histograms depicts the adjusted p-value obtained per each analysed gene set.



C**D**

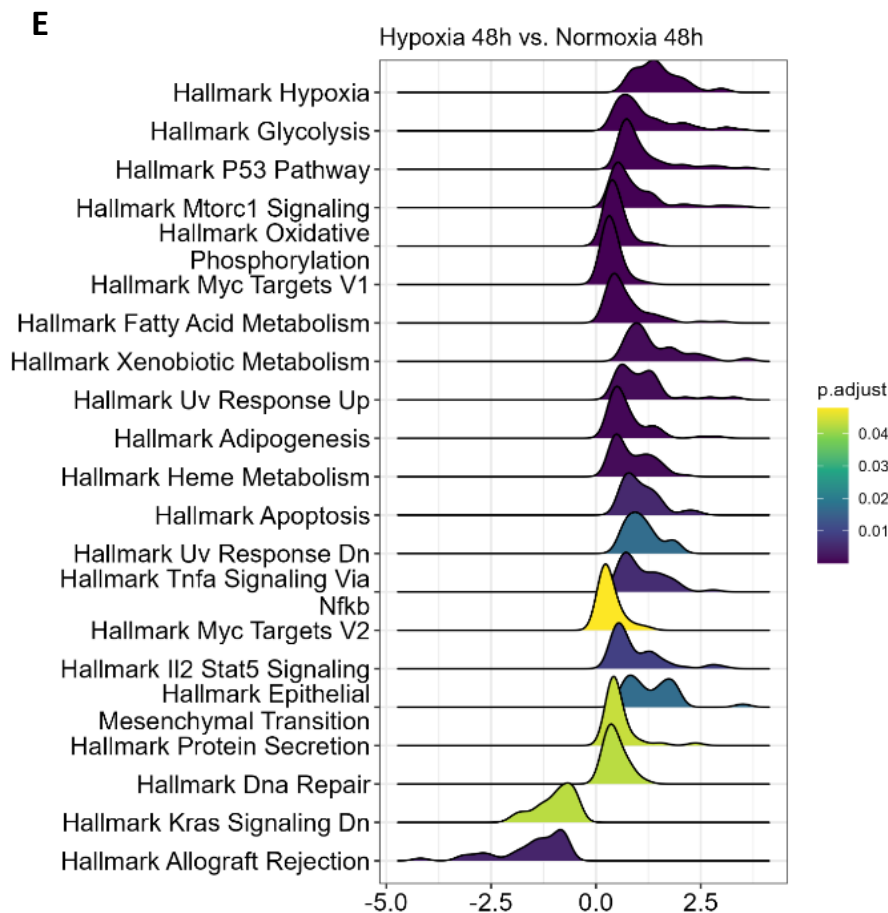


Figure 21. Hypoxia induces early and sustained changes in the transcriptional program of T_{MBP} cells. GSEA plots representing the \log_2FC of gene sets found enriched in the experimental groups at the different time points of the study. **A**, 3h; **B**, 6h; **C**, 12h; **D**, 24h; **E**, 48h. Only statistically significant findings are represented in the plots. Power of the statistical significance is coded by colour according to the legend.

In all the analysed time points, the hallmarks “Hypoxia”, including genes up-regulated in response to low oxygen levels, “Glycolysis” which aggregates genes encoding proteins involved in glycolysis and gluconeogenesis and “mTORC1 activation” were found positively enriched in the hypoxic samples in comparison with the normoxic counterpart. The measured enrichment of these gene sets was expected (hypoxia was the stimulus to which we submitted our cells and the variable distinguishing the experimental groups) and proved the validity of our analytic approach. We also observed that already at the earliest time point, i.e. 3 hours after antigen stimulation, the gene-set hallmarks “response to interferon alpha-signalling”, “response to interferon-gamma signalling” and “inflammatory responses” were downregulated in the group of T_{MBP} cells activated under hypoxic conditions compared to the normoxic control. Similar behaviour was observed in the gene set hallmarks, “G2m checkpoint” and “E2f targets” which include genes involved in DNA replication and progression through the cell cycle. These data confirmed our previous flow-cytometry data that showed a reduction of activation and proliferation in T_{MBP} cells stimulated under hypoxic conditions.

The dynamic of the gene set hallmark “IL2-Stat5 signalling” was also noteworthy, since it was upregulated in the first 3 hours in the normoxic group and then from 24 hours onwards was instead upregulated in the hypoxic group. A similar “biphasic” dynamic was observed also in the hallmark gene set “Oxidative phosphorylation” that was upregulated in the normoxic vs the hypoxic groups at the time points 12 hours and 24 hours when proliferative programme are particularly prominent. In the following time points, the upregulation of genes was reversed; this gene set being more upregulated in the hypoxic cohort.

Taken together the GSEA data indicated that the oxygen-deprived environment affects the metabolism of T_{MBP} cells very rapidly and in a sustained manner, triggering among others the upregulation of gene sets related to glycolysis, fatty acid metabolism or heme metabolism. These metabolic changes were associated with very early changes in T_{MBP} cell functional programme related to activation and proliferation.

4.10 An oxygen-deprived environment during T_{MBP} activation triggers the upregulation of specific transcripts related to the glycolytic pathway

It has been extensively reported that upon activation, effector T cells experience the so-called Warburg effect, by which their metabolism switches towards aerobic glycolysis (Kouidhi et al., 2017). The function of the Warburg effect in activated effector T cells is incompletely understood (Salmond, 2018).

The GSEA revealed the hallmark gene set “Glycolysis” as upregulated within the hypoxic group at every time point. To investigate in more detail the changes in the glycolytic pathway over time due to hypoxic stimulus, we retrieved genes annotated with glycolysis from the Reactome-database (Gillespie et al., 2022), and used it for data-mining, i.e. inspecting expression patterns at the different time points using heat maps as visualisation tool (*Figure 22*). Of note, this selection of genes included both genes encoding enzymes directly involved in the metabolic processing of glucose, as well as glycolysis-associated genes.

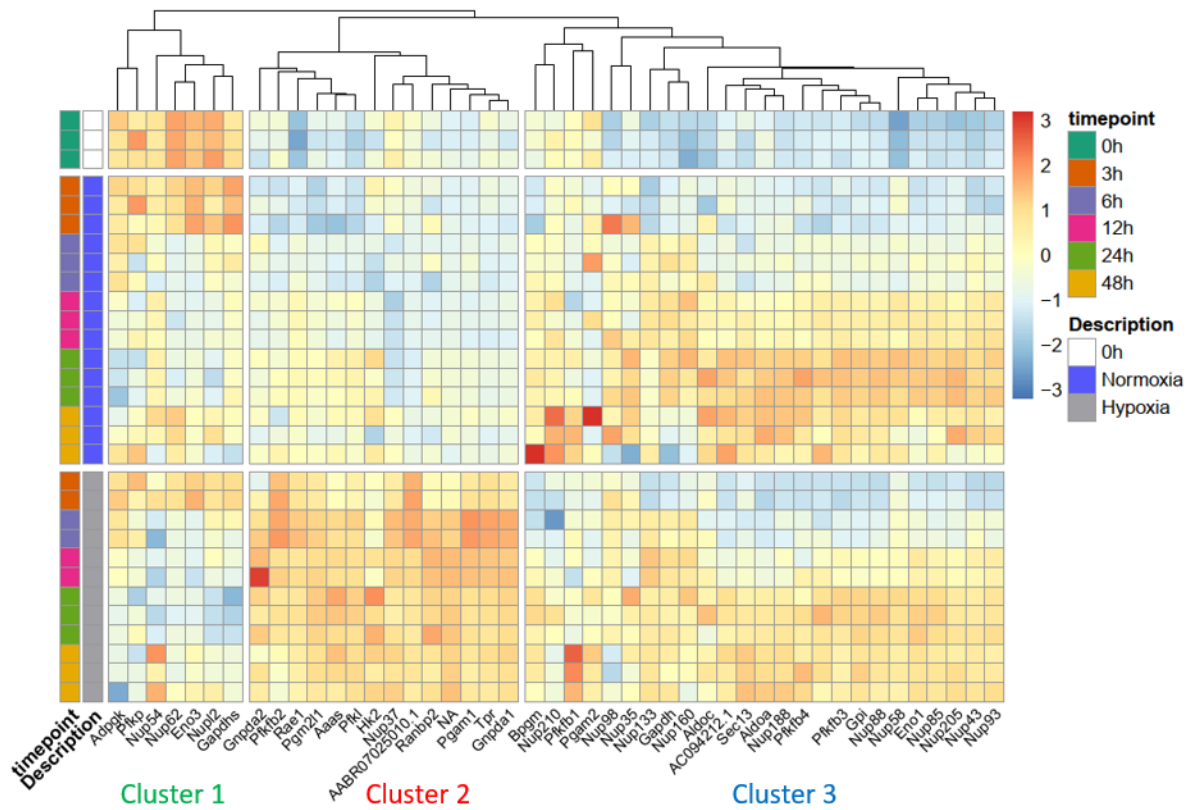


Figure 22. Hypoxia triggers the overexpression of a specific subset of hypoxia-related genes. Heat map showing the expression level of genes related to the glycolytic pathway in the Reactome database (Gillespie et al., 2022). Three different patterns of expressions (clusters 1 to 3) could be identified. Time point and experimental description appear colour-coded according to the provided legend.

The hierarchical cluster analysis revealed the existence of three main clusters, based on the gene expression pattern. A first cluster, including only seven transcripts, contained genes whose expression was high in resting T_{MBP} cells (time point 0 hours) and decreased in similar manner in both the experimental groups over time. A second cluster counting 14 transcripts, included genes whose expression was low in resting T_{MBP} cells, promptly increased upon hypoxia and remained high in all the investigated time points. In normoxic conditions, the expression of this gene set did not change initially, but it slowly and moderately increased over time. The third cluster included 25 different transcripts whose expression was low in basal conditions and increased over time in a similar manner in both experimental groups.

Interestingly, both clusters 2 and 3 contained transcripts encoding for key glycolytic enzymes. However, cluster 3 included transcripts encoding enzymes in the “core” of the glycolytic pathway, catalysing the reactions from β -D-Fructose-1,6P₂ to Phosphoenolpyruvate. Cluster 2 included transcripts encoding enzymes localized at the very beginning of the pathway, catalysing the first chemical changes that the molecule of glucose undergoes in order to be “assigned” to the glycolytic

pathway. A scheme of the glycolytic pathway with highlighted enzymes encoded in each of the hierarchical clusters is provided in Figure 23.

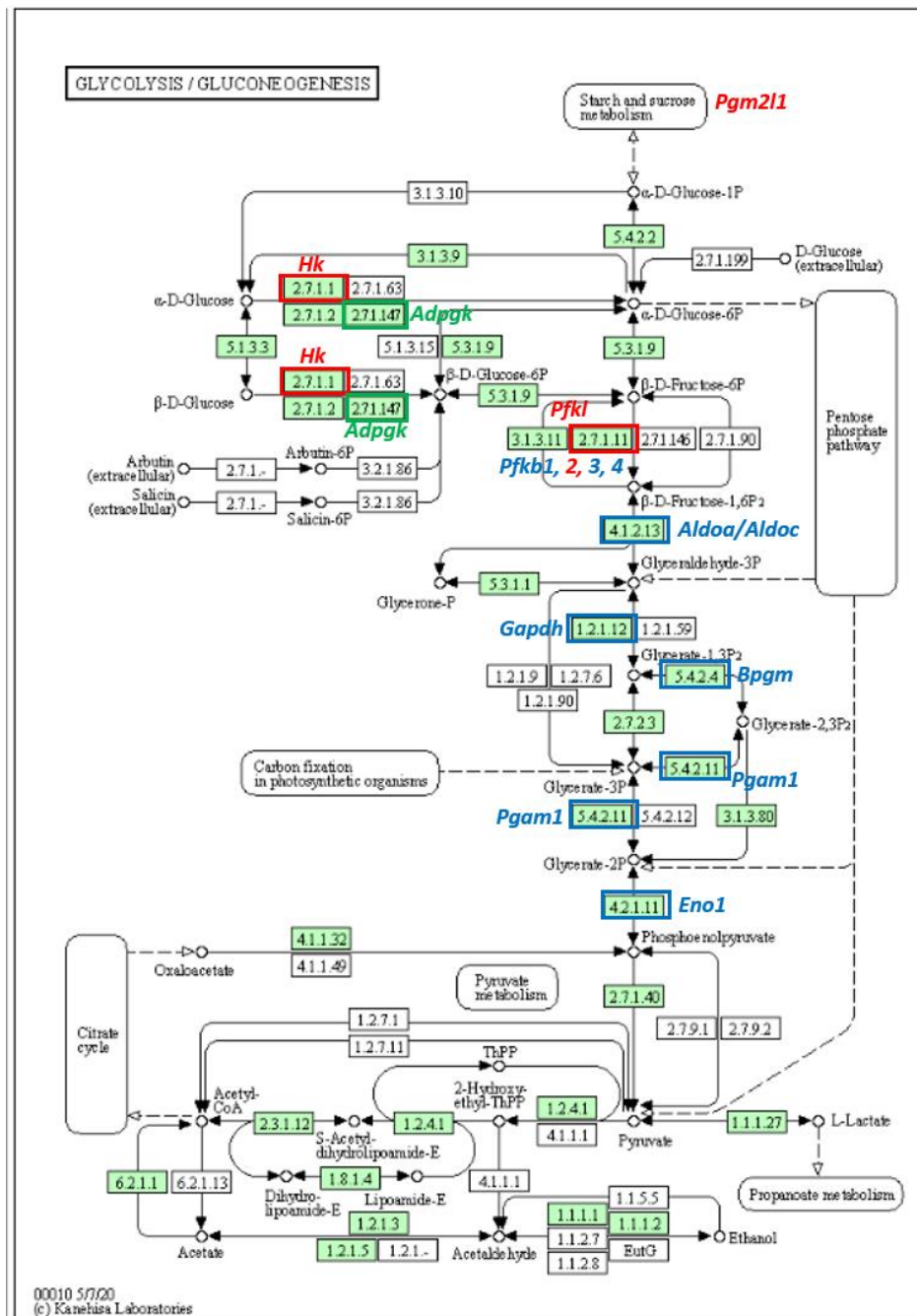


Figure 23. Hypoxia promotes the upregulation of glycolysis rate-limiting enzymes. Scheme of the metabolic pathway Glycolysis/gluconeogenesis from the KEGG database. Proteins encoded by genes localized in the previously identified cluster are colour-coded. Cluster 1: green; cluster 2: red; cluster 3: blue.

Taken together, the results of this transcriptomic study showed that an oxygen-deprived environment promotes rather than hinders the transcriptional program in T_{MBP} cells. In the first 24 hours upon antigen stimulation, the number of transcripts upregulated in the hypoxic group was strikingly higher

than the downregulated ones. At the same time, the hypoxic stimulus induced metabolic and functional changes in T_{MBP} cells. At the metabolic level, the glycolytic program, which is normally switched on in T cells upon activation was further pushed by the upregulation of a unique set of glycolytic genes responsible for the entry of the glucose moieties in the pathway. At the functional level, programme related to activation and proliferation were tuned down.

4.11 Environmental oxygen conditions during *in vitro* T cell activation affect the encephalitogenic potential of T_{MBP} cells

Up to this point, our data showed that the *in vitro* antigen-driven stimulation of T_{MBP} cells under oxygen-limited conditions has pleiotropic effects on T_{MBP} cell proliferation and cytokine production. Next, we wanted to assess whether the oxygen availability during T cell activation would also have an effect on the encephalitogenic potential of T_{MBP} cells. For this purpose, we used a model of EAE, induced in rats by i.v. transfer of fully activated T_{MBP} cells. In this model, the animals develop a monophasic paralytic disease that resembles the relapse phase of MS. The advantage of this system is the possibility to track and functionally characterize the pathogenic T cells over the entire disease course.

To test their encephalitogenic potential, T_{MBP} cells were stimulated *in vitro* in the presence of an optimal dose of the cognate antigen (10 µg MBP/ml) under either normoxic (approx. 20% O₂, normoxic blasts) or hypoxic conditions (1% O₂, hypoxic blasts). Two days later, 2x10⁶ T_{MBP} cell blasts were transferred intravenously into naïve recipient Lewis rats. An infographic of the experimental setup is depicted in *Figure 24*.

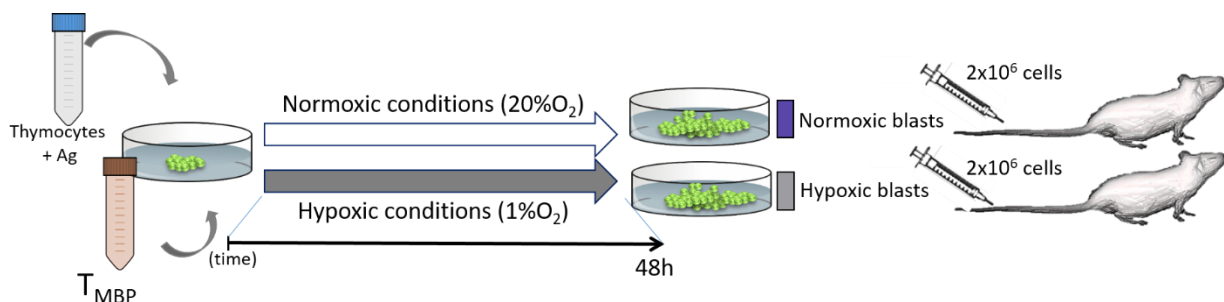


Figure 24. Experimental design of transfer EAE experiments. T_{MBP} cells were stimulated with the cognate antigen *in vitro* under normoxic (approx. 20% O₂) or hypoxic conditions (1% O₂). After 48 hours, 2x10⁶ T_{MBP} cell blasts were transferred intravenously into naïve recipients. The animals were scored on a daily basis. Infographics generated by the author.

Upon transfer, all the animals developed a classic paralytic monophasic disease (*Figure 25B*). Nevertheless, several significant differences could be observed between the two cohorts (*Figure 25C-F*). Overall, the disease was less severe in the group that received hypoxic T_{MBP} cells in comparison with the group that received normoxic cells. More specifically, in the hypoxic group the disease started one day later, the clinical signs at the disease onset (Hypoxic cohort: 0.55 ±0.06; Normoxic cohort: 1.6 ±0.07) and at the peak of the disease (Hypoxic cohort: 1.66 ±0.10; Normoxic cohort: 2.35 ±0.04) were milder. Accordingly a lower cumulative EAE score (Hypoxic cohort: 6.11 ±0.14; Normoxic cohort: 7.48 ±0.1) could be observed.

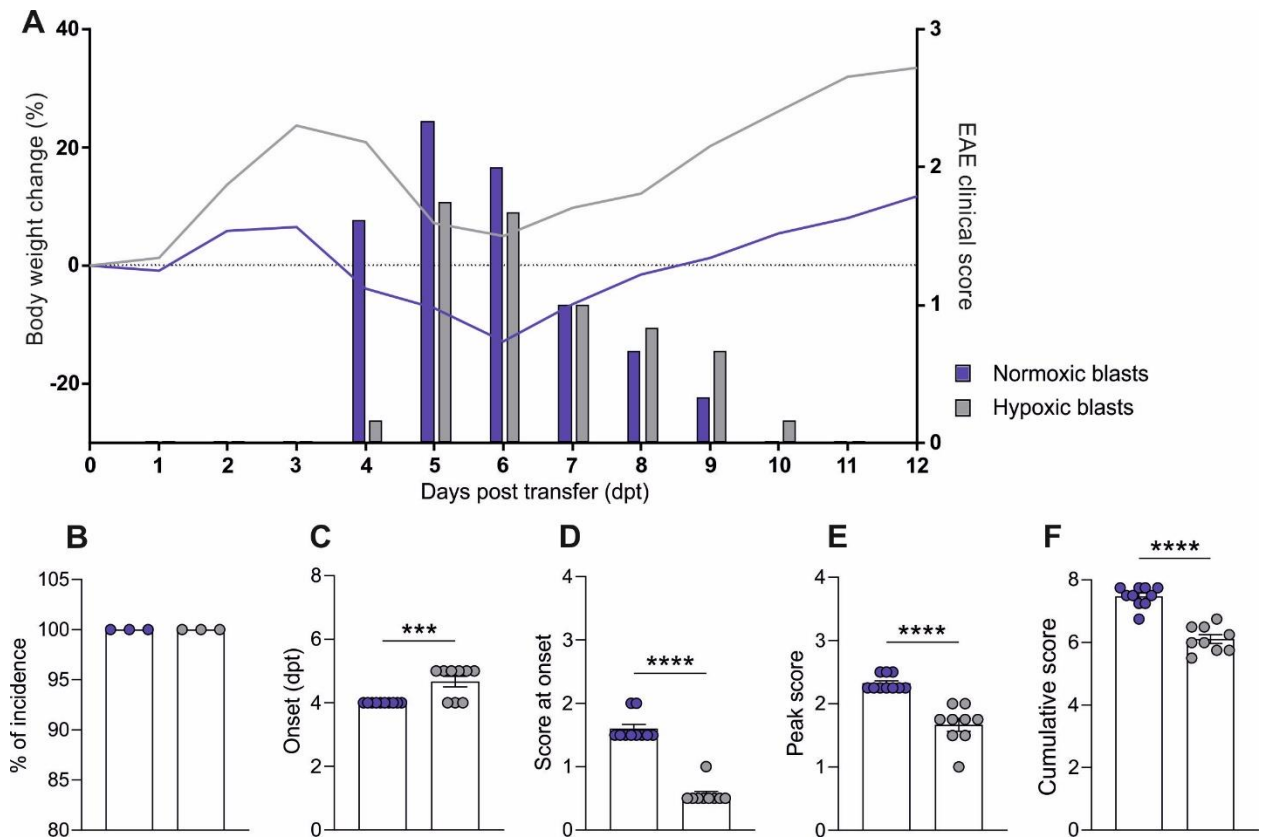


Figure 25. *T*_{MBP} cell blasts stimulated in vitro under hypoxic conditions trigger milder clinical signs in the transfer EAE. A-F EAE was induced by i.v. transferred of 2×10^6 normoxic or hypoxic *T*_{MBP} cell blasts as described in Figure 26. **A.** Mean body weight changes (lines) and mean clinical score (bars) during the course of EAE. **B.** Incidence. **C.** Disease onset. **D.** Disease peak. **E.** Cumulative score. **B-F:** Mean \pm SEM. Cumulative data from three independent experiments (Normoxic blasts: n=10; hypoxic blasts n=9). Unpaired t-Test. *** $p \leq 0.001$; **** $p \leq 0.0001$.

Subtle differences in clinical parameters could potentially have been masked by an overshooting immune response induced by the transfer of a high number of cells. In order to see more pronounced differences between the two groups, we applied the same experimental design as above but lowered the number of transferred *T*_{MBP} blasts from 2×10^6 to 0.25×10^6 (Figure 26).

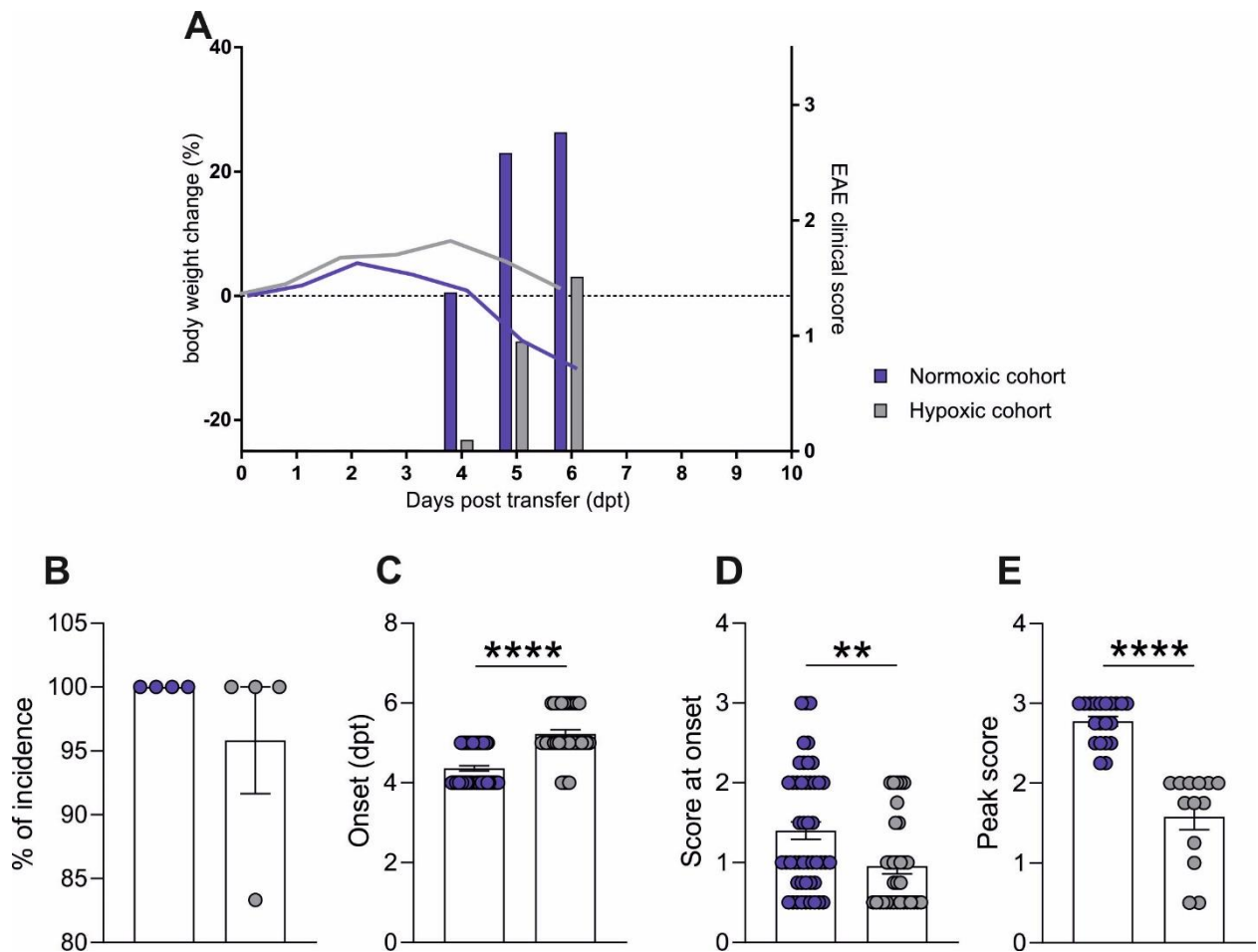


Figure 26. Low numbers of hypoxic T_{MBP} cell blasts trigger a delayed and weaker clinical signs in the transfer EAE. Transfer EAE was induced by transfer of 0.25×10^6 T_{MBP} cell blasts previously activated *in vitro* under either normoxic or hypoxic conditions. **A.** Mean body weight changes (lines) and mean clinical score (bars) during the course of EAE. **B.** Incidence. **C.** Disease onset. **D.** Disease peak. **E.** Cumulative score. **B-F:** Mean \pm SEM. Cumulative data from three independent experiments (Normoxic blasts: $n=48$; hypoxic blasts $n=33$). Unpaired t-Test. ****** $p \leq 0.01$; ******** $p \leq 0.0001$.

As expected, the progression of the disease was slightly dampened. In both groups, the disease started on day 4 –as it was the case when a higher number of T cells was transferred– but the clinical signs progressively worsened over 48 hours and reached the peak on day 6 after transfer (Figure 27A). More importantly, also in this setup, there were significant differences between the two experimental groups. The cohort that received T_{MBP} blasts stimulated under hypoxic conditions showed a delayed disease onset by at least one day (Hypoxic cohort: 5.2 ± 0.1 ; Normoxic cohort: 4.3 ± 0.06) and a significantly lower clinical score both at the onset (Hypoxic cohort: 0.9 ± 0.1 ; Normoxic cohort: 1.4 ± 0.1) and at the peak (Hypoxic cohort: 1.58 ± 0.06 ; Normoxic cohort: 2.78 ± 0.06) of the disease (Figure 26.C- E).

Taken together, these data indicate that the encephalitogenic potential of T_{MBP} cells stimulated under hypoxic conditions is impaired.

4.12 An oxygen-deprived environment during *in vitro* activation impairs T_{MBP} cell ability to invade the CNS

In previous work from our group (Odoardi et al., 2012), it could be observed that upon intravenous transfer, T_{MBP} cells follow a precise migratory pattern. They first home in the lung, before moving to the mediastinal lymph nodes 2 to 3 days later. From there, they egress back into the blood circulation and can be found in peripheral organs such the spleen before invading the CNS.

The ameliorated disease course observed in animals transferred with hypoxic T_{MBP} cell blasts could potentially have been caused by a disturbance in this behavior. Consequently, we next wanted to investigate if the *in vitro* exposure to a hypoxic environment affected the migratory pattern of T_{MBP} cells and their potential to invade the CNS.

We stimulated T_{MBP} cells under normoxic or hypoxic conditions as described above and after 48 hours transferred them into recipient animals (0.25 x10⁶/rat). We then quantified the number of T_{MBP} cells by FACS in peripheral organs (lung, mediastinal lymph nodes, spleen and blood) and spinal cord from day 3 to day 6 p.t. (*Figure 27*).

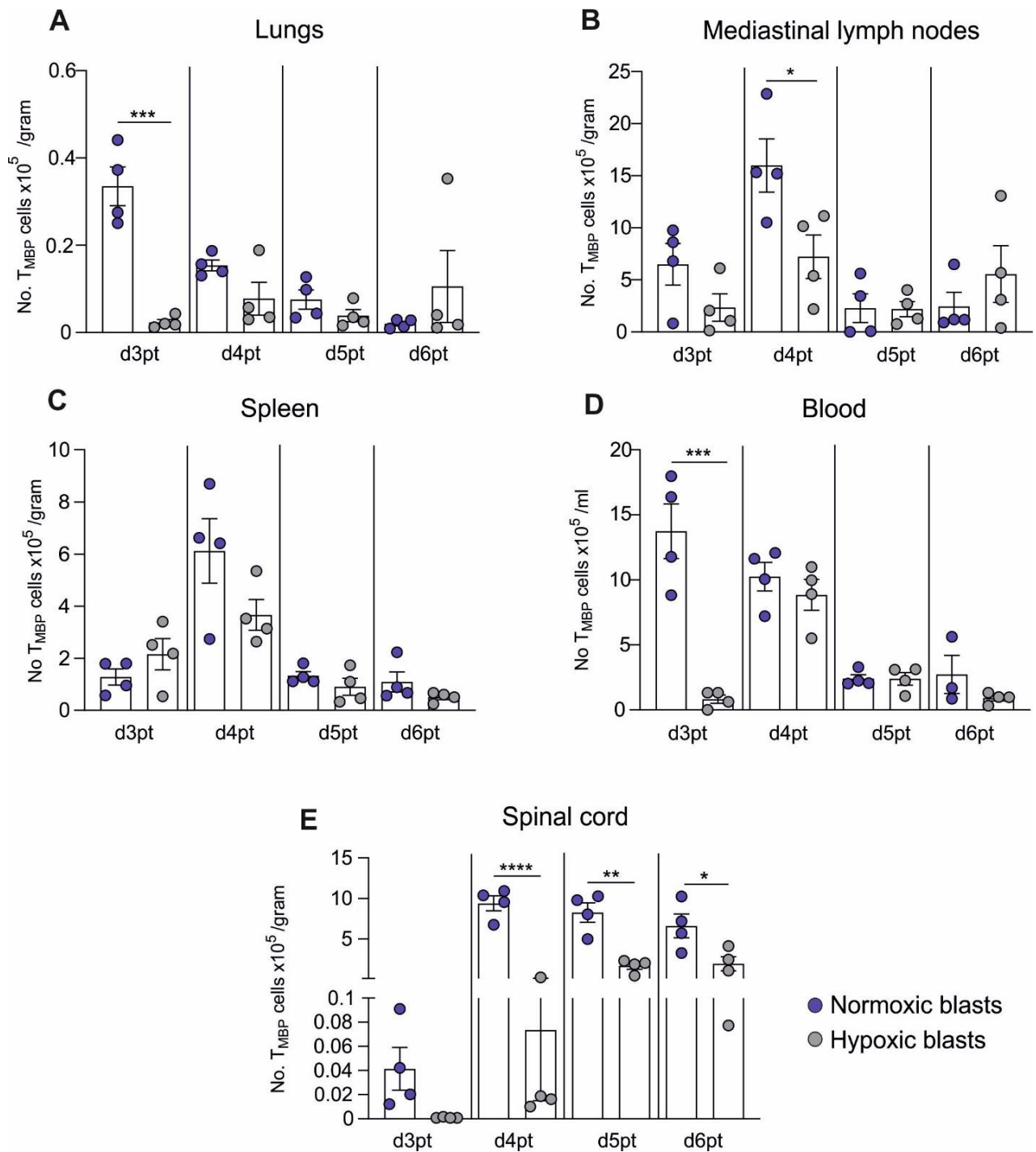


Figure 27. Hypoxic T_{MBP} cell blasts display a reduced capacity to infiltrate the CNS. Number of T_{MBP} cells detected in the indicated organs during the course of EAE induced by transfer of hypoxic or normoxic T_{MBP} cells as in Figure 28. **A.** Lungs, **B.** Mediastinal lymph nodes; **C.** Spleen; **D.** Blood and **E.** CNS. Each dot represents a single animal. Mean \pm SEM. Representative data of 3 independent experiments including at least 4 animals/group/time point. Unpaired t-Test. * $p \leq 0.05$; ** $p \leq 0.01$; *** $p \leq 0.001$; **** $p < 0.0001$.

In the lungs of the group transferred with normoxic T_{MBP} cell (normoxic group) blasts, the number of T_{MBP} cells reached a maximum on day 3p.t. and then progressively decreased over time. In the animals that received hypoxic T_{MBP} cell blasts (hypoxic group), the peak of T_{MBP} cell numbers in the lung was

observed one day later i.e. on day 4 p.t. Except for day 6 p.t., at all other time points the number of T_{MBP} cells was higher in the normoxic than in the hypoxic group. This difference reached statistical significance on day 3 p.t. when the numbers of T_{MBP} cells in the hypoxic group was 14 times lower than the ones in the normoxic controls (*Figure 27A*).

In the mediastinal lymph nodes and spleen, the kinetics of T_{MBP} cell numbers was very similar between the two groups with a peak on day 4 p.t. followed by a progressive reduction in the T_{MBP} cell number over time. In the mediastinal lymph nodes, on day 3 and day 4 p.t. the number of T_{MBP} cells was 2.7- and 2.2-fold lower in the hypoxic than in the normoxic group. No main differences were observed in the other time points. In the spleen, a lower number of T_{MBP} cells (1.6-fold difference) was observed exclusively on day 4 p.t. (*Figure 27 B-C*).

In the blood, the kinetics of T_{MBP} cell numbers was different in the two groups. In the normoxic group, T_{MBP} cell numbers reached the peak on day 3 p.t. and then progressively decreased in the following days, coinciding with the infiltration of T_{MBP} cells into the spinal cord. In the hypoxic group, the maximum number of T_{MBP} cells in the blood was reached on day 4 p.t. On day 3 p.t., the number of T_{MBP} cells was on average 16 times lower in the hypoxic vs the normoxic group but no differences were observed at the other time points (*Figure 27 D*).

In the spinal cord, on day 3 p.t., T_{MBP} cells could be already detected in the normoxic group. T_{MBP} cell numbers increased more than twenty-fold during the following 24 hours. This difference lasted until the end of the observation period on day 6 p.t. In the hypoxic group, T_{MBP} cells started to invade the spinal cord on day 4 p.t. and dramatically increased (about 22 times) 24 hours later. This difference lasted until the end of the observation period. Of note, the maximal number of T_{MBP} cells found in the spinal cord in the hypoxic group was three to four times lower than the amount of T_{MBP} cells in the CNS of the reference cohort at the peak of T_{MBP} cell infiltration (*Figure 27 E*).

Taken together, these data indicate that the reduced encephalitogenic potential of T_{MBP} cells stimulated under hypoxic conditions is associated with a reduced number of T_{MBP} cells both in the peripheral organs and in the CNS.

4.13 CNS inflammation correlates with the invasion pattern of T_{MBP} cells

We next measured the expression of *Ifng*, *Il17a* and *Foxp3* in the CNS over the disease course by real-time quantitative PCR in the spinal cord (Figure 28).

For all the transcripts, in the normoxic group the maximal expression was detected on day 4 p.t. coinciding with the peak of T_{MBP} cell invasion of the CNS and was 31-fold higher for *Ifng* and about 27-fold higher for *Il17a* than the corresponding expression in the hypoxic group. In the hypoxic cohort, the maximal cytokine expression was observed on day 5 p.t., i.e. at the peak of T_{MBP} cell infiltration. At this time point, the expression of *Ifng* was 3-fold higher and of *Il17a* twice higher in the hypoxic than in normoxic group (Figure 28A-C). Notably, when the maximal values in each group were compared, the expression of *Ifng* and *Il17a* detected in the hypoxic cohort was about half of the expression detected in the reference cohort (*Ifng*; Normoxic group: 0.0051 ±0.0002, Hypoxic group: 0.0023 ±0.0003; *Il17a*; Normoxic group: 0.0036 ±0.0002; Hypoxic group: 0.0017 ±0.000) (Figure 28A-B). For *Foxp3*, the expression in the CNS tissue was low and no main differences between the two groups were observed (Normoxic group: 0.0007 ±0.0001 Hypoxic group: 0.0007 ±0.0001) (Figure 28C).

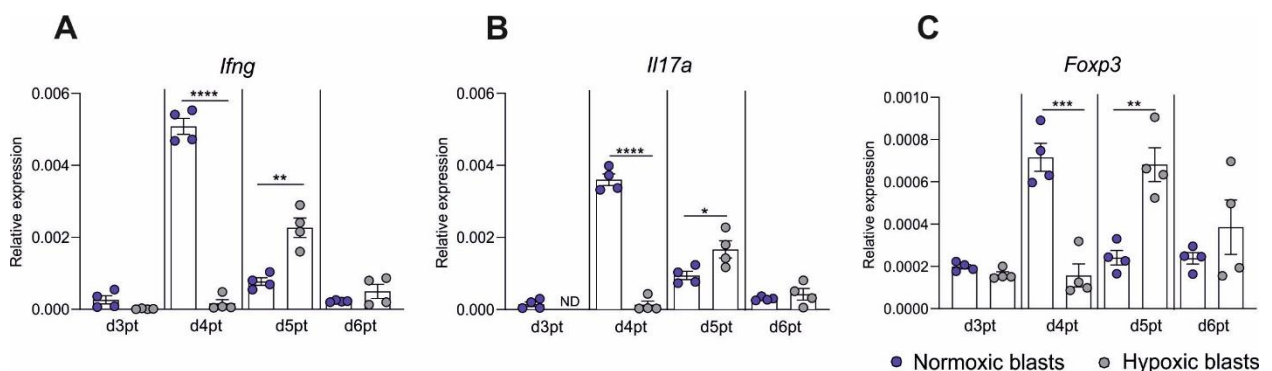


Figure 28 . Different expression pattern of pro-inflammatory cytokines and *Foxp3* in hypoxic and normoxic T_{MBP} cells in the CNS. Expression of *Ifng* (A), *Il17a* (B) and *Foxp3* (C) in total spinal cord at the indicated time points after transfer of hypoxic or normoxic blasts as in Figure 26. Quantitative PCR. Housekeeping-gene: β -actin. Mean \pm SEM. Representative data of 3 independent experiments including at least 4 animals/group/time point. Each dot represents a single animal. Unpaired t-Test. * $P \leq 0.05$; ** $p \leq 0.01$; *** $p \leq 0.001$; **** $p < 0.0001$.

4.14 The reactivation of hypoxic T_{MBP} cells in the target tissue is not impaired

The local reactivation of CNS-reactive T cells in the target organ is a crucial step for disease pathogenesis (Bartholomäus et al., 2009; Lodygin et al., 2013). Therefore, we asked if an impaired capacity of the hypoxic T_{MBP} cells to be restimulated *in vivo* in the target tissue could explain the lower level of pro-inflammatory cytokines observed in the spinal cord and the milder clinical course. To address this question we measured the expression of the surface activation markers CD134 and CD25 (Figure 29) and the production of pro-inflammatory cytokines IFN γ and IL17a (Figure 30) in T_{MBP} cells sorted from blood and spinal cord daily from days 3 to 6 p.t.

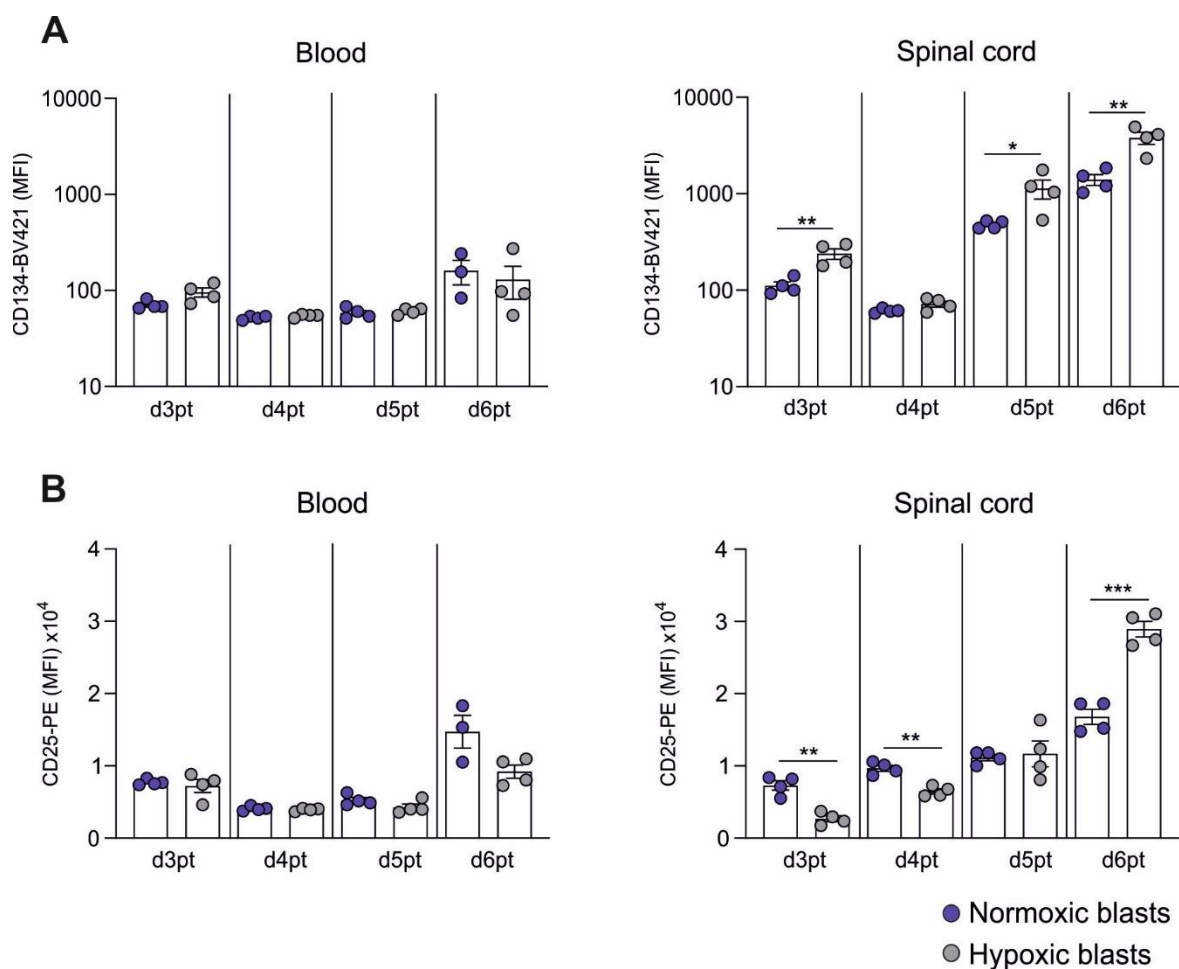


Figure 29. The expression of surface of activation markers in hypoxic T_{MBP} cells is not impaired in the CNS. EAE was induced by transfer of hypoxic or normoxic T_{MBP} cells as in Figure 26. Median fluorescence intensity (MFI) of CD134 (A) and CD25 (B) in T_{MBP} cells isolated from blood and spinal cord through the course of EAE. Each dot represents a single animal. Mean \pm SEM. Representative data of three independent experiments including at least 4 animals/group/time point. Statistical significance was assessed by non-parametric t-Test. * $p \leq 0.05$; ** $p \leq 0.01$; *** $p \leq 0.001$; **** $p < 0.0001$.

Regarding the surface activation markers, no differences in CD134 expression between the two groups could be observed in the blood at any time point. When comparing blood and CNS, in both the groups on day 5 and day 6 p.t. the expression of CD134 in T_{MBP} cells was higher in the CNS than in the blood, indicating that T_{MBP} cells could be reactivated in situ in the target organ in both the experimental conditions. At the same time points, in the CNS, the expression of CD134 was significantly higher in the hypoxic T_{MBP} cells in comparison with the normoxic ones. This was also the case on day 3 p.t. when very few T_{MBP} cells could be found in the CNS of animals that received the hypoxic T_{MBP} blasts (Figure 30A).

Regarding CD25, we did not observe major differences in the blood between the two groups. In line with the CD134 expression data, CD25 expression was higher in the CNS compared to the blood in both the groups on days 4, 5 and 6 p.t. The expression of this marker progressively increased from day 3 p.t. to day 6 p.t. in both groups with the increase being more pronounced in the group that received hypoxic T_{MBP} cells. CD25 was higher in the group transferred with normoxic T_{MBP} cells on day 3 and 4 p.t. However, at the peak of CD25 expression on day 6p.t. the hypoxic T_{MBP} cells expressed on their surface significantly more CD25 than the normoxic counterpart (Hypoxic group: 28935 ±1083; Normoxic group: 16804 ±1047).

We next assessed the capacity of T_{MBP} cells previously stimulated under normoxic or hypoxic conditions and isolated from blood and CNS to produce pro-inflammatory cytokines under basal conditions and after stimulation with Phorbol 12-myristate 13-acetat and Ionomycin (PMA/IONO) over the relevant clinical phase (from day 3 to day 6 p.t.)

No difference between the two cohorts was observed in blood-derived T_{MBP} cells at any time point (Figure 30 A). In both the groups at any time point, the production of cytokines in basal conditions was higher in the CNS than in the blood-derived counterpart (Figure 31 A-B), further confirming that T_{MBP} cells could be reactivated in the CNS. In the CNS, the highest percentage of normoxic T_{MBP} cells able to produce cytokines was observed on day 3p.t. coinciding with the initial T-cell infiltration. At this time point, the few T_{MBP} cells that could be retrieved from the CNS in animals transferred with hypoxic blasts were not able to produce cytokines both in basal conditions and upon stimulation (Figure 30 B).

In the hypoxic cohort, the peak of IFN γ production was reached on day 4 p.t. coinciding with the initial infiltration of hypoxic T_{MBP} into the CNS. At this time point, the percentage of IFN γ -producing T_{MBP} cells was significantly higher in the hypoxic than in the normoxic cohort and was also two-fold higher than the value observed the day before in the CNS of the reference cohort (Figure 30 B).

On days 5 and 6 p.t. the percentage of cytokine-producing T_{MBP} cells found in the CNS of animals transferred with hypoxic blasts was higher than in the group transferred with normoxic blasts, the difference being statistically significant on day 5 p.t. but no longer so on day 6 p.t. (Figure 30 B).

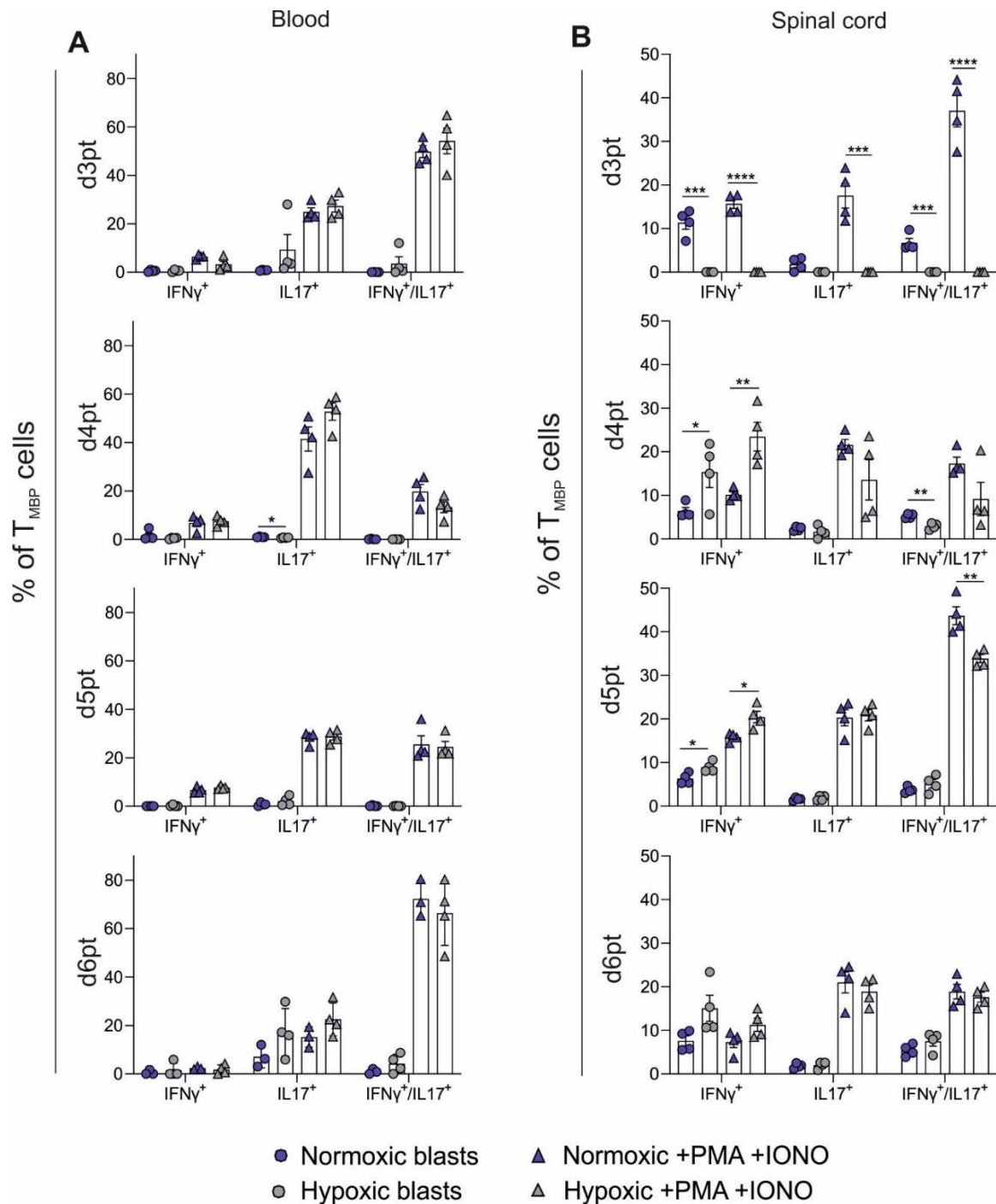


Figure 30. The expression of pro-inflammatory cytokines by hypoxic T_{MBP} cells in the CNS is not impaired. EAE was induced as in Figure 26 by transfer of normoxic or hypoxic blasts. Percentage of IFN γ^+ , IL17a $^+$ and IFN γ^+ /IL17a $^+$ T_{MBP} cells in blood (A) and spinal cord (B) of animals throughout the EAE course in steady-state and upon PMA/IONO stimulation. Flow cytometry. Each dot represents a single animal. Mean \pm SEM. Representative data of three independent experiments including at least four animals/group/time point. Statistical significance was assessed by non-parametric t-Test. * $p \leq 0.05$; ** $p \leq 0.01$; *** $p \leq 0.001$; **** $p < 0.0001$.

Next, we quantified the absolute number of T_{MBP} cells able to produce IFN γ , IL17 and IFN γ -IL17 in both cohorts in blood and spinal cord (Figure 31). A relatively higher number of cytokine producing cells (IFN γ^+ , IL17a $^+$ or IFN γ^+ /IL17a $^+$) could be found in the blood of the normoxic cohort in comparison with the hypoxic cohort (Figure 31A). This observation is consistent with the higher numbers of T_{MBP} cells found in the blood of hypoxic animals. In the CNS, consistent with the pattern of infiltration (Figure 27), the cytokine-producing T_{MBP} cells peaked on day 4 and on day 5p.t. in the normoxic and hypoxic group, respectively. Their number was always higher in the normoxic than in the hypoxic group (Figure 31B).

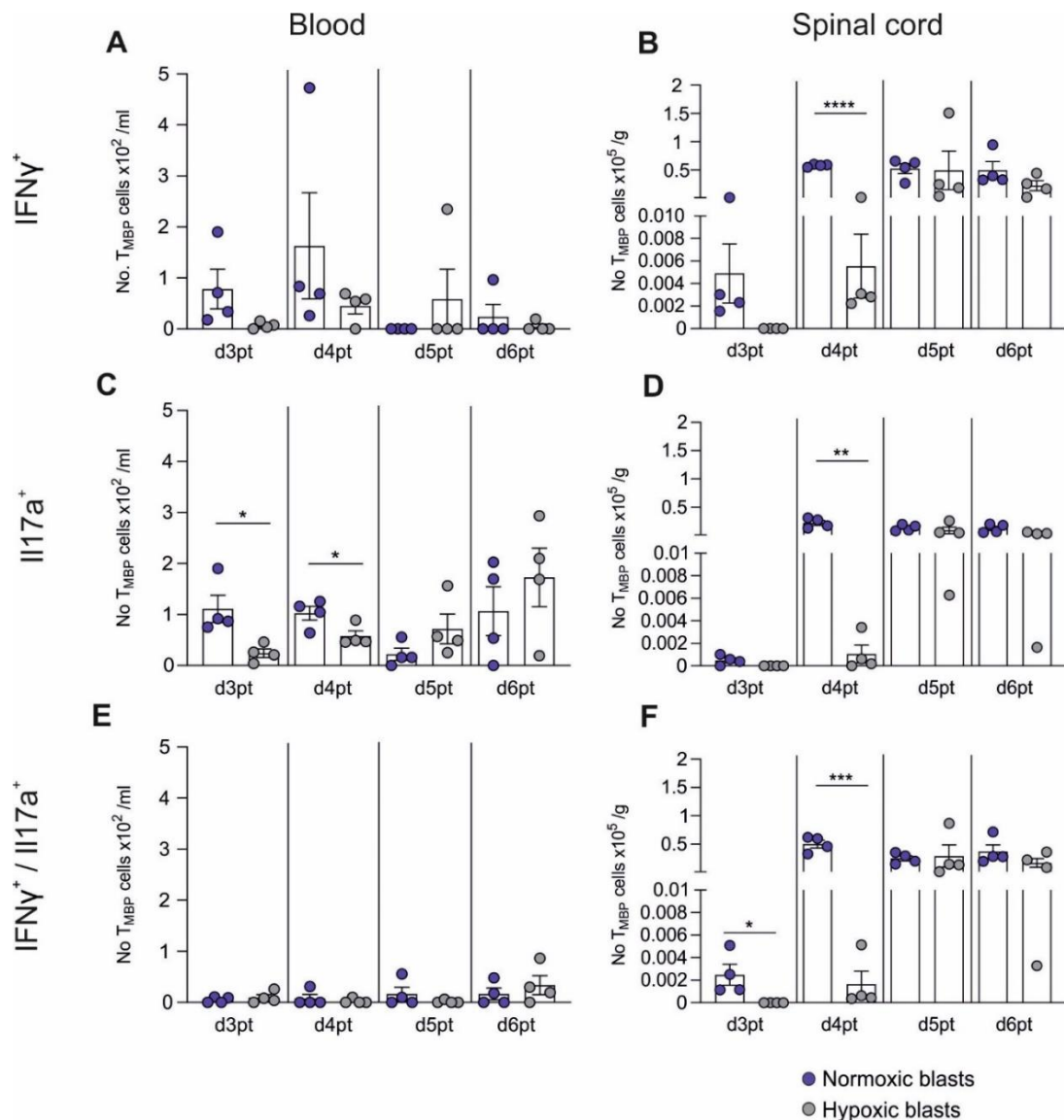


Figure 31. The number of hypoxic T_{MBP} cells producing pro-inflammatory cytokines is reduced in the CNS. EAE was induced as in Figure 25 by transfer of normoxic or hypoxic blasts. Absolute number of IFN γ^+ , IL17a $^+$ and IFN γ^+ /IL17a $^+$ T_{MBP} cells in blood (A) and spinal cord (B) throughout the EAE course. Flow cytometry. Each dot represents a single animal. Mean \pm SEM. Representative data of three independent experiments including at least four animals/group/time point. Statistical significance was assessed by non-parametric t-Test. * $P \leq 0.05$; ** $P \leq 0.01$; *** $P \leq 0.001$; **** $p < 0.0001$.

Finally, we quantified the expression of FOXP3 in blood and CNS-derived T_{MBP} cells (Figure 32). No differences between the normoxic and hypoxic groups were observed in the blood at any time point (Figure 33A). In the CNS, in the normoxic group the percentage of FOXP3⁺ T_{MBP} cells was similar at all examined time points (around 2.5%). In the hypoxic group, almost no FOXP3⁺ T_{MBP} cells were detected on day 3 and day 4 p.t. On day 5p.t. the percentage of FOXP3⁺ T_{MBP} cells increased to 9% and became significantly higher than in the reference group (Normoxic group: 2.8% \pm 0.35%; Hypoxic group: 9.4% \pm 1.7%). On day 6 p.t. both groups displayed a very similar percentage of FOXP3⁺ T_{MBP} cells. Regarding the total number of FOXP3⁺ T_{MBP} cells, very few positive cells could be detected at any time point in blood or CNS and no main differences between the two groups could be found between different time points (Figure 32B).

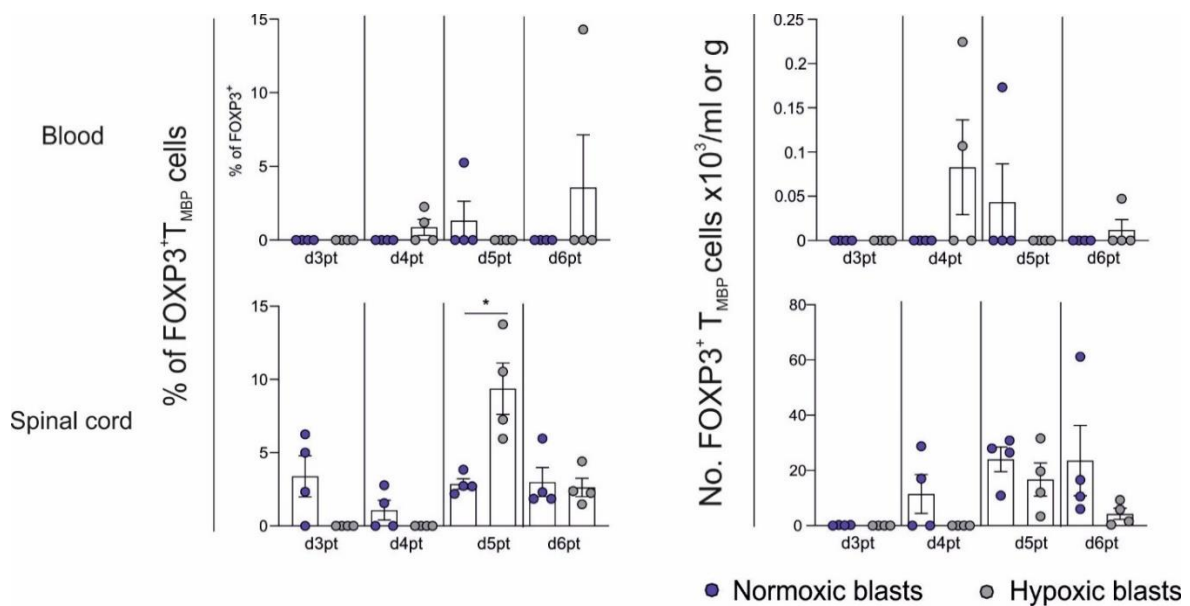


Figure 32. Hypoxic blasts do not acquire a regulatory phenotype in the spinal cord. EAE was induced as in Figure 26 by transfer of normoxic or hypoxic blasts. Percentage and absolute numbers of FOXP3⁺ T_{MBP} cells assessed by FACS. Each dot represents a single animal. Mean \pm SEM. Representative data of three independent experiments including at least 4 animals /group /time point. Statistical significance was assessed by non-parametric t-Test. * $p \leq 0.05$.

Taken together, these results show that the total number of hypoxic T_{MBP} cells able to produce pro-inflammatory cytokines in the CNS is reduced but their capacity to be reactivated in situ is not impaired. No shift towards a regulatory phenotype is observed.

4.15 Endogenous T cell recruitment to the CNS is reduced in animals that receive hypoxic T_{MBP} cells

The local reactivation of T_{MBP} cells in the CNS induces the release of pro-inflammatory cytokines and chemokines that drive the recruitment of endogenous $CD4^+$ and $CD8^+$ T cells. We therefore aimed to assess the recruitment of endogenous T cells in animals transferred with T_{MBP} cells stimulated under normoxic or hypoxic conditions. For this purpose, we quantified the number of endogenous $GFP^- CD4^+$ and $CD8^+$ T cells in the CNS daily from day 3 to day 6 p.t. (Figure 33) and measured their capacity to produce $IFN\gamma$ and $IL17$ (Figure 34).

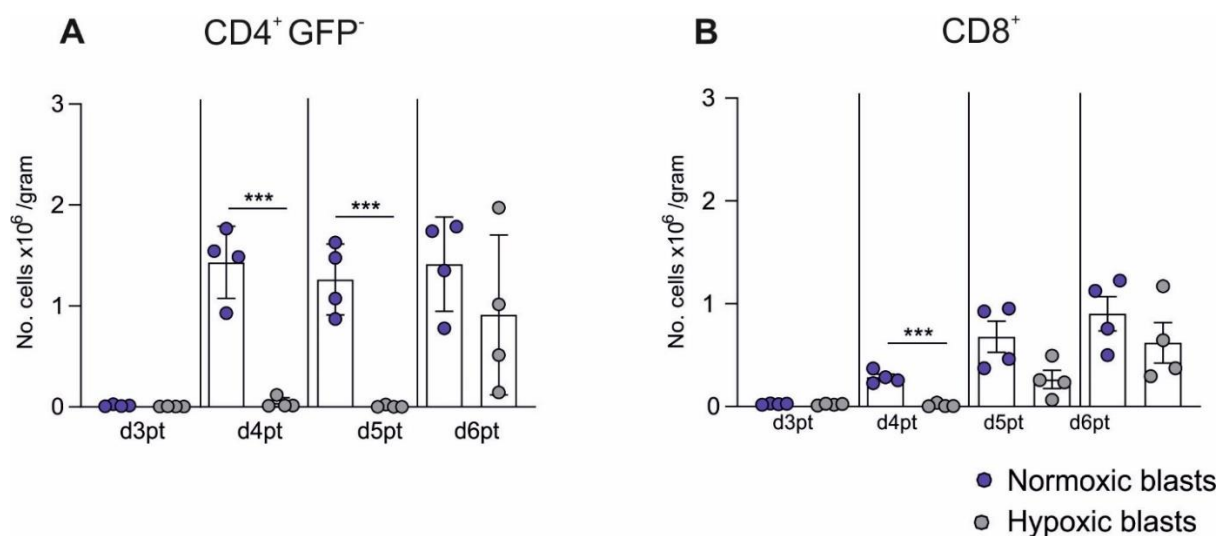


Figure 33. Reduced infiltration of endogenous T cells in the target tissue upon transfer of hypoxic T_{MBP} cells. EAE was induced as in Figure 26 by transfer of normoxic or hypoxic blasts. Number of endogenous $\alpha\beta TCR^+ CD4^+$ and $CD8^+$ T cells in the spinal cord. Each dot represents a single animal. Mean \pm SEM. Representative data of three independent experiments including at least 4 animals/group/time point. Statistical significance was assessed by non-parametric t-Test. * $P \leq 0.05$; ** $P \leq 0.01$; *** $P \leq 0.001$; **** $p < 0.0001$.

In the normoxic group, both $GFP^- CD4^+$ and $CD8^+$ T cells started to invade the CNS on day 4p.t. In the hypoxic group, $GFP^- CD4^+$ T cells were detectable on day 6p.t., whereas $CD8^+$ T cell invasion started on day 5p.t. At any time point, the number of $GFP^- CD4^+$ T cells and $CD8^+$ T cells was higher in the normoxic than in the hypoxic group.

We then measured in the same animals the production of pro-inflammatory cytokines in CNS-derived $GFP^- CD4^+$ and $CD8^+$ T cells (Figure 34). We could not observe any difference between the two cohorts in the percentage of cytokine positive $CD4^+$ or $CD8^+$ T cells. However, when we quantified the absolute number of $CD4^+$ or $CD8^+$ T cells able to produce cytokines, we observed that at any time point the number of $IFN\gamma$ -producing T cells was higher in the normoxic than in the hypoxic group. The number

of IL17a-producing T cells was significantly higher in the normoxic group on day 4 p.t. whereas no main differences were detected at the other time points.

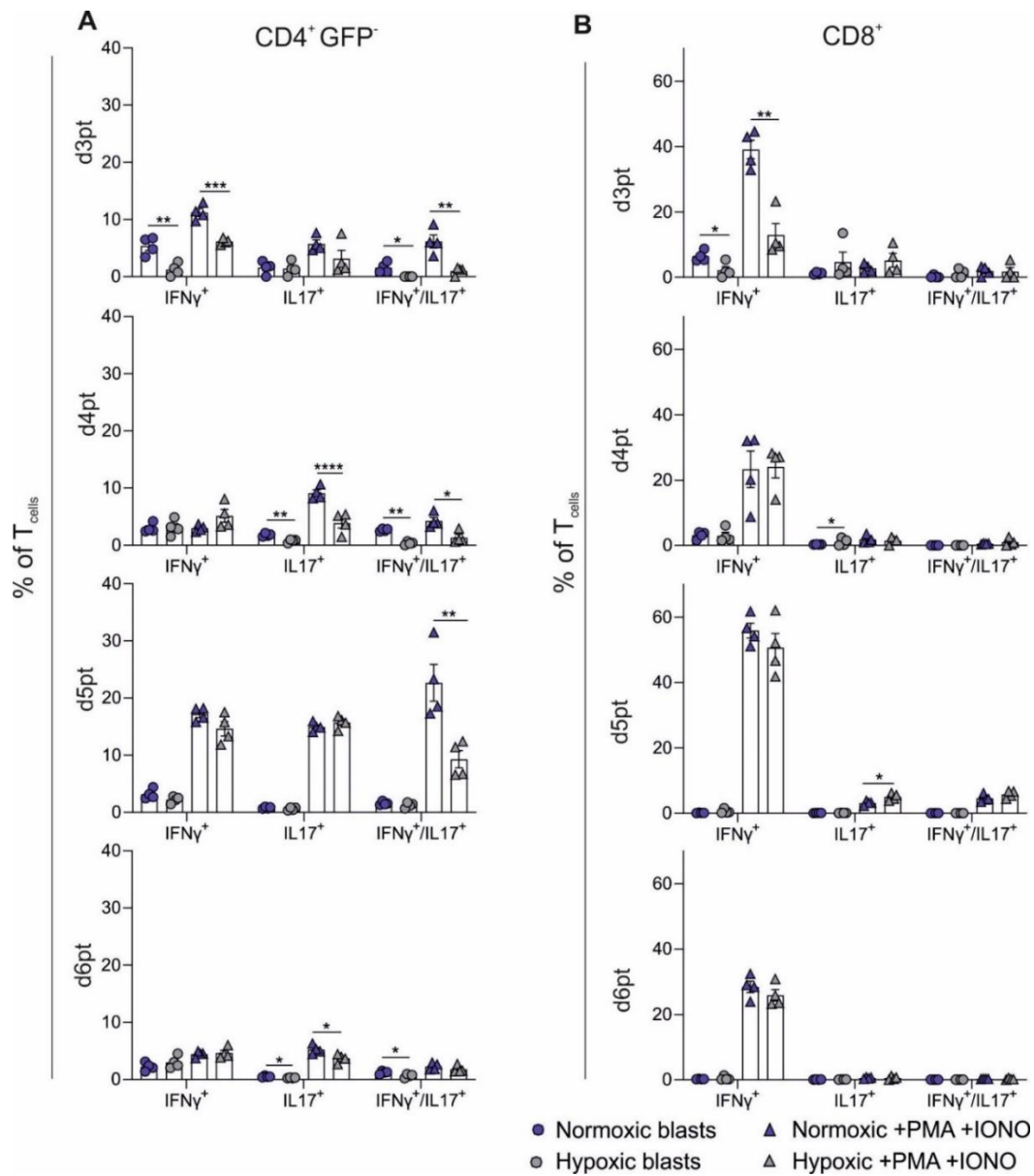


Figure 34. Endogenous T cells recruited in the CNS upon transfer of hypoxic T_{MBP} cells are not functionally impaired. EAE was induced as in Figure 26 by transfer of normoxic or hypoxic blasts. Percentage of $\alpha\beta$ TCR⁺ CD4⁺ (A) and CD8⁺ (B) endogenous T cells expressing IFN γ , IL17a and IFN γ /IL17a in spinal cord throughout the EAE course in steady state and upon PMA/IONO stimulation. Each dot represents a single animal. Mean \pm SEM. Representative data of three independent experiments including at least 4 animals/group/time point. Statistical significance was assessed by non-parametric t-Test. * $P \leq 0.05$; ** $P \leq 0.01$; *** $P \leq 0.001$; **** $P < 0.0001$.

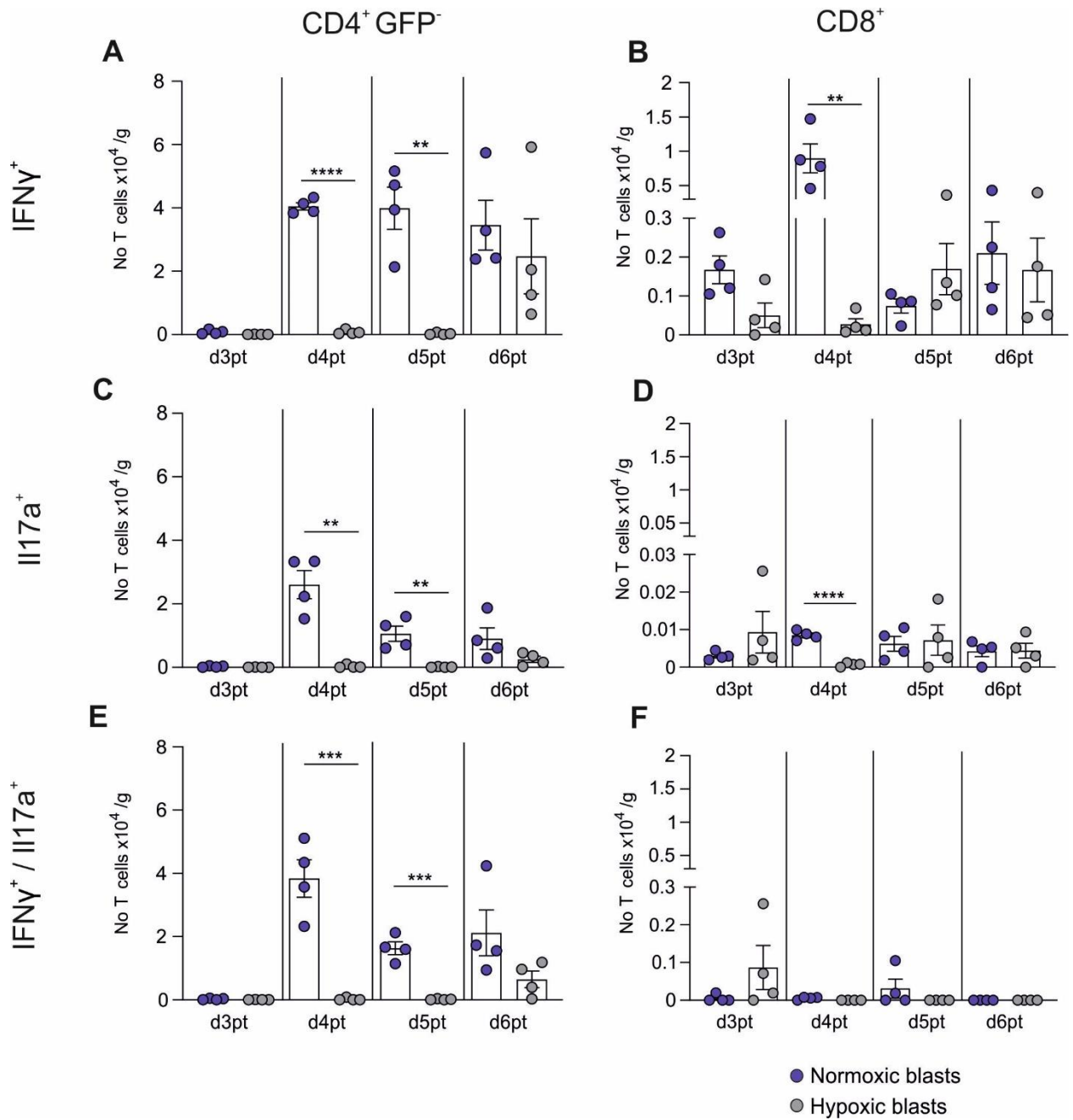


Figure 35. Activated endogenous T cells in the CNS are reduced upon transfer of hypoxic T_{MBP} cells. EAE was induced as in Figure 25 by transfer of normoxic or hypoxic blasts. Absolute number of $\alpha\beta TCR^+$ CD4⁺ (A) and CD8⁺ (B) endogenous T cells expressing IFN γ , IL17a and IFN γ /IL17a in spinal cord throughout the EAE course. Each dot represents a single animal. Mean \pm SEM. Representative data of three independent experiments including at least 4 animals/group/time point. Statistical significance was assessed by non-parametric t-Test. * $P \leq 0.05$; ** $P \leq 0.01$; *** $P \leq 0.001$; **** $P < 0.0001$.

Taken together, these results show an impaired and decreased ability of hypoxic T_{MBP} cells not only to invade the CNS but also to recruit endogenous T cells into the inflamed tissue.

4.16 Hypoxyprobe-1 allows the detection of the oxygenation status of T_{MBP} cells *in vitro*

We next aimed to detect if individual T_{MBP} cells can sense the level of oxygenation. For this purpose, we used the commercial system Hypoxyprobe-1 (HP1) from Hypoxyprobe, which can detect hypoxia as low as 10 mmHg oxygen. This system consists in the nitroimidazole compound pimonidazole hydrochloride in combination with a polyclonal antibody against pimonidazole adducts that can be detected by FACS or imaging techniques. Pimonidazole is reduced under hypoxic environments and binds to thiol-containing intracellular molecules such as glutathione and proteins. The resulting complexes can be detected by immuno-labelling (Raleigh et al., 1987). The more hypoxic a cell is, the more reduced is its inner environment, and therefore a higher amount of pimonidazole-SH adducts are formed and the staining is more intense.

We used the HP1 system to test the oxygenations status of T_{MBP} cells *in vitro*. To this end we cultured resting T_{MBP} cells under normoxic or hypoxic conditions in presence of pimonidazole. Two hours later, the samples were fixed, stained according to the manufacturer's protocol and acquired by flow cytometry. After two hours under a hypoxic environment, resting T_{MBP} cells showed an increase in the staining intensity of HP1 in comparison with the normoxic counterpart (Figure 36).

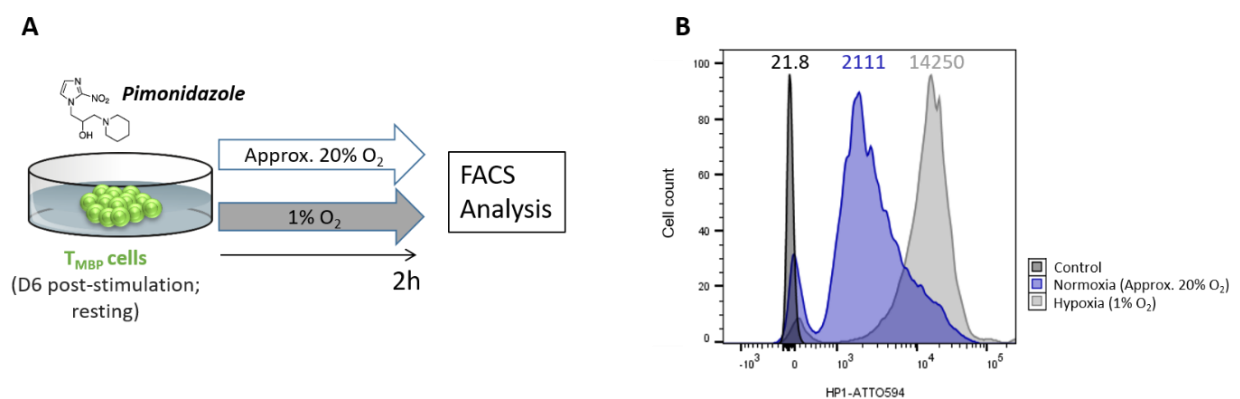


Figure 36. T_{MBP} cells *in vitro* display a more intense HP1-staining in hypoxic than in normoxic conditions. **A.** Scheme of the experimental set up. Resting T_{MBP} cells were cultured under either hypoxic or normoxic conditions for two hours in presence of pimonidazole. HP-1 binding was assessed two hours later by flow cytometry. **B.** Histogram overlay comparing the HP1-binding in T_{MBP} cells in hypoxic or normoxic conditions. Not stained T_{MBP} cells were used as negative control (dark grey). Numbers indicates the median fluorescence intensity in each group. Representative data of 2 independent experiments.

4.17 T cells in different organs displayed a different oxygenation status

We next investigated if the HP1 system would allow to identify the oxygenation level of $\alpha\beta\text{TCR}^+\text{GFP}^+$ T_{MBP} cells and $\alpha\beta\text{TCR}^+\text{GFP}^-$ endogenous T cells in peripheral organs and CNS tissue during tEAE. To this end, we transferred naïve recipient Lewis rats with *in vitro* activated T_{MBP} cells (Figure 37A). At different time points of the disease, namely on d1 p.t. (preclinical phase), d3 p.t. (disease onset) and d5 p.t. (disease peak), the animals received intraperitoneally pimonidazole and shortly after they were euthanized. At each time point, peripheral organs and spinal cord were retrieved and processed for FACS analysis. Single cell suspension underwent the manufacturer's protocol for HP1- staining.

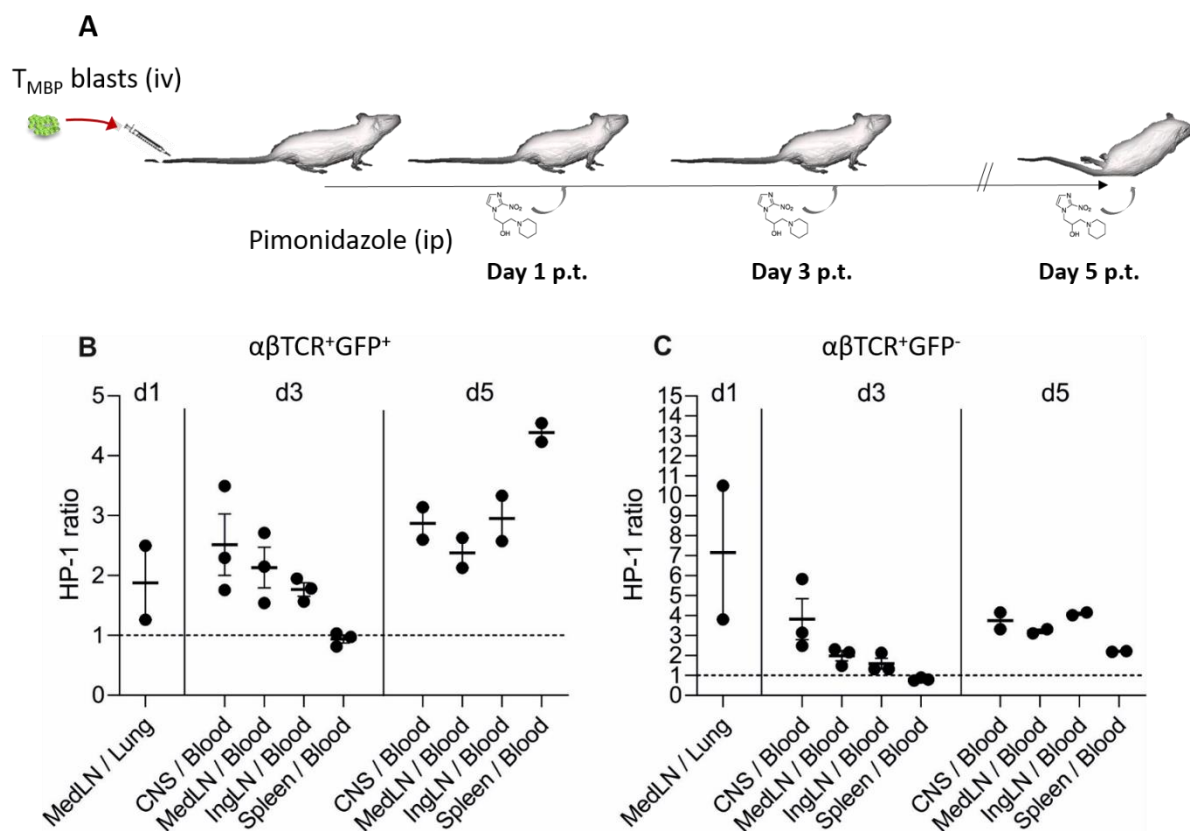


Figure 37. T cells in different organs displayed different levels of oxygenation through the course of EAE. **A.** Scheme of the experimental set up. EAE was induced in Lewis rat by transfer of T_{MBP} cell blasts. At the indicated time points the animals were injected intraperitoneally with pimonidazole shortly before being euthanized and their organs were analysed by FACS. **B.** Pairwise comparisons of HP1-binding intensity in T_{MBP} cells isolated from the indicated organs on day 1, day 3 and day 5 p.t. **C.** Corresponding quantification in $\alpha\beta\text{TCR}^+\text{GFP}^-$ endogenous T cells. Dotted lines are set at 1, indicating no differences between both compared organs. Mean \pm SEM. Representative data of 2 independent experiments including 2-3 animals/group.

By using this approach, we could detect differences in the oxygenation status of T cells in the investigated organs (Figure 37B). Due to the high variability in the pharmacokinetic of pimonidazole between the animals, we calculated per each animal and per each time point the ratio of intensity of HP1 detected in the different organs. At day 1 p.t., when T_{MBP} cells are almost exclusively located in

lung and mediastinal lymph nodes, the ratio of HP1 intensity in T_{MBP} cells between the mediastinal lymph nodes and the lung was 1.9 ± 0.6 , meaning that the oxygenation level of T_{MBP} cells in the lung was approximately the double than the one the same cells experimented in the mediastinal lymph nodes.

At the following time points, namely day 3 p.t. and day 5 p.t. T_{MBP} cells appeared in the blood that was used as reference tissue. At the disease onset (day 3 p.t.), T_{MBP} cells in peripheral tissues (mediastinal and inguinal lymph nodes) and in CNS, displayed on average at least 2-fold higher staining intensity of HP1 than the ones localized in the blood (mediastinal lymph nodes: 2.1 ± 0.3 ; inguinal lymph nodes 1.8 ± 0.1 ; CNS: 2.5 ± 0.5). T_{MBP} cells in the spleen at the same time point showed no difference in HP1 intensity compared with the blood (0.9 ± 0.1).

At the peak of the disease (day 5 p.t.) the ratios of HP1-staining intensity was qualitatively similar than what we observed at day 3 p.t., but displayed consistently increased values than the ones observed at the previous time point (mediastinal lymph nodes: 2.4 ± 0.3 ; inguinal lymph nodes: 3.0 ± 0.4 ; CNS: 2.8 ± 0.3). The staining intensity of HP1 observed in T_{MBP} cells localized in the spleen was on average 4.4 times higher than the one measured in blood isolated T_{MBP} cells.

The observed differences in the intensity of HP1-staining may also depend –at least in part- on the activation and metabolic status of T_{MBP} cells in the different tissues at the different time points of the disease course. To correct for those factors, we then performed HP-1 staining on $\alpha\beta TCR^+ GFP^-$ endogenous T cells in the same tissues and at the same time point as for T_{MBP} cells (*Figure 39C*). Overall, $\alpha\beta TCR^+ GFP^-$ T cells behaved very similar to T_{MBP} cells. More specifically, on day 1p.t. the staining intensity of HP1 of $\alpha\beta TCR^+ GFP^-$ cells in the mediastinal lymph nodes was 7.2 times higher (± 3.3) than the one measured in the same subset of cells isolated from the lung. On day 3p.t $\alpha\beta TCR^+ GFP^-$ T cells isolated from CNS, mediastinal lymph nodes and inguinal lymph nodes were more oxygenated than the ones in the blood (CNS: 3.8 ± 1 ; mediastinal lymph nodes: 2 ± 0.25 ; inguinal lymph nodes: 1.6 ± 0.3). At the same time point, $\alpha\beta TCR^+ GFP^-$ T cells isolated from spleen and blood did not show any difference (0.8 ± 0.1). At the peak of the disease (day 5 p.t.), $\alpha\beta TCR^+ GFP^-$ cells displayed an intensity of HP1-staining higher in all studied organs than in the blood (CNS: 3.7 ± 0.4 ; mediastinal lymph nodes: 3.2 ± 0.1 ; inguinal lymph nodes: 4.1 ± 0.1 ; spleen: 2.2 ± 0).

Taken together these results demonstrate that T cells can sense the level of oxygen and display different oxygenation statuses in different tissues, the lung and the CNS being the most and the least oxygenated organs, respectively.

4.18 *In vivo* hypoxia impairs T_{MBP} cell proliferation in EAE induced via the lung

Up to now our data showed that hypoxic condition impacted *in vitro* T_{MBP} cell activation and proliferation upon antigen exposure. Furthermore, *in vivo*, T cells were able to sense different environmental oxygen conditions. We next sought to clarify whether an oxygen-restricted environment would also affect the reactivation of autoreactive T_{EM} cells *in vivo*.

To this end, we exposed a whole animal to hypoxia (10% oxygen) and combined it with a model of EAE induced via immunisation in the lung, recently established in our lab (Nature, 2022). First we sought to investigate whether whole-body hypoxia would affect the proliferation of T_{MBP} cells reactivated through intratracheal immunisation with the cognate antigen. To this end, we stained resting T_{MBP} cells with the proliferation marker cell trace violet prior to injecting them into naïve recipient animals. After 3 hours, recipients were immunised into the lung by intratracheal administration of MBP emulsified in CFA. Immediately after intratracheal immunisation, the animals were divided in three experimental groups: a “0-24h” group was submitted to whole body hypoxia (10% O_2) immediately after immunisation for 24 hours; a second group, namely 24-48h, was kept under normoxic conditions for the first 24 hours after immunisation but submitted to the oxygen-restricted atmosphere for the following 24 hours; a third group was kept under normoxic conditions for 48 hours. 48 hours after immunisation, all animals were euthanised and their lungs and mediastinal lymph nodes were analysed by FACS. A detailed infographic depicting the experimental set up can be found in *Figure 38*.

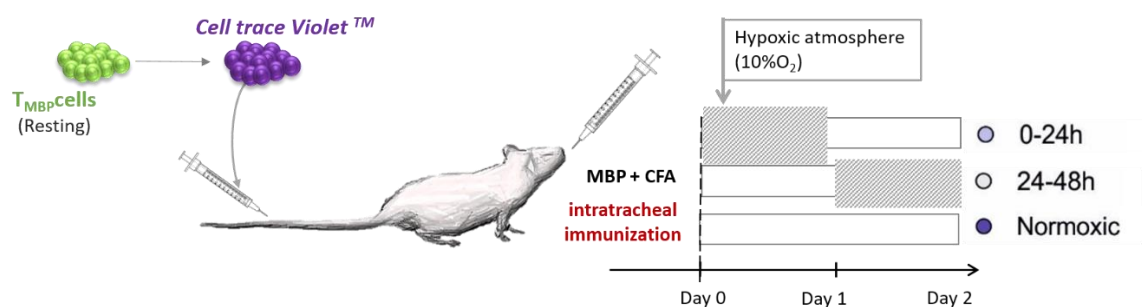


Figure 38. Effect of hypoxic environment on T_{MBP} cell reactivation into the lung. Scheme of the experimental set up. Lewis rats were transferred intravenously with resting T_{MBP} cells previously labelled with cell trace violet; shortly after, animals were immunised into the lung with an emulsion of MBP and CFA and exposed to the indicated ambient oxygen conditions. 48 hours after immunisation, all animals were euthanised and T_{MBP} cells retrieved from different organs were analysed by FACS.

We first measured the number of T_{MBP} cells in lungs and mediastinal lymph nodes (*Figure 39*). A significant lower number of T_{MBP} cells was found in the lungs of animals exposed to an oxygen-reduced atmosphere between 24 hours and 48 hours after lung immunisation in comparison with the normoxic

group (T_{MBP} cells per gram: Normoxic: $1.6 \times 10^6 \pm 0.2 \times 10^6$; 24-48h: $0.5 \times 10^6 \pm 0.2 \times 10^6$). The other group exposed to an oxygen-deprived atmosphere for the first 24 hours upon intratracheal immunisation, showed also a moderate, non-statistically significant reduction in T_{MBP} cell number ($0.9 \times 10^6 \pm 0.2 \times 10^6$) in comparison with the control group.

In the mediastinal lymph nodes, no statistical significant difference was found between any of the experimental groups. Nevertheless, both groups subjected to the oxygen-deprived environment showed a reduced number of T_{MBP} cells compared to the normoxic control (T_{MBP} cells per gram: Normoxic: $22 \times 10^6 \pm 0.7 \times 10^6$; 0-24h: $7.8 \times 10^6 \pm 1.5 \times 10^6$; 24-48h: $13.5 \times 10^6 \pm 1.9 \times 10^6$).

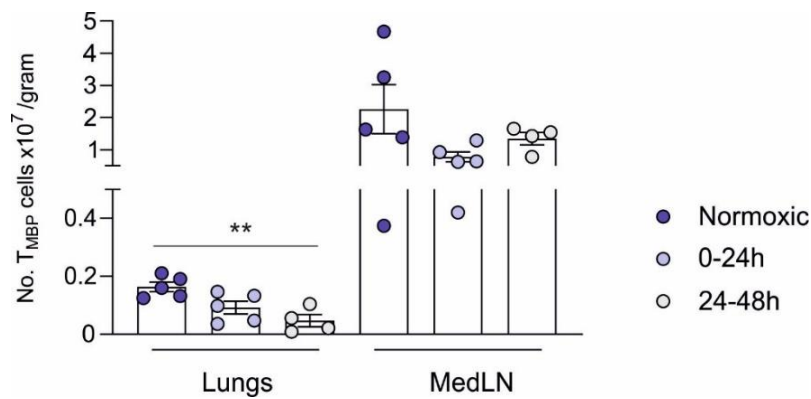


Figure 39. Hypoxia affects T_{MBP} cell proliferation in vivo upon lung immunisation. Number of T_{MBP} cells in lungs and mediastinal lymph nodes 48 hours after intra-lung immunisation of animals previously transferred with resting T_{MBP} cells. Each dot represents one animal. Mean \pm SEM. Representative data of three independent experiments. Statistical significance was assessed by one-way ANOVA with Turkey's correction for multiple comparisons. **: $p < 0.01$.

The inclusion of the proliferation dye cell trace violet in our experimental design allowed us to perform a more refined analysis of the proliferative activity of T_{MBP} cells in the different experimental groups. *Figures 40A* and *41A* show representative graphs of the distribution of the intensity of the proliferation dye in T_{MBP} cells isolated from lung and mediastinal lymph nodes in each experimental group. In the lung, the percentage of dividing T_{MBP} cells was significantly reduced in the 24-48h group ($58\% \pm 2\%$) when compared with the normoxic group ($66\% \pm 1.3\%$) while no differences could be detected between the control group and the group exposed to the oxygen-restricted environment directly upon immunisation (0-24h: $59\% \pm 2\%$; *Figure 42B*). Division and expansion indices were significantly reduced in both hypoxic groups compared to the normoxic control (*Figure 40C-D*).

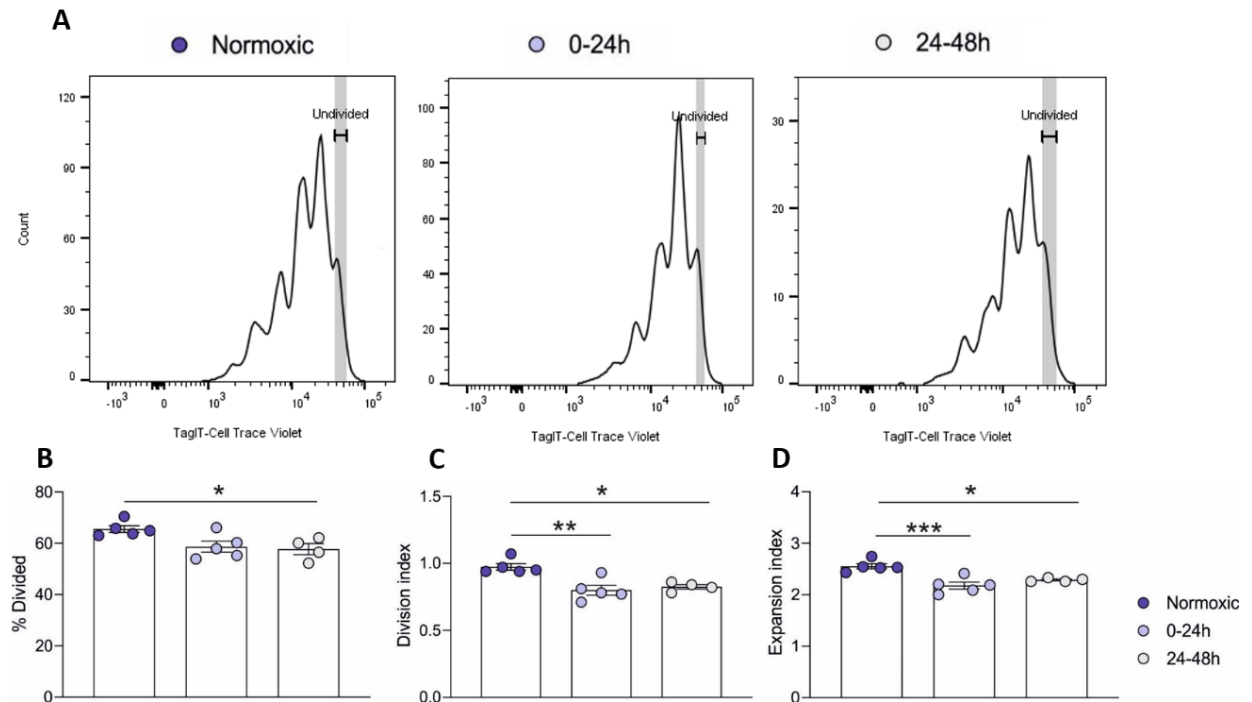


Figure 40. T_{MBP} cell proliferation in the lung is affected by a hypoxic environment. A-D. Animals were treated as in Figure 40. T_{MBP} cell analysis was performed in lung-isolated cells 48 hours after in situ immunisation. **A.** T_{MBP} cell proliferation measured by dilution of the cell trace violet. **B.** Percentage of T_{MBP} cells that underwent at least one division cycle. **C.** Division index (Number of divisions for each cell). **D.** Expansion index (Ratio between the total numbers of T_{MBP} cells at the end and at the beginning of the experiment). **B-D.** Mean \pm SEM. Each dot represents one animal. Statistical significance was assessed by one-way ANOVA with Tukey's correction for multiple comparisons. Representative data of 2 independent experiments including 4-5 animals per group. * $p \leq 0.05$; ** $p \leq 0.01$; *** $p \leq 0.001$.

In the mediastinal lymph nodes the results pointed in the same direction but the differences were even more accentuated. Specifically, all the analysed indices (percentage of dividing cells, division and expansion indices) were significantly reduced in the two experimental groups submitted to the decreased oxygen environments compared to the normoxic group. Of note, all the parameters were significantly lower in the experimental group exposed to the oxygen-restricted environment immediately after immunisation than in the group exposed to the hypoxic environment 24 hours after immunisation (Figure 41).

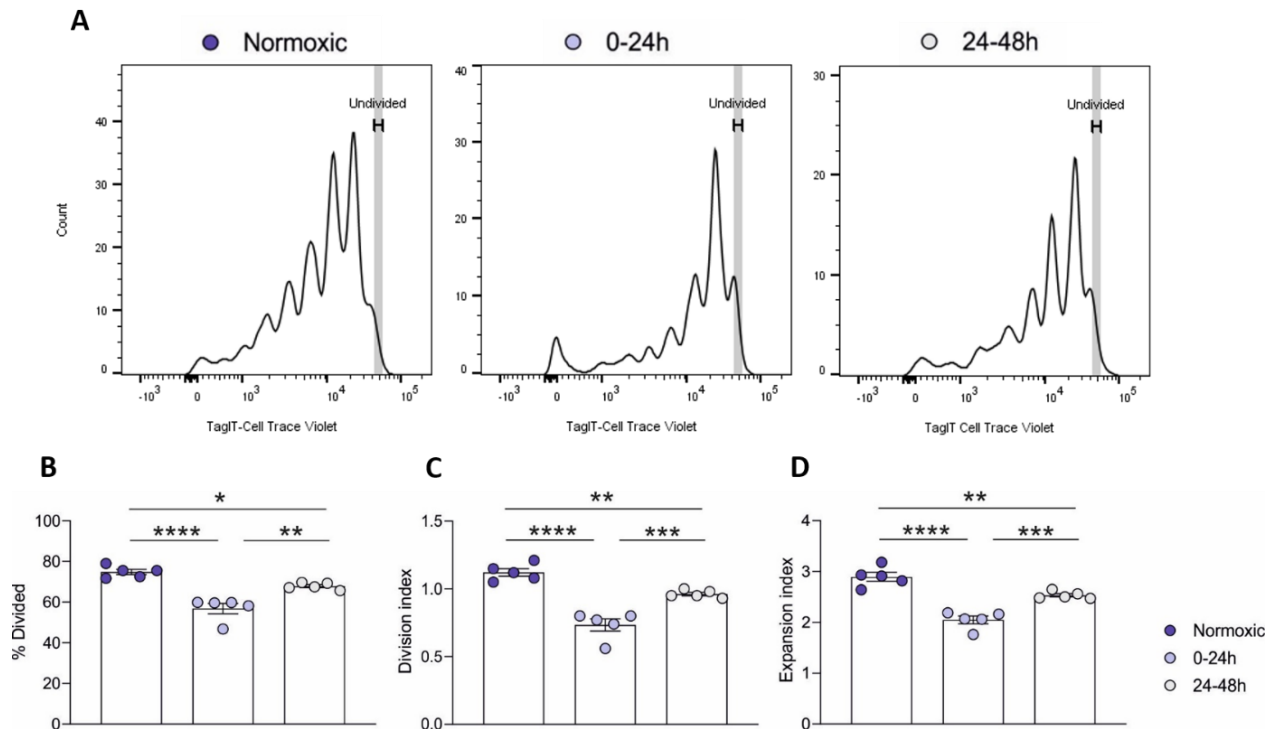


Figure 41. Proliferative status of T_{MBP} cells in the mediastinal lymph nodes is affected by a hypoxic environment. A-D. Animals were treated as in Figure 40. T_{MBP} cell analysis was performed in cells isolated from the mediastinal lymph nodes 48 hours after in situ immunisation. **A.** T_{MBP} cell proliferation measured by dilution of the cell trace violet. **B.** Percentage of T_{MBP} cells that underwent at least one division cycle. **C.** Division index. **D.** Expansion index. **B-D.** Mean \pm SEM. Each dot represents one animal. Statistical significance was assessed by one-way ANOVA with Tukey's correction for multiple comparisons. Representative data of 2 independent experiments including 4-5 animals per group. *, $p \leq 0.05$; **, $p \leq 0.01$; ***, $p \leq 0.001$.

Taken together, these results suggest that the exposure to whole body hypoxia impairs the proliferation of T_{MBP} cells in the lung upon in situ reactivation. The exposure to an oxygen-reduced atmosphere for 24 hours immediately after antigen exposure was able to impair the proliferation of T_{MBP} cells in lungs and mediastinal lymph nodes 48h after reactivation. The dampening effect on proliferation in lung-derived T_{MBP} cells was even more prominent in the group submitted to hypoxia 24 hours after immunisation.

4.19 *In vivo* hypoxia impairs cytokine expression in T_{MBP} cells in EAE induced via the lung.

We next asked whether the *in vivo* effect of whole-body hypoxia on T_{MBP} cell proliferation observed at 48h after reactivation in the lung was associated with impaired cytokine production.

In T_{MBP} cell isolated from lung or mediastinal lymph nodes 48 hours after immunisation, we did not detect any differences in IFN γ and IL17a production between the normoxic group and the two experimental groups exposed to hypoxia at different time points (*Figure 42*).

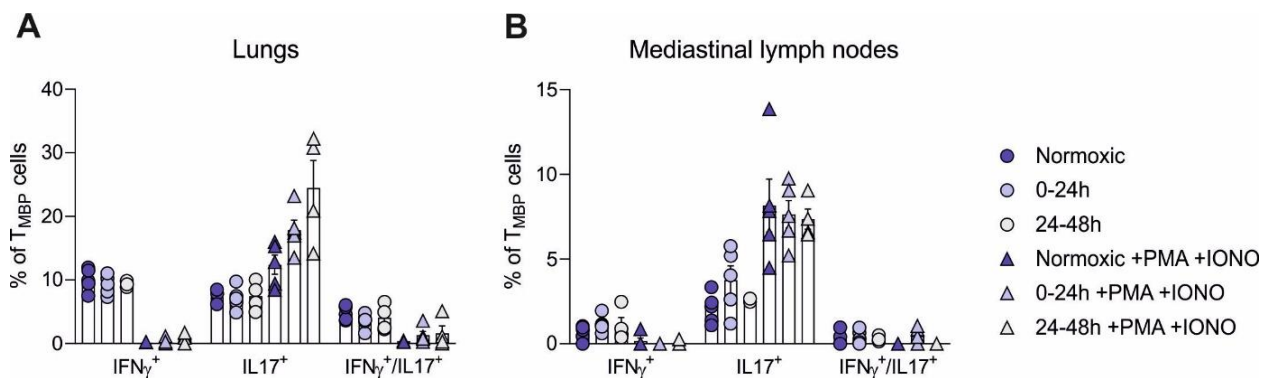


Figure 42. Hypoxia does not affect cytokine production by T_{MBP} at 48h after reactivation in the lung. A-B. Animals were treated as in *Figure 40*. FACS quantification of T_{MBP} cells producing pro-inflammatory cytokine in steady state or upon stimulation with PMA/IONO. Analysis was performed in T_{MBP} cells isolated from lung (A) or mediastinal lymph nodes (B) 48 hours after intra-lung immunisation in animals kept in the indicated environmental oxygen conditions. Mean \pm SEM. Each dot represents one animal. Representative data of 2 independent experiments including 4-5 animals per group.

We reasoned that cytokine production by T_{MBP} cells was maximally affected *in vitro* when T cells were exposed to hypoxia in the first 24 hours upon antigen encounter. Therefore, we set-up to assess cytokine production in lung-derived T_{MBP} cells 24 hours after in situ antigen exposure in animal kept in normoxic or hypoxic conditions. The experimental set up is depicted in *Figure 43A*.

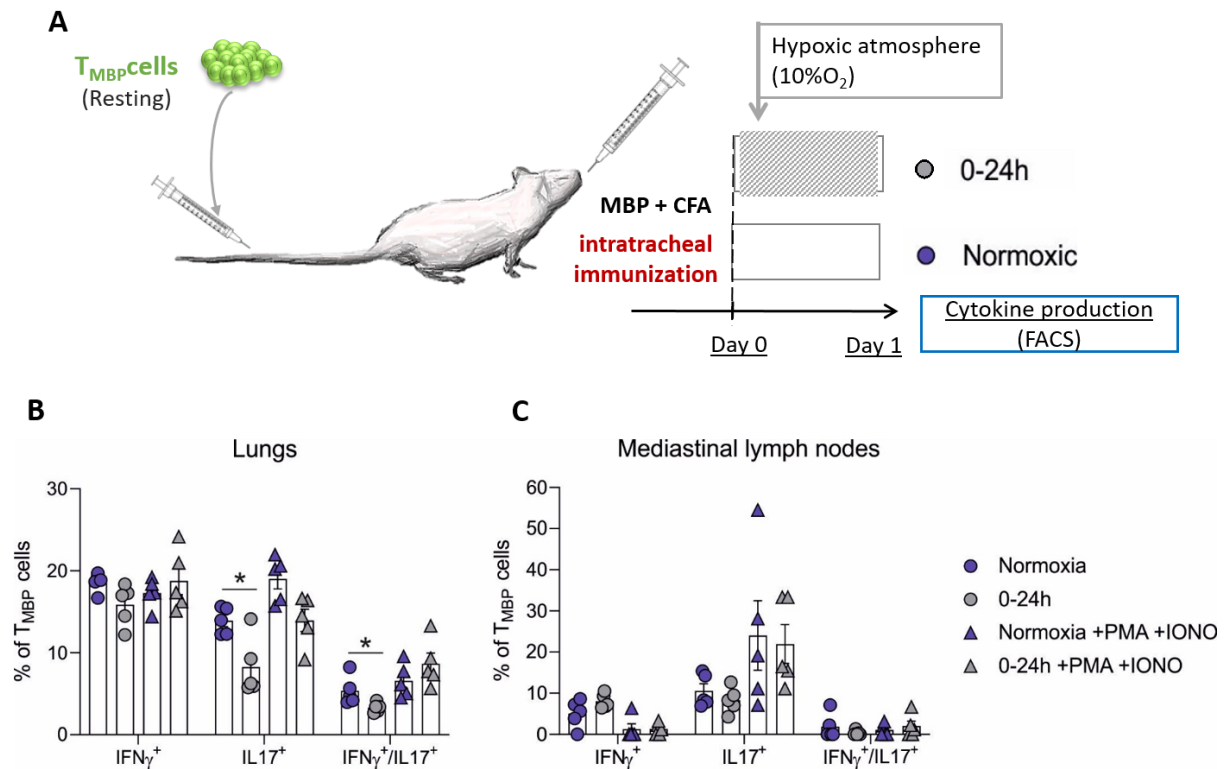


Figure 43. Hypoxia affects cytokine production by T_{MBP} at 24h after reactivation in the lung. **A.** Scheme of the experimental set up. Rats were transferred intravenously with resting T_{MBP} cells and shortly after immunised into the lung. Immediately after immunisation the animals were submitted to normoxic or hypoxic conditions. **B-C.** FACS quantification of T_{MBP} cells producing IFN γ , IL17a or IFN γ and IL17⁺ in lungs (**B**) and mediastinal lymph nodes (**C**) as in Fig. 8. Analysis was performed 24h after intra-lung immunisation. Mean \pm SEM. Each dot represents one animal. Representative dat of 2 independent experiments including 4-5 animals per group. Statistical significance of pairwise comparisons was assessed by non-parametric t-Test. *= $p \leq 0.05$.

The percentage of T_{MBP} cells expressing pro-inflammatory cytokines measured in the lung at steady-state was higher at 24 hours than at 48 hours (*Figures 43 and 42*, respectively) suggesting that the activation programme in T_{MBP} cells upon lung reactivation is very rapidly induced but also very rapidly declines. Notably, we observed that in the lung the percentage of T_{MBP} cells expressing pro-inflammatory cytokines was lower in animals exposed to an oxygen-restricted environment compared to the normoxic counterpart (*Figure 42B*). This reduced expression of cytokines in the hypoxic group reached statistical significance in IL17⁺ T_{MBP} cells (Normoxic: 13.9 ± 0.7 ; 0-24h: 8.2 ± 1.6) and in the IFN γ ⁺/IL17⁺ subset of T_{MBP} cells (Normoxic: $5.4\% \pm 0.8\%$; 0-24h: $3.3\% \pm 0.3\%$) but not in the IFN γ ⁺-producing T_{MBP} cells (Normoxic: $18.6\% \pm 0.5\%$; 0-24h: $15.9\% \pm 1.1\%$). No difference between the two experimental groups was observed in T_{MBP} cells isolated at the same time point from mediastinal lymph nodes (*Figure 42C*).

4.20 *In vivo* hypoxia does not induce a main shift toward a regulatory phenotype in T_{MBP} cells in lung-EAE

We next used the *in vivo* set-up for investigating if the oxygen-deprived environment would induce a shift in T_{MBP} cells toward a regulatory phenotype by measuring the expression of FOXP3 24 and 48 hours upon lung immunisation (Figure 44). At 24 hours after immunisation, a very low percentage of FOXP3⁺ T_{MBP} cells was detectable in lung (0.4% ±0.2%) and mediastinal lymph nodes (3.3% ±1.7%) in normoxic conditions. No quantitative or qualitative changes were induced by subjecting the animals to hypoxia (Figure 44A). At 48 hours upon lung immunisation, 0.4% ±0.1% and 5.7% ±1.8% of FOXP3⁺ T_{MBP} cells could be detected in the lungs and mediastinal lymph nodes, respectively. Upon exposure of the animals to hypoxic conditions, we observed in the lung a statistical significant increase in FOXP3⁺ T_{MBP} cells in the group exposed to hypoxia 24 hours after immunisation. However, the percentage of FOXP3⁺ T_{MBP} cells remained low (2.7% ±0.9%). In mediastinal lymph nodes, at the same time point no differences were observed in FOXP3⁺ T_{MBP} cells; however, the 24-48h group displayed lower levels of FOXP3 expression (0.9% ±0.3%) that did not reach the statistical significance compared to the other two experimental groups (Figure 44B).

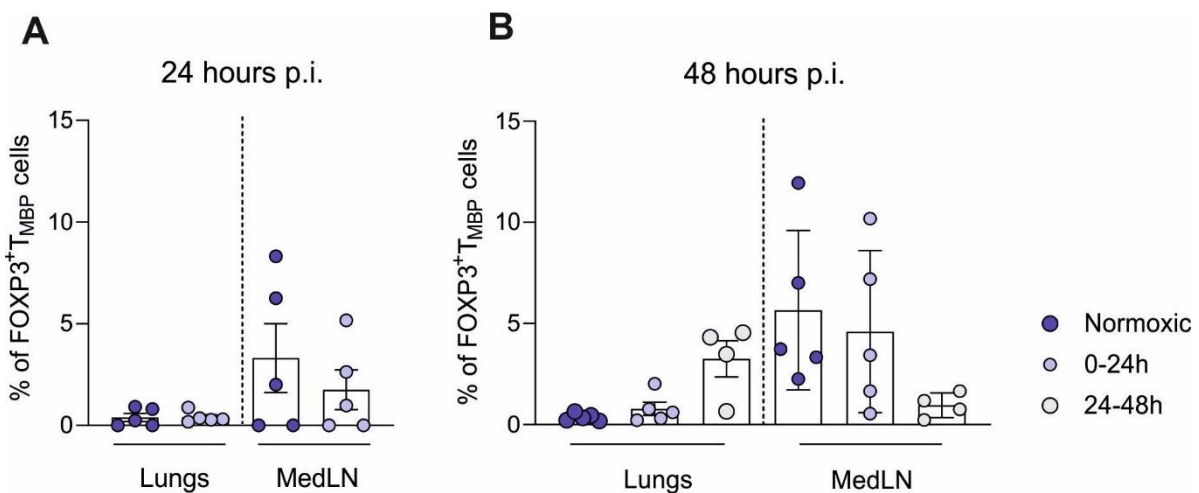


Figure 44. Hypoxia promotes a mild increase in the expression of FOXP3 in T_{MBP} cells in the lungs. **A.** Percentage of FOXP3⁺ T_{MBP} cells assessed 24 hours after intra-lung immunisation in animals kept in normoxic or hypoxic condition. Flow cytometry. **B.** Percentage of FOXP3⁺ T_{MBP} cells assessed 48 hours after intra-lung immunisation in animals kept in normoxic conditions or in the two indicated hypoxic conditions. Flow cytometry. **A-B.** Mean ± SEM. Each dot represents one animal. Representative data of 2 independent experiments including 4-5 animals per group. Statistical significance was assessed by non-parametric t-Test (**A**) or by one-way ANOVA with Tukey's correction for multiple comparisons (**B**). *= $p \leq 0.05$, **= $p \leq 0.01$.

4.21 *In vivo* hypoxia affects the encephalitogenic potential of T_{MBP} cells

Finally, we investigated if the whole-body hypoxia would impair the encephalitogenic potential of T_{MBP} cells stimulated *in vivo*. To this end, as described in *Figure 43*, we induced EAE via the lung in animals previously transferred with resting T_{MBP} cells. The animals were then kept in hypoxic condition for the first 24 hours after immunisation or for the interval 24-48 hours after immunisation. Animals kept in normoxic conditions were used as control. Clinical course was assessed daily (*Figure 45A*).

All animals developed clinical symptoms. In the normoxic group the disease started on day 4 p.i. whereas in the two experimental groups exposed to an oxygen-restricted atmosphere the EAE started one day later (*Figure 45B*). The onset and peak disease scores showed no differences between the groups (*Figure 45C and D*). However, the disease lasted longer and was overall more severe in the normoxic group as reflected by the cumulative EAE score that was significantly higher in the normoxic than in the hypoxic groups (Normoxic: 6.4 ± 0.3 ; 0-24h: 3.9 ± 0.6 ; 24-48h: 3.3 ± 0.3). No differences were found between the cumulative EAE score of the two experimental groups exposed at different times to the oxygen-restricted environment (*Figure 45F*).

Remarkably, whereas all the animal kept in normoxic conditions developed a classical EAE characterized by ascendant paralysis, an elevated proportion of animals in the hypoxic groups developed “atypical” EAE symptoms. Three out of the 5 animals in the 0-24h group and 4 out of the 5 animals in the 24-48h group showed ataxia and gait disturbance with no signs of paresis nor loss of the tail tone (*Figure 45B*).

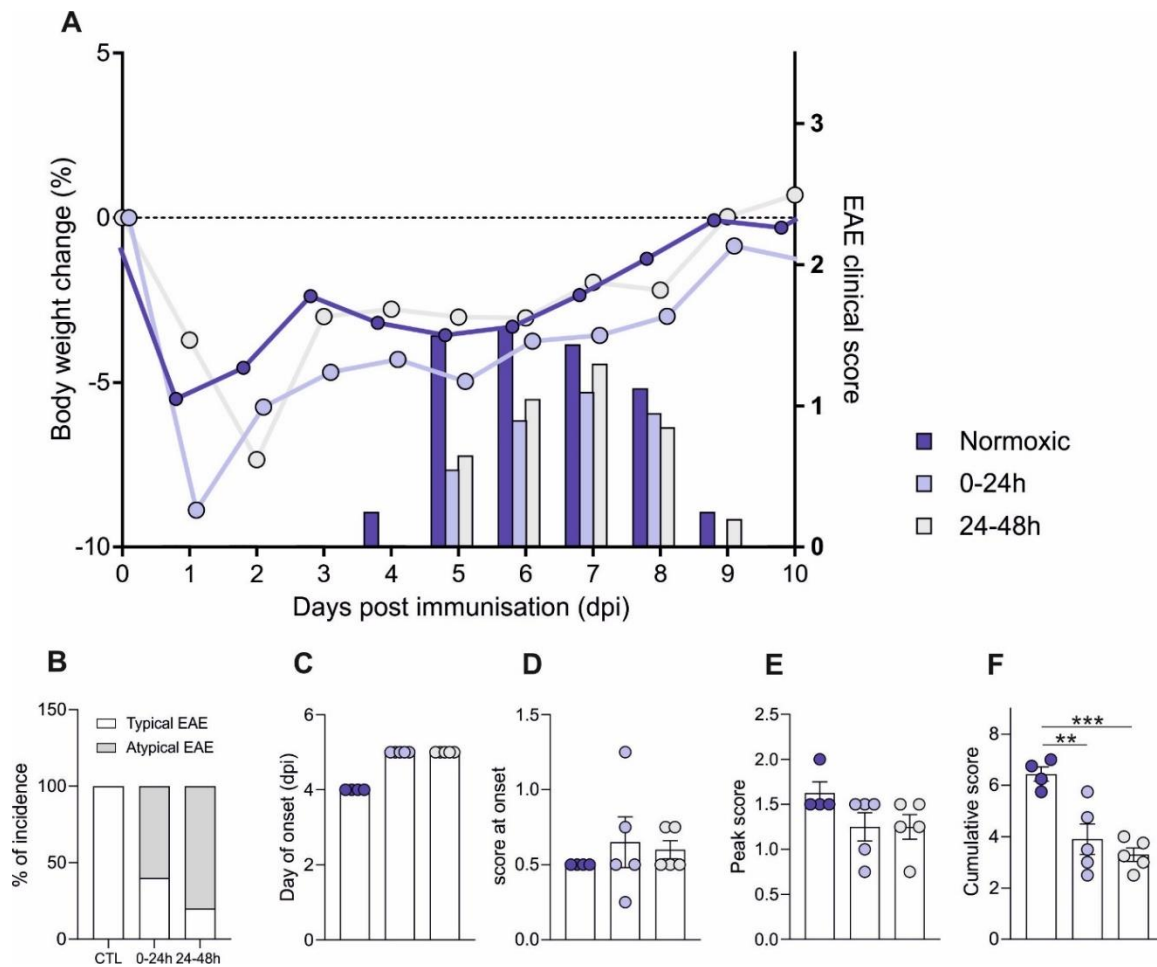


Figure 45. Hypoxia induce clinical differences in EAE induced via the lung. EAE was induced via intra-lung immunisation in animals previously transferred with resting T_{MBP} cells. Immediately after, animals were exposed, or not, to an oxygen deprived atmosphere as indicated. **A.** Body weight changes (lines) and clinical score (bars) during the course of EAE. **B.** Global incidence (%) and percentage of animals with typical and atypical symptoms. **C.** Disease onset (days). **D.** Clinical score at disease onset. **E.** Clinical score at disease peak. **F.** Cumulative score. **C–F.** Mean \pm SEM. Each dot represents one animal. Representative dat of 2 independent experiments including 4-5 animals per group. Statistical significance was assessed by one-way ANOVA with Tukey's correction for multiple comparisons. *** $P \leq 0.01$; ** $p \leq 0.001$

Taken together, these *in vivo* results suggest that the exposure of T_{MBP} cells to an oxygen-restricted environment within the first 48h after their reactivation by intra-lung immunisation affects T_{MBP} cell proliferation and activation. Furthermore, this hypoxic stimulus also impacts the clinical phase with a disease course that is less severe and frequently atypical.

5. Discussion

Multiple sclerosis is an autoimmune, inflammatory disorder affecting the central nervous system. Despite intense investigation, the pathogenesis of the disease is still under discussion. Based also on experimental data, it is thought that T cells reactive against CNS antigen are the culprits of the disease (Hohlfeld et al., 2016; Sospedra & Martin, 2016). These autoreactive T cells, which can be also present in the immune repertoire of healthy people, are presumably activated in the peripheral organs before attacking the CNS. Where and how this peripheral activation takes place remain unclear. Gut and lung, due to their direct connection with the external environment, have been suggested as potential trigger sites (Ochoa-Repáraz et al., 2009; Odoardi et al., 2012). A similar role has also been ascribed to cervical lymph nodes and more recently to the dural sinus due to their potential role in draining CNS antigens (Rustenhoven et al., 2021).

Regarding the lung as a potential trigger site, epidemiological reports indicate that smoking, chronic lung disease and upper respiratory infections can play a role in MS (Ascherio, 2013; Bjornevik et al., 2022; Jafari & Hintzen, 2011). Furthermore, experimental data also suggested that the lung could play a role in CNS autoimmunity (Odoardi et al., 2012). However, the role of the lung in initiating autoimmune processes has not yet been thoroughly investigated.

To address this question, we established a system to induce EAE via intratracheal immunisation of animals previously transferred with encephalitogenic T_{EM} cells, i.e. the T cells reached the lung directly via the trachea rather than via the bloodstream as in intravenous transfer. Surprisingly, we observed that doses of antigen 75 to 150 times lower than the ones classically used in protocols for subcutaneous immunisation triggered a severe EAE. A mild form of the disease was induced by immunising the animals with a 750 to 1500-fold reduced dose.

Such a highly efficient capacity to reactivate encephalitogenic T cells prompted us to further study the unique features of the lung that may explain its special role in triggering CNS autoimmunity. The main task for the lungs in mammal organisms is to provide the whole organism with the oxygen required for cell respiration and therefore for proper cell function. By virtue of its intricate and folded anatomy, in a human adult the lung represents about 70 m² of direct contact surface with the external environment (Wiebe & Laursen, 1998). Because of its nature of being open to the outside environment, the lung is equipped with a specialised immune system and it is colonized by a distinct microbiome to provide a barrier to pathogens (O'Dwyer et al., 2016). In a work recently published by our group (Hosang et al., 2022), we could show that the lung microbiota modulates CNS autoimmunity, not by affecting the local immune response but rather by exerting a remote control on microglial activation status through LPS, a main component of the bacterial cellular wall.

As a repercussion of their main function, the lungs and the airways represent one of the most oxygenated tissues in mammals (Ast & Mootha, 2019; Caldwell et al., 2001; De Santis & Singer, 2015) and it is well documented that the oxygen level can induce pleiotropic effects on the immune function. In this work we investigated the effect that an oxygen-rich lung microenvironment may have on autoreactive T cells in the context of CNS autoimmunity.

Overall, our results showed that the function of T cells by oxygen levels, both *in vitro* and *in vivo*.

In vitro, upon antigen stimulation under hypoxic conditions (1% oxygen), T_{MBP} cells displayed a reduction in their proliferation as well as a decrease in cytokine production. These results confirmed numerous previous works reporting a reduced proliferation of CD8⁺ T cells cultured under poorly oxygenated atmospheres (1 to 5 % O₂) (Atkuri et al., 2005, 2007; Larbi et al., 2010; Loeffler et al., 1992; Naldini et al., 1997), as well as a decrease in the production of cytokines such IFN γ and IL-2 (Caldwell et al., 2001; Kim et al., 2008; Roman et al., 2010; Zuckerberg et al., 1994).

Despite the severe hypoxia, the viability of CD4⁺ T cells was not impaired. Similar observations were obtained upon stimulation of CD8⁺ T cells under hypoxic condition (Gropper et al., 2017) and are perhaps not so surprising since T cells *in vivo* are activated in lymph nodes where the oxygen levels range from 0.5 to 6% (Huang et al., 2007). The lack of the effect of hypoxia on viability also implies that during activation T cells adapt rapidly to the hypoxic condition rather than undergoing a selection process.

Furthermore, hypoxia did not promote the acquisition of a regulatory phenotype in T_{MBP} cells. The discrepancy with previous data (Clambey et al., 2012; McNamee et al., 2013) can be due to the different type of T cells used in the set-ups. Most of the previous data is based on naïve-T cells (McNamee et al., 2013). In our experiments, we used antigen-experience effector memory T cells that are already polarized toward a Th1/Th17 phenotype and are therefore much less prone to reprogram their phenotype compared to naïve T cells.

Upon antigen encounter, T cells undergo profound transcriptional and metabolic changes with the final goal to cover the energetic demands and produce the biosynthetic precursors required for T cell proliferation and effector function very rapidly (Chang et al., 2013). This reprogramming occurs within the first 24 hours after antigen encounter when T cells depends critically on translational induction of metabolic enzymes and very rapidly up-regulate genes related to effector function. During the subsequent 24-72 hours, T cells actively proliferate and mRNA translation of ribosomal proteins is markedly up-regulated (Ricciardi et al., 2018). Our results indicate that oxygen levels could crucially affect both these stages, independently. Indeed T cell effector functions, such as cytokine production were maximally affected when T_{MBP} cells were submitted to the hypoxic stimulus within the first 24

hours upon antigen encounter. Conversely, T_{MBP} cell proliferation was mainly affected when the hypoxic stimulus was provided in the subsequent 24 hours after antigen recognition.

To further gauge the global impact of oxygen on T_{EM} cells during the reactivation process, we performed a transcriptome study comparing T_{MBP} cells stimulated *in vitro* under normoxic or hypoxic conditions at different time points after antigen encounter. We observed that the hypoxic stimulus did not block the transcriptional programme set in motion by the antigen stimulation. Indeed the number of upregulated genes in hypoxic samples exceeded by far the number of downregulated genes in the first 24 hours. Furthermore, when the two variables i.e. time after antigen stimulation and environmental conditions were taken into account by PC analysis, the largest source of variance between samples was time after stimulation, further indicating that oxygen is mainly involved in shaping the ongoing activation program rather than blocking it. These data fit with the fact that T cells are able to perform their function also in low-oxygen environments such as found in the lymph nodes or in inflammatory sites.

We then performed GSEA to understand which molecular pathways induced in T cells by antigen encounter are impacted by oxygen. Consistently with our flow cytometry data, we observed that programme linked to T cell activation and proliferation were down-regulated in T cells stimulated under normoxic conditions. Genes related to the $IFN\gamma$ pathway and the G2/M checkpoint of the cell cycle were specially affected. Of note, these genes were already significantly down-regulated 3h after antigen encounter, indicating a very early effect of oxygen on T cell function. It is known that immediately after antigen encounter, T cells undergo metabolic changes, switching towards a glycolytic profile. Such changes are not only a requirement for the latter proliferation of the T cells, but are also an indispensable requirement for the successful performance of their effector functions (Chang et al., 2013). Indeed, the gene sets more consistently and significantly upregulated in the hypoxic group were “response to hypoxic stimulus” and “glycolysis”.

The metabolic switch to glycolysis in all eukaryotic cells including immune cells in a hypoxic environment has been extensively studied (Cho et al., 2019; Michiels, 2004; Taylor & Colgan, 2017). Such metabolic change is mainly but not exclusively orchestrated by transcription factors belonging to the hypoxia inducible factors (HIF) family, which trigger a set of transcriptional programme for ensuring metabolic and functional adaptation to oxygen shortages (Semenza, 2011, 2014). Indeed, in our analysis, transcripts directly regulated by HIF1 were among the most upregulated genes under hypoxic conditions. Hypoxia can regulate the glycolytic pathway at many levels: the lack of oxygen necessary for the oxidative phosphorylation (OXPHOS) will inhibit this mechanism and the molecules of ATP available in the cell will be consumed, thus preventing them to exert their usual allosteric

inhibition on the principal glycolytic enzymes (Henderson, 1969). At the same time, HIF1 α will induce the expression of solute transporters, e.g. GLUT1, of several rate-limiting glycolytic enzymes and will mediated suppression of OXPHOS (Palmer et al., 2015). Several other mechanisms are also responsible for the regulation of glycolysis under hypoxic conditions, including the activation of the PI3K/Akt pathway (Xie et al., 2019) and post-translational mechanisms triggering glycolytic enzymes (Agbor et al., 2011).

Our transcriptome data indicated that the metabolic switch to glycolysis was not a prerogative of T cells stimulated in hypoxic conditions. Also in the normoxic group, effector T cells upregulated glycolytic genes. These results were expected because, upon TCR engagement effector T cells are known to undergo a metabolic reprogramming called the Warburg effect in which they shift their metabolism towards aerobic glycolysis to the detriment of oxidative phosphorylation despite the availability of oxygen (Warburg, 1956; Peng et al., 2016; Kouidhi et al., 2017; Salmond, 2018).

Cluster analysis of the expression of glycolytic enzymes helped to discriminate between common and divergent gene sets in the two experimental conditions. Transcripts encoding proteins involved in the core-enzymatic process of glycolysis were overexpressed to a similar extent in both experimental groups compared to basal conditions at any analysed time point. However, a specific cluster of genes encoding for rate-limiting glycolytic enzymes such as hexokinase (*Hk*) and Phosphofructokinase (*Pfk*) were selectively upregulated in the hypoxic cohort. These enzymes catalyse reactions that determine the fate of glucose molecules in the glycolytic pathway and are crucial in the regulation of glycolytic flux (Chaneton et al., 2012; Jurica et al., 1998; Kemp & Gunasekera, 2002). Glycolysis supports cellular function energetically but it is also pivotal for the acquisition of effector functions (Peng et al., 2016) and cytokine synthesis (Chang et al., 2013). Therefore, it is plausible that oxygen levels can finely tune T cell function by directly controlling the glycolytic flow. Further studies including a detailed metabolic profiling will foreseeably shed more light on the effect that low tension of oxygen has on T cell function.

The *in vitro* data convincingly showed that the local oxygen concentrations shape the transcriptional profile and the effector function of antigen-experienced effector T cells. These studies also imply that T cells are extremely plastic and able to perform their tasks in a large range of oxygen conditions. This capacity of adaptation can be of relevance *in vivo*. It has to be kept in mind that T cells *in vivo*, in order to exert their effector functions, circulate throughout different organs where they are exposed to different levels of oxygen. Indeed direct measurements of oxygen inside the tissue by microelectrode demonstrated that the oxygen ranged from 0.65% to 13% approximately, the lungs having the highest and some regions of the small intestine the lowest (Braun et al., 2001; Caldwell et al., 2001; Keeley &

Mann, 2019). More recently, the use of nitroimidazole compounds, which form stable covalent adducts with cellular proteins under hypoxia, allowed for the measurement of oxygen levels in several tissues at single cell level (Arteel et al., 1998; Bergeron et al., 1999; Shabsigh et al., 2001). By using this approach, we showed that both autoreactive T cells and non-autoreactive endogenous T cells were able to sense the different oxygenation levels in different tissues. We therefore asked if the level of oxygen *in vivo* could also affect effector T cells function as it was observed *in vitro*.

To address this question, we subjected animals in which EAE was induced via the lung to whole-body hypoxia (10%). This disease model has been recently established in our lab (Hosang et al., 2022) and is based on intra-lung immunisation of animals transferred few hours earlier with resting T_{MBP} cells. In this way, CNS-reactive T cells in the lung can be identified and therefore, the initial events of antigen-specific T_{MBP} cell activation and proliferation in the lung and the impact of oxygen on these processes can be investigated. By using this system, we observed a substantial reduction in T cell proliferation and cytokine production upon reactivation of T_{MBP} cells in the lung in animals subjected to whole-body hypoxia. These results confirmed our previous *in vitro* data, indicating that the level of oxygen *in vivo* also shaped effector T cell function. Furthermore, these data may indicate that oxygen levels can differentially affect the pulmonary immune response depending on the nature of the stimulus. In steady-state conditions, oxygen levels contribute to create an immunosuppressive environment in the lung by permitting the differentiation of iTreg cells and by restraining the inflammatory responses of CD4⁺ and CD8⁺ T cells towards an innocuous stimulus, such as house dust mite (Clever et al., 2016). However, this “default state” is not absolute and can be bypassed, as is the case in our setup in which the (auto) antigen in CFA is provided. In such conditions, the high level of oxygen in the lung promotes rather than restrains the immune response. Similar results were obtained by Ohta and colleagues, who showed that the extent of T cell activation *in vivo* depends on their localisation and is decreased in environments with lower oxygen tension (Ohta et al., 2011).

We finally sought whether these effects on the initial stages of T cell reactivation would also affect the encephalitogenic potential of T_{EM} cells directed against myelin antigens. To this end, we used the same experimental design as for the assessment of T cell reactivation *in vivo*, combining the exposition to whole body hypoxia with the local reactivation of T_{MBP} cells into the lung. Upon lung immunisation, all animals developed EAE. However, in animals exposed at any time to the hypoxic environment, T_{MBP} cell reactivation in the lung triggered milder and delayed symptoms. Unexpectedly, a high proportions of animals exposed to the hypoxic atmosphere developed an atypical EAE phenotype, characterised by severe ataxia in absence of paresis or paralysis. The hypoxic stimulus can have pleiotropic systemic effects. For example it can affect the local lung milieu, disrupt the integrity of the blood-brain barrier (Halder & Milner, 2020), modulate the activation status of microglial cells (Tadmouri et al., 2014) or

induce a stress response (Leonard et al., 2005). All these effects can influence EAE in a T cell-independent manner. Therefore, in order to evaluate if environmental oxygen availability affected the encephalitogenic potential of T_{MBP} cells, we took a reductionist approach and injected the animals with T_{MBP} cells previously reactivated *in vitro* under either normoxic or hypoxic atmosphere. When tracking the encephalitogenic T_{MBP} cells on their way to the CNS and in the spinal cord (Flügel et al., 1999), we did not observe any differences between the two cohorts in their migratory pattern in peripheral organs, neither showing any impairment in overcoming the BBB nor in being reactivated in the CNS upon invasion. Instead, in the CNS, T_{MBP} cells activated under hypoxic *in vitro* conditions displayed a higher level of activation through surface markers and cytokine production. Of note, a HIF1-dependent increase in effector function was previously observed in $CD8^+$ T cells stimulated under hypoxic conditions (Doedens et al., 2013), suggesting that a similar mechanism can take place also in our setup. Nevertheless, we detected a lower amount of T_{MBP} cells both in the peripheral organs and in the CNS of the hypoxic group. Accordingly, EAE was delayed and milder, suggesting that the *in vitro* hypoxic preconditioning was able to imprint T_{MBP} cells and affect their function *in vivo* in the context of CNS autoimmunity. In perspective, we aim to perform criss-cross experiments and 1) we will retrieve recently activated T_{MBP} cells from hypoxic and normoxic lungs and retransfer them to naïve recipient animals and 2) we will induce transfer EAE in animals previously subjected to normoxia or hypoxia. With this approach, we aim to characterize in detail the T cell intrinsic and extrinsic effects of oxygen on EAE.

In summary, our data indicate that T cells are sensitive to environmental oxygen tensions and can rapidly adapt their transcriptional program and their effector function accordingly. Likely through fine-tuneable metabolic changes, T cells encountering the antigen in an oxygen rich environment display a higher proliferative capacity and a higher encephalitogenic potential. As consequence, the lung, due to its high oxygenation status and its constant contact with the external environment, can represent a very efficient trigger site for CNS autoimmunity.

6. List of references

- Agbor, T. A., Cheong, A., Comerford, K. M., Scholz, C. C., Bruning, U., Clarke, A., Cummins, E. P., Cagney, G., & Taylor, C. T. (2011). Small ubiquitin-related modifier (SUMO)-1 promotes glycolysis in hypoxia. *The Journal of Biological Chemistry*, *286*(6), 4718–4726. <https://doi.org/10.1074/jbc.M110.115931>
- Alonso, A., & Hernán, M. A. (2008). Temporal trends in the incidence of multiple sclerosis. *Neurology*, *71*(2), 129–135. <https://doi.org/10.1212/01.wnl.0000316802.35974.34>
- Angelini, D. F., Serafini, B., Piras, E., Severa, M., Coccia, E. M., Rosicarelli, B., Ruggieri, S., Gasperini, C., Buttari, F., Centonze, D., Mechelli, R., Salvetti, M., Borsellino, G., Aloisi, F., & Battistini, L. (2013). Increased CD8+ T Cell Response to Epstein-Barr Virus Lytic Antigens in the Active Phase of Multiple Sclerosis. *PLoS Pathogens*, *9*(4), e1003220. <https://doi.org/10.1371/journal.ppat.1003220>
- Arteel, G. E., Thurman, R. G., & Raleigh, J. A. (1998). Reductive metabolism of the hypoxia marker pimonidazole is regulated by oxygen tension independent of the pyridine nucleotide redox state. *European Journal of Biochemistry*, *253*(3), 743–750. <https://doi.org/10.1046/j.1432-1327.1998.2530743.x>
- Ascherio, A. (2013). Environmental factors in multiple sclerosis. *Expert Review of Neurotherapeutics*, *13*(sup2), 3–9. <https://doi.org/10.1586/14737175.2013.865866>
- Ascherio, A., & Munger, K. L. (2007a). Environmental risk factors for multiple sclerosis. Part I: The role of infection. *Annals of Neurology*, *61*(4), 288–299. <https://doi.org/10.1002/ana.21117>
- Ascherio, A., & Munger, K. L. (2007b). Environmental risk factors for multiple sclerosis. Part II: Noninfectious factors. *Annals of Neurology*, *61*(6), 504–513. <https://doi.org/10.1002/ana.21141>
- Ast, T., & Mootha, V. K. (2019). Oxygen and mammalian cell culture: Are we repeating the experiment of Dr. Ox? *Nature Metabolism*, *1*(9), 858–860. <https://doi.org/10.1038/s42255-019-0105-0>
- Atkuri, K. R., Herzenberg, L. A., & Herzenberg, L. A. (2005). Culturing at atmospheric oxygen levels impacts lymphocyte function. *Proceedings of the National Academy of Sciences of the United States of America*, *102*(10), 3756–3759. <https://doi.org/10.1073/pnas.0409910102>
- Atkuri, K. R., Herzenberg, L. A., Niemi, A.-K., Cowan, T., & Herzenberg, L. A. (2007). Importance of culturing primary lymphocytes at physiological oxygen levels. *Proceedings of the National Academy of Sciences of the United States of America*, *104*(11), 4547–4552. <https://doi.org/10.1073/pnas.0611732104>
- Bahbouhi, B., Pettré, S., Berthelot, L., Garcia, A., Elong Ngonu, A., Degauque, N., Michel, L., Wiertlewski, S., Lefrère, F., Meyniel, C., Delcroix, C., Brouard, S., Laplaud, D.-A., & Soullillou, J.-P. (2010). T cell recognition of self-antigen presenting cells by protein transfer assay reveals a high frequency of anti-myelin T cells in multiple sclerosis. *Brain*, *133*(6), 1622–1636. <https://doi.org/10.1093/brain/awq074>
- Baranzini, S. E., & Oksenberg, J. R. (2017). The Genetics of Multiple Sclerosis: From 0 to 200 in 50 Years. *Trends in Genetics*, *33*(12), 960–970. <https://doi.org/10.1016/j.tig.2017.09.004>

- Bartholomäus, I., Kawakami, N., Odoardi, F., Schläger, C., Miljkovic, D., Ellwart, J. W., Klinkert, W. E. F., Flügel-Koch, C., Issekutz, T. B., Wekerle, H., & Flügel, A. (2009). Effector T cell interactions with meningeal vascular structures in nascent autoimmune CNS lesions. *Nature*, *462*(7269), 94–98. <https://doi.org/10.1038/nature08478>
- Beecham, A. H., Patsopoulos, N. A., Xifara, D. K., Davis, M. F., Kempainen, A., Cotsapas, C., Shah, T. S., Spencer, C., Booth, D., Goris, A., Oturai, A., Saarela, J., Fontaine, B., Hemmer, B., Martin, C., Zipp, F., D'Alfonso, S., Martinelli-Boneschi, F., Taylor, B., ... International IBD Genetics Consortium (IIBDGC). (2013). Analysis of immune-related loci identifies 48 new susceptibility variants for multiple sclerosis. *Nature Genetics*, *45*(11), 1353–1360. <https://doi.org/10.1038/ng.2770>
- Ben-Nun, A., Wekerle, H., & Cohen, I. R. (1981). The rapid isolation of clonable antigen-specific T lymphocyte lines capable of mediating autoimmune encephalomyelitis. *European Journal of Immunology*, *11*(3), 195–199. <https://doi.org/10.1002/eji.1830110307>
- Bergeron, M., Evans, S. M., Sharp, F. R., Koch, C. J., Lord, E. M., & Ferriero, D. M. (1999). Detection of hypoxic cells with the 2-nitroimidazole, EF5, correlates with early redox changes in rat brain after perinatal hypoxia-ischemia. *Neuroscience*, *89*(4), 1357–1366. [https://doi.org/10.1016/s0306-4522\(98\)00377-7](https://doi.org/10.1016/s0306-4522(98)00377-7)
- Bjornevik, K., Cortese, M., Healy, B. C., Kuhle, J., Mina, M. J., Leng, Y., Elledge, S. J., Niebuhr, D. W., Scher, A. I., Munger, K. L., & Ascherio, A. (2022). Longitudinal analysis reveals high prevalence of Epstein-Barr virus associated with multiple sclerosis. *Science*, *375*(6578), 296–301. <https://doi.org/10.1126/science.abj8222>
- Braun, R. D., Lanzen, J. L., Snyder, S. A., & Dewhirst, M. W. (2001). Comparison of tumor and normal tissue oxygen tension measurements using OxyLite or microelectrodes in rodents. *American Journal of Physiology. Heart and Circulatory Physiology*, *280*(6), H2533-2544. <https://doi.org/10.1152/ajpheart.2001.280.6.H2533>
- Caldwell, C. C., Kojima, H., Lukashev, D., Armstrong, J., Farber, M., Apasov, S. G., & Sitkovsky, M. V. (2001). Differential effects of physiologically relevant hypoxic conditions on T lymphocyte development and effector functions. *Journal of Immunology (Baltimore, Md.: 1950)*, *167*(11), 6140–6149. <https://doi.org/10.4049/jimmunol.167.11.6140>
- Cerychova, R., & Pavlinkova, G. (2018). HIF-1, Metabolism, and Diabetes in the Embryonic and Adult Heart. *Frontiers in Endocrinology*, *9*. <https://www.frontiersin.org/article/10.3389/fendo.2018.00460>
- Chaneton, B., Hillmann, P., Zheng, L., Martin, A. C. L., Maddocks, O. D. K., Chokkathukalam, A., Coyle, J. E., Jankevics, A., Holding, F. P., Vousden, K. H., Frezza, C., O'Reilly, M., & Gottlieb, E. (2012). Serine is a natural ligand and allosteric activator of pyruvate kinase M2. *Nature*, *491*(7424), 458–462. <https://doi.org/10.1038/nature11540>
- Chang, C.-H., Curtis, J. D., Maggi, L. B., Faubert, B., Villarino, A. V., O'Sullivan, D., Huang, S. C.-C., van der Windt, G. J. W., Blagih, J., Qiu, J., Weber, J. D., Pearce, E. J., Jones, R. G., & Pearce, E. L. (2013). Posttranscriptional control of T cell effector function by aerobic glycolysis. *Cell*, *153*(6), 1239–1251. <https://doi.org/10.1016/j.cell.2013.05.016>

- Cho, S. H., Raybuck, A. L., Blagih, J., Kemboi, E., Haase, V. H., Jones, R. G., & Boothby, M. R. (2019). Hypoxia-inducible factors in CD4⁺ T cells promote metabolism, switch cytokine secretion, and T cell help in humoral immunity. *Proceedings of the National Academy of Sciences*, *116*(18), 8975–8984. <https://doi.org/10.1073/pnas.1811702116>
- Clambey, E. T., McNamee, E. N., Westrich, J. A., Glover, L. E., Campbell, E. L., Jedlicka, P., de Zoeten, E. F., Cambier, J. C., Stenmark, K. R., Colgan, S. P., & Eltzschig, H. K. (2012). Hypoxia-inducible factor-1 alpha-dependent induction of FoxP3 drives regulatory T-cell abundance and function during inflammatory hypoxia of the mucosa. *Proceedings of the National Academy of Sciences of the United States of America*, *109*(41), E2784-2793. <https://doi.org/10.1073/pnas.1202366109>
- Clever, D., Roychoudhuri, R., Constantinides, M. G., Askenase, M. H., Sukumar, M., Klebanoff, C. A., Eil, R. L., Hickman, H. D., Yu, Z., Pan, J. H., Palmer, D. C., Phan, A. T., Goulding, J., Gattinoni, L., Goldrath, A. W., Belkaid, Y., & Restifo, N. P. (2016). Oxygen Sensing by T Cells Establishes an Immunologically Tolerant Metastatic Niche. *Cell*, *166*(5), 1117-1131.e14. <https://doi.org/10.1016/j.cell.2016.07.032>
- Compston, A., & Coles, A. (2008). Multiple sclerosis. *The Lancet*, *372*(9648), 1502–1517. [https://doi.org/10.1016/S0140-6736\(08\)61620-7](https://doi.org/10.1016/S0140-6736(08)61620-7)
- De Santis, V., & Singer, M. (2015). Tissue oxygen tension monitoring of organ perfusion: Rationale, methodologies, and literature review. *British Journal of Anaesthesia*, *115*(3), 357–365. <https://doi.org/10.1093/bja/aev162>
- Deng, B., Zhu, J.-M., Wang, Y., Liu, T.-T., Ding, Y.-B., Xiao, W.-M., Lu, G.-T., Bo, P., & Shen, X.-Z. (2013). Intratumor Hypoxia Promotes Immune Tolerance by Inducing Regulatory T Cells via TGF- β 1 in Gastric Cancer. *PLOS ONE*, *8*(5), e63777. <https://doi.org/10.1371/journal.pone.0063777>
- Dobson, R., & Giovannoni, G. (2019). Multiple sclerosis – a review. *European Journal of Neurology*, *26*(1), 27–40. <https://doi.org/10.1111/ene.13819>
- Doedens, A. L., Phan, A. T., Stradner, M. H., Fujimoto, J. K., Nguyen, J. V., Yang, E., Johnson, R. S., & Goldrath, A. W. (2013). Hypoxia-inducible factors enhance the effector responses of CD8⁺ T cells to persistent antigen. *Nature Immunology*, *14*(11), 1173–1182. <https://doi.org/10.1038/ni.2714>
- Ebers, G. C., Yee, I. M. L., Sadovnick, A. D., & Duquette, P. (2000). Conjugal multiple sclerosis: Population-based prevalence and recurrence risks in offspring. *Annals of Neurology*, *48*(6), 927–931. [https://doi.org/10.1002/1531-8249\(200012\)48:6<927::AID-ANA14>3.0.CO;2-F](https://doi.org/10.1002/1531-8249(200012)48:6<927::AID-ANA14>3.0.CO;2-F)
- Feigin, V. L., Abajobir, A. A., Abate, K. H., Abd-Allah, F., Abdulle, A. M., Abera, S. F., Abyu, G. Y., Ahmed, M. B., Aichour, A. N., Aichour, I., Aichour, M. T. E., Akinyemi, R. O., Alabed, S., Al-Raddadi, R., Alvis-Guzman, N., Amare, A. T., Ansari, H., Anwari, P., Ärnlöv, J., ... Vos, T. (2017). Global, regional, and national burden of neurological disorders during 1990–2015: A systematic analysis for the Global Burden of Disease Study 2015. *The Lancet Neurology*, *16*(11), 877–897. [https://doi.org/10.1016/S1474-4422\(17\)30299-5](https://doi.org/10.1016/S1474-4422(17)30299-5)
- Flügel, A., Willem, M., Berkowicz, T., & Wekerle, H. (1999a). Gene transfer into CD4⁺ T lymphocytes: Green fluorescent protein-engineered, encephalitogenic T cells illuminate brain autoimmune responses. *Nature Medicine*, *5*(7), 843–847. <https://doi.org/10.1038/10567>

- Flügel, A., Willem, M., Berkowicz, T., & Wekerle, H. (1999b). Gene transfer into CD4+ T lymphocytes: Green fluorescent protein-engineered, encephalitogenic T cells illuminate brain autoimmune responses. *Nature Medicine*, *5*(7), 843–847. <https://doi.org/10.1038/10567>
- Fong, G.-H., & Takeda, K. (2008). Role and regulation of prolyl hydroxylase domain proteins. *Cell Death & Differentiation*, *15*(4), 635–641. <https://doi.org/10.1038/cdd.2008.10>
- Ford, H. (2020). Clinical presentation and diagnosis of multiple sclerosis. *Clinical Medicine*, *20*(4), 380–383. <https://doi.org/10.7861/clinmed.2020-0292>
- Freund, J., Thomson, K. J., Sommer, H. E., Walter, A. W., & Schenkein, E. L. (1945). IMMUNIZATION OF RHESUS MONKEYS AGAINST MALARIAL INFECTION (P. KNOWLESI) WITH KILLED PARASITES AND ADJUVANTS. *Science (New York, N.Y.)*, *102*(2643), 202–204. <https://doi.org/10.1126/science.102.2643.202>
- Gillespie, M., Jassal, B., Stephan, R., Milacic, M., Rothfels, K., Senff-Ribeiro, A., Griss, J., Sevilla, C., Matthews, L., Gong, C., Deng, C., Varusai, T., Ragueneau, E., Haider, Y., May, B., Shamovsky, V., Weiser, J., Brunson, T., Sanati, N., ... D'Eustachio, P. (2022). The reactome pathway knowledgebase 2022. *Nucleic Acids Research*, *50*(D1), D687–D692. <https://doi.org/10.1093/nar/gkab1028>
- Goodin, D. S. (2014). The epidemiology of multiple sclerosis: Insights to disease pathogenesis. *Handbook of Clinical Neurology*, *122*, 231–266. <https://doi.org/10.1016/B978-0-444-52001-2.00010-8>
- Gropper, Y., Feferman, T., Shalit, T., Salame, T.-M., Porat, Z., & Shakhar, G. (2017). Culturing CTLs under Hypoxic Conditions Enhances Their Cytotoxicity and Improves Their Anti-tumor Function. *Cell Reports*, *20*(11), 2547–2555. <https://doi.org/10.1016/j.celrep.2017.08.071>
- Halder, S. K., & Milner, R. (2020). Mild hypoxia triggers transient blood–brain barrier disruption: A fundamental protective role for microglia. *Acta Neuropathologica Communications*, *8*(1), 175. <https://doi.org/10.1186/s40478-020-01051-z>
- Halenius, A., & Hengel, H. (2014). Human Cytomegalovirus and Autoimmune Disease. *BioMed Research International*, *2014*, e472978. <https://doi.org/10.1155/2014/472978>
- Hatton, O. L., Harris-Arnold, A., Schaffert, S., Krams, S. M., & Martinez, O. M. (2014). The interplay between Epstein-Barr virus and B lymphocytes: Implications for infection, immunity, and disease. *Immunologic Research*, *58*(2–3), 268–276. <https://doi.org/10.1007/s12026-014-8496-1>
- Hawkins, K. E., Sharp, T. V., & McKay, T. R. (2013). The role of hypoxia in stem cell potency and differentiation. *Regenerative Medicine*, *8*(6), 771–782. <https://doi.org/10.2217/rme.13.71>
- Hedström, A. K., Bäärnhielm, M., Olsson, T., & Alfredsson, L. (2011). Exposure to environmental tobacco smoke is associated with increased risk for multiple sclerosis. *Multiple Sclerosis (Houndmills, Basingstoke, England)*, *17*(7), 788–793. <https://doi.org/10.1177/1352458511399610>
- Hedström, A. K., Hillert, J., Olsson, T., & Alfredsson, L. (2013). Smoking and multiple sclerosis susceptibility. *European Journal of Epidemiology*, *28*(11), 867–874. <https://doi.org/10.1007/s10654-013-9853-4>

- Hemmer, B., Archelos, J. J., & Hartung, H.-P. (2002). New concepts in the immunopathogenesis of multiple sclerosis. *Nature Reviews Neuroscience*, 3(4), 291–301. <https://doi.org/10.1038/nrn784>
- Henderson, A. R. (1969). Biochemistry of hypoxia: Current concepts. I. An introduction to biochemical pathways and their control. *British Journal of Anaesthesia*, 41(3), 245–250. <https://doi.org/10.1093/bja/41.3.245>
- Hernán, M. A., Oleky, M. J., & Ascherio, A. (2001). Cigarette Smoking and Incidence of Multiple Sclerosis. *American Journal of Epidemiology*, 154(1), 69–74. <https://doi.org/10.1093/aje/154.1.69>
- Hohlfeld, R., Dornmair, K., Meinl, E., & Wekerle, H. (2016). The search for the target antigens of multiple sclerosis, part 1: Autoreactive CD4+ T lymphocytes as pathogenic effectors and therapeutic targets. *The Lancet Neurology*, 15(2), 198–209. [https://doi.org/10.1016/S1474-4422\(15\)00334-8](https://doi.org/10.1016/S1474-4422(15)00334-8)
- Holt, P. G., Strickland, D. H., Wikström, M. E., & Jahnsen, F. L. (2008). Regulation of immunological homeostasis in the respiratory tract. *Nature Reviews Immunology*, 8(2), 142–152. <https://doi.org/10.1038/nri2236>
- Hosang, L., Canals, R. C., van der Flier, F. J., Hollensteiner, J., Daniel, R., Flügel, A., & Odoardi, F. (2022). The lung microbiome regulates brain autoimmunity. *Nature*, 603(7899), 138–144. <https://doi.org/10.1038/s41586-022-04427-4>
- Huang, J. H., Cárdenas-Navia, L. I., Caldwell, C. C., Plumb, T. J., Radu, C. G., Rocha, P. N., Wilder, T., Bromberg, J. S., Cronstein, B. N., Sitkovsky, M., Dewhirst, M. W., & Dustin, M. L. (2007). Requirements for T Lymphocyte Migration in Explanted Lymph Nodes. *The Journal of Immunology*, 178(12), 7747–7755. <https://doi.org/10.4049/jimmunol.178.12.7747>
- Hubbi, M. E., & Semenza, G. L. (2015). Regulation of cell proliferation by hypoxia-inducible factors. *American Journal of Physiology. Cell Physiology*, 309(12), C775–782. <https://doi.org/10.1152/ajpcell.00279.2015>
- Jafari, N., & Hintzen, R. Q. (2011). The association between cigarette smoking and multiple sclerosis. *Journal of the Neurological Sciences*, 311(1), 78–85. <https://doi.org/10.1016/j.jns.2011.09.008>
- Jurica, M. S., Mesecar, A., Heath, P. J., Shi, W., Nowak, T., & Stoddard, B. L. (1998). The allosteric regulation of pyruvate kinase by fructose-1,6-bisphosphate. *Structure (London, England: 1993)*, 6(2), 195–210. [https://doi.org/10.1016/s0969-2126\(98\)00021-5](https://doi.org/10.1016/s0969-2126(98)00021-5)
- Karhausen, J., Haase, V. H., & Colgan, S. P. (2005). Inflammatory hypoxia: Role of hypoxia-inducible factor. *Cell Cycle (Georgetown, Tex.)*, 4(2), 256–258.
- Kawakami, N., Odoardi, F., Ziemssen, T., Bradl, M., Ritter, T., Neuhaus, O., Lassmann, H., Wekerle, H., & Flügel, A. (2005). Autoimmune CD4+ T Cell Memory: Lifelong Persistence of Encephalitogenic T Cell Clones in Healthy Immune Repertoires. *The Journal of Immunology*, 175(1), 69–81. <https://doi.org/10.4049/jimmunol.175.1.69>

- Keeley, T. P., & Mann, G. E. (2019). Defining Physiological Normoxia for Improved Translation of Cell Physiology to Animal Models and Humans. *Physiological Reviews*, *99*(1), 161–234. <https://doi.org/10.1152/physrev.00041.2017>
- Kemp, R. G., & Gunasekera, D. (2002). Evolution of the allosteric ligand sites of mammalian phosphofructo-1-kinase. *Biochemistry*, *41*(30), 9426–9430. <https://doi.org/10.1021/bi020110d>
- Kim, H., Peng, G., Hicks, J. M., Weiss, H. L., Van Meir, E. G., Brenner, M. K., & Yotnda, P. (2008). Engineering human tumor-specific cytotoxic T cells to function in a hypoxic environment. *Molecular Therapy: The Journal of the American Society of Gene Therapy*, *16*(3), 599–606. <https://doi.org/10.1038/sj.mt.6300391>
- Koritschoner, R., & Schweinburg, F. (1925). Induktion von Paralyse und Rückenmarksentzündung durch Immunisierung von Kaninchen mit menschlichem Rückenmarksgewebe. *Zeitschrift fuer Immunitaetsforschung und eyperimentelle Therapie*, *42*, 217–283.
- Koudhi, S., Elgaaid, A. B., & Chouaib, S. (2017). Impact of Metabolism on T-Cell Differentiation and Function and Cross Talk with Tumor Microenvironment. *Frontiers in Immunology*, *8*, 270. <https://doi.org/10.3389/fimmu.2017.00270>
- Krzywinska, E., & Stockmann, C. (2018). Hypoxia, Metabolism and Immune Cell Function. *Biomedicines*, *6*(2), E56. <https://doi.org/10.3390/biomedicines6020056>
- Lang, H. L. E., Jacobsen, H., Ikemizu, S., Andersson, C., Harlos, K., Madsen, L., Hjorth, P., Sondergaard, L., Svejgaard, A., Wucherpfennig, K., Stuart, D. I., Bell, J. I., Jones, E. Y., & Fugger, L. (2002). A functional and structural basis for TCR cross-reactivity in multiple sclerosis. *Nature Immunology*, *3*(10), 940–943. <https://doi.org/10.1038/ni835>
- Lanz, T. V., Brewer, R. C., Ho, P. P., Moon, J.-S., Jude, K. M., Fernandez, D., Fernandes, R. A., Gomez, A. M., Nadj, G.-S., Bartley, C. M., Schubert, R. D., Hawes, I. A., Vazquez, S. E., Iyer, M., Zuchero, J. B., Teegen, B., Dunn, J. E., Lock, C. B., Kipp, L. B., ... Robinson, W. H. (2022). Clonally expanded B cells in multiple sclerosis bind EBV EBNA1 and GialCAM. *Nature*, *603*(7900), 321–327. <https://doi.org/10.1038/s41586-022-04432-7>
- Larbi, A., Zelba, H., Goldeck, D., & Pawelec, G. (2010). Induction of HIF-1 α and the glycolytic pathway alters apoptotic and differentiation profiles of activated human T cells. *Journal of Leukocyte Biology*, *87*(2), 265–273. <https://doi.org/10.1189/jlb.0509304>
- Leonard, M. O., Godson, C., Brady, H. R., & Taylor, C. T. (2005). Potentiation of glucocorticoid activity in hypoxia through induction of the glucocorticoid receptor. *Journal of Immunology (Baltimore, Md.: 1950)*, *174*(4), 2250–2257. <https://doi.org/10.4049/jimmunol.174.4.2250>
- Lodygin, D., Odoardi, F., Schläger, C., Körner, H., Kitz, A., Nosov, M., van den Brandt, J., Reichardt, H. M., Haberl, M., & Flügel, A. (2013). A combination of fluorescent NFAT and H2B sensors uncovers dynamics of T cell activation in real time during CNS autoimmunity. *Nature Medicine*, *19*(6), 784–790. <https://doi.org/10.1038/nm.3182>
- Loeffler, D. A., Juneau, P. L., & Masseran, S. (1992). Influence of tumour physico-chemical conditions on interleukin-2-stimulated lymphocyte proliferation. *British Journal of Cancer*, *66*(4), 619–622. <https://doi.org/10.1038/bjc.1992.326>

- Lucas, R. M., Byrne, S. N., Correale, J., Ilschner, S., & Hart, P. H. (2015). Ultraviolet radiation, vitamin D and multiple sclerosis. *Neurodegenerative Disease Management*, 5(5), 413–424. <https://doi.org/10.2217/nmt.15.33>
- Makino, Y., Nakamura, H., Ikeda, E., Ohnuma, K., Yamauchi, K., Yabe, Y., Poellinger, L., Okada, Y., Morimoto, C., & Tanaka, H. (2003). Hypoxia-Inducible Factor Regulates Survival of Antigen Receptor-Driven T Cells. *The Journal of Immunology*, 171(12), 6534–6540. <https://doi.org/10.4049/jimmunol.171.12.6534>
- McKay, K. A., Kwan, V., Duggan, T., & Tremlett, H. (2015). Risk Factors Associated with the Onset of Relapsing-Remitting and Primary Progressive Multiple Sclerosis: A Systematic Review. *BioMed Research International*, 2015, 817238. <https://doi.org/10.1155/2015/817238>
- McKeown, S. R. (2014). Defining normoxia, physoxia and hypoxia in tumours-implications for treatment response. *The British Journal of Radiology*, 87(1035), 20130676. <https://doi.org/10.1259/bjr.20130676>
- McNamee, E. N., Korn Johnson, D., Homann, D., & Clambey, E. T. (2013). Hypoxia and hypoxia-inducible factors as regulators of T cell development, differentiation, and function. *Immunologic Research*, 55(1–3), 58–70. <https://doi.org/10.1007/s12026-012-8349-8>
- Michiels, C. (2004). Physiological and Pathological Responses to Hypoxia. *The American Journal of Pathology*, 164(6), 1875–1882.
- Mix, E., Meyer-Rienecker, H., Hartung, H.-P., & Zettl, U. K. (2010). Animal models of multiple sclerosis—Potentials and limitations. *Progress in Neurobiology*, 92(3), 386–404. <https://doi.org/10.1016/j.pneurobio.2010.06.005>
- Mootha, V. K., Lindgren, C. M., Eriksson, K.-F., Subramanian, A., Sihag, S., Lehar, J., Puigserver, P., Carlsson, E., Ridderstråle, M., Laurila, E., Houstis, N., Daly, M. J., Patterson, N., Mesirov, J. P., Golub, T. R., Tamayo, P., Spiegelman, B., Lander, E. S., Hirschhorn, J. N., ... Groop, L. C. (2003). PGC-1 α -responsive genes involved in oxidative phosphorylation are coordinately downregulated in human diabetes. *Nature Genetics*, 34(3), 267–273. <https://doi.org/10.1038/ng1180>
- Munger, K. L., Levin, L. I., Hollis, B. W., Howard, N. S., & Ascherio, A. (2006). Serum 25-Hydroxyvitamin D Levels and Risk of Multiple Sclerosis. *JAMA*, 296(23), 2832–2838. <https://doi.org/10.1001/jama.296.23.2832>
- Naldini, A., Carraro, F., Silvestri, S., & Bocci, V. (1997). Hypoxia affects cytokine production and proliferative responses by human peripheral mononuclear cells. *Journal of Cellular Physiology*, 173(3), 335–342. [https://doi.org/10.1002/\(SICI\)1097-4652\(199712\)173:3<335::AID-JCP5>3.0.CO;2-O](https://doi.org/10.1002/(SICI)1097-4652(199712)173:3<335::AID-JCP5>3.0.CO;2-O)
- Ochoa-Repáraz, J., Mielcarz, D. W., Ditrio, L. E., Burroughs, A. R., Foureau, D. M., Haque-Begum, S., & Kasper, L. H. (2009). Role of gut commensal microflora in the development of experimental autoimmune encephalomyelitis. *Journal of Immunology (Baltimore, Md.: 1950)*, 183(10), 6041–6050. <https://doi.org/10.4049/jimmunol.0900747>
- Odoardi, F., Sie, C., Strey, K., Ulaganathan, V. K., Schläger, C., Lodygin, D., Heckelsmiller, K., Nietfeld, W., Ellwart, J., Klinkert, W. E. F., Lottaz, C., Nosov, M., Brinkmann, V., Spang, R., Lehrach, H., Vingron, M., Wekerle, H., Flügel-Koch, C., & Flügel, A. (2012). T cells become licensed in the

- lung to enter the central nervous system. *Nature*, 488(7413), 675–679. <https://doi.org/10.1038/nature11337>
- O'Dwyer, D. N., Dickson, R. P., & Moore, B. B. (2016). The Lung Microbiome, Immunity, and the Pathogenesis of Chronic Lung Disease. *The Journal of Immunology*, 196(12), 4839–4847. <https://doi.org/10.4049/jimmunol.1600279>
- Ohta, A., Diwanji, R., Kini, R., Subramanian, M., Ohta, A., & Sitkovsky, M. (2011). In vivo T cell activation in lymphoid tissues is inhibited in the oxygen-poor microenvironment. *Frontiers in Immunology*, 2, 27. <https://doi.org/10.3389/fimmu.2011.00027>
- Oikonen, M., Laaksonen, M., Aalto, V., Ilonen, J., Salonen, R., Erälinna, J.-P., Panelius, M., & Salmi, A. (2011). Temporal relationship between environmental influenza A and Epstein-Barr viral infections and high multiple sclerosis relapse occurrence. *Multiple Sclerosis (Houndmills, Basingstoke, England)*, 17(6), 672–680. <https://doi.org/10.1177/1352458510394397>
- Palazon, A., Goldrath, A. W., Nizet, V., & Johnson, R. S. (2014). HIF Transcription Factors, Inflammation, and Immunity. *Immunity*, 41(4), 518–528. <https://doi.org/10.1016/j.immuni.2014.09.008>
- Palmer, C. S., Ostrowski, M., Balderson, B., Christian, N., & Crowe, S. M. (2015). Glucose Metabolism Regulates T Cell Activation, Differentiation, and Functions. *Frontiers in Immunology*, 6. <https://www.frontiersin.org/article/10.3389/fimmu.2015.00001>
- Pasteur, L., & Illo, J. (1996). Pasteur and rabies: An interview of 1882. *Medical History*, 40(3), 373–377.
- Paterson, P. Y. (1960). Transfer of allergic encephalomyelitis in rats by means of lymph node cells. *Journal of Experimental Medicine*, 111(1), 119–136.
- Pender, M. P., Csurhes, P. A., Smith, C., Beagley, L., Hooper, K. D., Raj, M., Coulthard, A., Burrows, S. R., & Khanna, R. (2014). Epstein-Barr virus-specific adoptive immunotherapy for progressive multiple sclerosis. *Multiple Sclerosis (Houndmills, Basingstoke, England)*, 20(11), 1541–1544. <https://doi.org/10.1177/1352458514521888>
- Peng, M., Yin, N., Chhangawala, S., Xu, K., Leslie, C. S., & Li, M. O. (2016). Aerobic glycolysis promotes T helper 1 cell differentiation through an epigenetic mechanism. *Science (New York, N.Y.)*, 354(6311), 481–484. <https://doi.org/10.1126/science.aaf6284>
- Prabhakar, N. R., & Semenza, G. L. (2015). Oxygen Sensing and Homeostasis. *Physiology (Bethesda, Md.)*, 30(5), 340–348. <https://doi.org/10.1152/physiol.00022.2015>
- Raleigh, J. A., Miller, G. G., Franko, A. J., Koch, C. J., Fuciarelli, A. F., & Kelly, D. A. (1987). Fluorescence immunohistochemical detection of hypoxic cells in spheroids and tumours. *British Journal of Cancer*, 56(4), 395–400. <https://doi.org/10.1038/bjc.1987.213>
- Ransohoff, R. M., Hafler, D. A., & Lucchinetti, C. F. (2015). Multiple sclerosis—A quiet revolution. *Nature Reviews Neurology*, 11(3), 134–142. <https://doi.org/10.1038/nrneurol.2015.14>
- Ricciardi, S., Manfrini, N., Alfieri, R., Calamita, P., Crosti, M. C., Gallo, S., Müller, R., Pagani, M., Abrignani, S., & Biffo, S. (2018). The Translational Machinery of Human CD4+ T Cells Is Poised for Activation and Controls the Switch from Quiescence to Metabolic Remodeling. *Cell Metabolism*, 28(6), 895–906.e5. <https://doi.org/10.1016/j.cmet.2018.08.009>

- Rivers, T. M., & Schwentker, F. F. (1935). ENCEPHALOMYELITIS ACCOMPANIED BY MYELIN DESTRUCTION EXPERIMENTALLY PRODUCED IN MONKEYS. *The Journal of Experimental Medicine*, 61(5), 689–702.
- Rivers, T. M., Sprunt, D. H., & Berry, G. P. (1933). OBSERVATIONS ON ATTEMPTS TO PRODUCE ACUTE DISSEMINATED ENCEPHALOMYELITIS IN MONKEYS. *The Journal of Experimental Medicine*, 58(1), 39–53.
- Robertson, N. P., Clayton, D., Fraser, M., Deans, J., & Compston, D. A. (1996). Clinical concordance in sibling pairs with multiple sclerosis. *Neurology*, 47(2), 347–352. <https://doi.org/10.1212/wnl.47.2.347>
- Roman, J., Rangasamy, T., Guo, J., Sugunan, S., Meednu, N., Packirisamy, G., Shimoda, L. A., Golding, A., Semenza, G., & Georas, S. N. (2010). T-cell activation under hypoxic conditions enhances IFN-gamma secretion. *American Journal of Respiratory Cell and Molecular Biology*, 42(1), 123–128. <https://doi.org/10.1165/rcmb.2008-0139OC>
- Rustenhoven, J., Drieu, A., Mamuladze, T., de Lima, K. A., Dykstra, T., Wall, M., Papadopoulos, Z., Kanamori, M., Salvador, A. F., Baker, W., Lemieux, M., Da Mesquita, S., Cugurra, A., Fitzpatrick, J., Sviben, S., Kossina, R., Bayguinov, P., Townsend, R. R., Zhang, Q., ... Kipnis, J. (2021). Functional characterization of the dural sinuses as a neuroimmune interface. *Cell*, 184(4), 1000-1016.e27. <https://doi.org/10.1016/j.cell.2020.12.040>
- Salmond, R. J. (2018). mTOR Regulation of Glycolytic Metabolism in T Cells. *Frontiers in Cell and Developmental Biology*, 6, 122. <https://doi.org/10.3389/fcell.2018.00122>
- Schwentker, F. F., & Rivers, T. M. (1934). THE ANTIBODY RESPONSE OF RABBITS TO INJECTIONS OF EMULSIONS AND EXTRACTS OF HOMOLOGOUS BRAIN. *The Journal of Experimental Medicine*, 60(5), 559–574.
- Semenza, G. L. (2003). Angiogenesis in ischemic and neoplastic disorders. *Annual Review of Medicine*, 54, 17–28. <https://doi.org/10.1146/annurev.med.54.101601.152418>
- Semenza, G. L. (2011). Oxygen sensing, homeostasis, and disease. *The New England Journal of Medicine*, 365(6), 537–547. <https://doi.org/10.1056/NEJMra1011165>
- Semenza, G. L. (2014). Oxygen sensing, hypoxia-inducible factors, and disease pathophysiology. *Annual Review of Pathology*, 9, 47–71. <https://doi.org/10.1146/annurev-pathol-012513-104720>
- Serafini, B., Scorsi, E., Rosicarelli, B., Rigau, V., Thouvenot, E., & Aloisi, F. (2017). Massive intracerebral Epstein-Barr virus reactivation in lethal multiple sclerosis relapse after natalizumab withdrawal. *Journal of Neuroimmunology*, 307, 14–17. <https://doi.org/10.1016/j.jneuroim.2017.03.013>
- Shabsigh, A., Ghafar, M. A., de la Taille, A., Burchardt, M., Kaplan, S. A., Anastasiadis, A. G., & Buttyan, R. (2001). Biomarker analysis demonstrates a hypoxic environment in the castrated rat ventral prostate gland. *Journal of Cellular Biochemistry*, 81(3), 437–444.
- Simpson, S., Blizzard, L., Otahal, P., Mei, I. V. der, & Taylor, B. (2011). Latitude is significantly associated with the prevalence of multiple sclerosis: A meta-analysis. *Journal of Neurology, Neurosurgery & Psychiatry*, 82(10), 1132–1141. <https://doi.org/10.1136/jnnp.2011.240432>

- Sospedra, M., & Martin, R. (2016). Immunology of Multiple Sclerosis. *Seminars in Neurology*, 36(2), 115–127. <https://doi.org/10.1055/s-0036-1579739>
- Subramanian, A., Tamayo, P., Mootha, V. K., Mukherjee, S., Ebert, B. L., Gillette, M. A., Paulovich, A., Pomeroy, S. L., Golub, T. R., Lander, E. S., & Mesirov, J. P. (2005). Gene set enrichment analysis: A knowledge-based approach for interpreting genome-wide expression profiles. *Proceedings of the National Academy of Sciences of the United States of America*, 102(43), 15545–15550. <https://doi.org/10.1073/pnas.0506580102>
- Sundström, P., & Nyström, L. (2008). Smoking worsens the prognosis in multiple sclerosis. *Multiple Sclerosis (Houndmills, Basingstoke, England)*, 14(8), 1031–1035. <https://doi.org/10.1177/1352458508093615>
- Tadmouri, A., Champagnat, J., & Morin-Surun, M. P. (2014). Activation of microglia and astrocytes in the nucleus tractus solitarius during ventilatory acclimatization to 10% hypoxia in unanesthetized mice. *Journal of Neuroscience Research*, 92(5), 627–633. <https://doi.org/10.1002/jnr.23336>
- Tao, J.-H., Barbi, J., & Pan, F. (2015). Hypoxia-inducible factors in T lymphocyte differentiation and function. A Review in the Theme: Cellular Responses to Hypoxia. *American Journal of Physiology. Cell Physiology*, 309(9), C580-589. <https://doi.org/10.1152/ajpcell.00204.2015>
- Taylor, C. T., & Colgan, S. P. (2017). Regulation of immunity and inflammation by hypoxia in immunological niches. *Nature Reviews Immunology*, 17(12), 774–785. <https://doi.org/10.1038/nri.2017.103>
- Tengvall, K., Huang, J., Hellström, C., Kammer, P., Biström, M., Ayoglu, B., Lima Bomfim, I., Stridh, P., Butt, J., Brenner, N., Michel, A., Lundberg, K., Padyukov, L., Lundberg, I. E., Svenungsson, E., Ernberg, I., Olafsson, S., Dilthey, A. T., Hillert, J., ... Kockum, I. (2019). Molecular mimicry between Anoctamin 2 and Epstein-Barr virus nuclear antigen 1 associates with multiple sclerosis risk. *Proceedings of the National Academy of Sciences of the United States of America*, 116(34), 16955–16960. <https://doi.org/10.1073/pnas.1902623116>
- Tripmacher, R., Gaber, T., Dziurla, R., Häupl, T., Erekul, K., Grützkau, A., Tschirschmann, M., Scheffold, A., Radbruch, A., Burmester, G.-R., & Buttgereit, F. (2008). Human CD4+ T cells maintain specific functions even under conditions of extremely restricted ATP production. *European Journal of Immunology*, 38(6), 1631–1642. <https://doi.org/10.1002/eji.200738047>
- Warburg, O. (1956). On respiratory impairment in cancer cells. *Science (New York, N.Y.)*, 124(3215), 269–270.
- Weidemann, A., & Johnson, R. S. (2008). Biology of HIF-1 α . *Cell Death & Differentiation*, 15(4), 621–627. <https://doi.org/10.1038/cdd.2008.12>
- Westendorf, A. M., Skibbe, K., Adamczyk, A., Buer, J., Geffers, R., Hansen, W., Pastille, E., & Jendrossek, V. (2017). Hypoxia Enhances Immunosuppression by Inhibiting CD4+ Effector T Cell Function and Promoting Treg Activity. *Cellular Physiology and Biochemistry*, 41(4), 1271–1284. <https://doi.org/10.1159/000464429>
- Wiebe, B. M., & Laursen, H. (1995). Human lung volume, alveolar surface area, and capillary length. *Microscopy Research and Technique*, 32(3), 255–262. <https://doi.org/10.1002/jemt.1070320308>

- Wiebe, B. M., & Laursen, H. (1998). Lung morphometry by unbiased methods in emphysema: Bronchial and blood vessel volume, alveolar surface area and capillary length. *APMIS*, *106*(1–6), 651–656. <https://doi.org/10.1111/j.1699-0463.1998.tb01395.x>
- Xie, Y., Shi, X., Sheng, K., Han, G., Li, W., Zhao, Q., Jiang, B., Feng, J., Li, J., & Gu, Y. (2019). PI3K/Akt signaling transduction pathway, erythropoiesis and glycolysis in hypoxia (Review). *Molecular Medicine Reports*, *19*(2), 783–791. <https://doi.org/10.3892/mmr.2018.9713>
- Zuckerberg, A. L., Goldberg, L. I., & Lederman, H. M. (1994). Effects of hypoxia on interleukin-2 mRNA expression by T lymphocytes. *Critical Care Medicine*, *22*(2), 197–203. <https://doi.org/10.1097/00003246-199402000-00008>

Acknowledgements

First of all, I would like to thank Prof. Dr. Alexander Flügel and Prof. Dr Francesca Odoardi for their leadership, diligent guidance, wise advice and visionary input. Thanks for giving me the chance to work, grow and develop in a brilliant scientific and professional atmosphere.

Thanks to Simone Hamann, for her unconceivable and unquantifiable support, for having always a listening ear for my complains and offering always the best answers and advices, thanks for showing me that there is always somebody nearby looking after you.

Special thanks are for Dr. Đorđe Miljković (University of Belgrade, Serbia), Dr. Jordi Pedragosa Ollé (Institute for Biomedical Investigations IIBB-CSIC, Spain) and Dr. Marc-André Lécuyer (Centre de recherché du CHUM –CRCHUM-, Canada, for their priceless help with planning, design and performance of some part of the animal experimentation.

Thanks to Prof. Dr. Dörthe M. Katschinski and Dr. Anke Zieseniss, for their collaboration and expertise I the field of hypoxic cell culture.

Thanks to Dr. Leon Hosang, for welcoming me into an encouraging and promising project, for being more than a teacher and a colleague.

Gràcies a la Sílvia Rodríguez i en Ferran Tarrés, per romandre amics, model i companys; per ser-hi sempre malgrat la distancia.

Thanks to Dr. Fred Lühder and Dr. Dmitri Lodygin, for being always ready to offer their challenging input and being open to discuss my progress anytime.

Special thanks to Dr. Arianna Merlini, for her brilliant comments and valuable opinions, for late night walks and thoughtful counselling for being a friend.

Thanks to Simon Mole, Martina Weig and Birgit Curdt for their impeccable technical support.

Thanks to Felicia Joy, Leonard, Lukas, Michael, Pari, Henrike, Marc-André, Judith and Hsin for being great colleagues and make the live and work in the laboratory so easy.

Thanks to Catherine Ludwig for proofreading my work and making great suggestions and to Omar L. Díaz for the great IT support.

Thanks to my chosen family, Cordero, Shama, Paola, Carlos, Txarli, Tommaso, Christin and Mahmoud; because they made me call a foreigner place home.

Thanks to Dr. Sebastian Jähne, for his patience with me and all his support, for being a good flatmate and an even better friend.

Thanks to Ava Jahangard, Iker Irisarri and Michelle Felletti, for the power and sincere warmth of new friendships.

Thanks to Júlia, Andrea, Ana, Ana, Carlos y Alba because we started this pathway together. Thanks to Mònica and Inés, to Agus, Carla, Elena and Laura, because in a friendship, when there is a will there are always several ways.

Finally yet importantly, I would also like to thank Dr. Francesc Jiménez-Altayó and Dr. Yara Onetti, because there is where everything started, to Prof. Dr. Anna Planas, for sprouting the seed of science, for giving me wings and letting my fly, to Jordi, Mattia, Ester, Amaia, Alba, Paqui, Núria, Francesc i Nuria and Angélica for having showed me from the beginning